Mapping Morphologic Change in the External Ear

by

Malcolm J. Grenness
B.D.Sc. (Melb) Dip. Prof. Mgt. (TCAE)
F.R.A.C.D.S.

Discipline of Anatomy and Physiology
School of Medicine
University of Tasmania

Submitted in fulfillment of the requirements for the Degree of
Master of Medical Science

University of Tasmania, September 1999

I hereby certify that this Thesis contains no material which has been accepted for a degree or diploma by the University or any other institution, except by way of background information and duly acknowledged in the Thesis, and to the best of my knowledge and belief no material previously published or written by another person except where due acknowledgement is made in the text of the Thesis.

Malcolm James Grenness

SUMMARY

The movement of the external ear canal, associated with jaw motion, relative to the concha region of the pinna has been studied. This issue is most relevant to the fitting and function of In-The-Ear hearing-aids. Pairs of open-jaw and closed-jaw silicone impressions were taken of 14 ears from 10 subjects. 3D coordinate data was obtained from the concha region and the anterior surface of the canal using a reflex microscope. The canal regions were plotted via an optical flat mirror. Proprietary area-based matching software was used to verify the stability of the concha region and evaluate distortion of the canal during jaw motion. The canal data from each pair was placed into the same coordinate system with their respective concha regions aligned using the area-matching software. Contour and difference maps of the canal data were used to demonstrate the amount of anterior-posterior (A-P), superior-inferior (S-I), and medial-lateral (M-L) movement that occurred between the open and closed-jaw impressions. Rotations were also evaluated.

Analysis confirmed that the concha regions did not undergo significant deformation during jaw movement. The canal regions underwent varying amounts of internal deformation with the majority of canals conforming within an RMS of 400 μm across the entire surface. The majority of canals underwent significant morphologic change relative to the concha. Movement of the canal in the M-L plane ranged from 0 to 3.8 mm with a mean of 1.4 mm; 8 canals moved laterally, 5 canals moved medially and 2 ears did not move in the M-L plane. Movement in the S-I plane ranged from 0 to 3.7 mm with a mean of 1.3 mm; 9 canals moved inferiorly, 2 canals moved superiorly and 3 canals did not moved in the S-I plane. Movement in the A-P plane ranged between +3.5 mm and –3 mm, with 5 canals moving anteriorly, 3 ears moved posteriorly, and 4 ears moving in a mixed fashion.

The geometry of the external ear has created difficulties in acquiring accurate surface maps for analysis. The study has focused on the key areas of the pinna and canal previously reported to undergo significant change.

This study does not support previous reports that suggest that the ear canal only widens with jaw opening. This study gives insights into the variability in the movements of the ear canal relative to the concha region of the pinna and will be of interest to clinicians involved in the fitting of hearing-aids.

ACKNOWLEDGEMENTS

When my wife Susan presented me with clinical material that defied the conventional wisdom, I thought that a simple quantitative study lay ahead. I approached the School of Surveying at the University of Tasmania and found that what I imagined to be a routine mapping exercise still lay in the realm of science fiction. I am indebted to Peter Zwart and Tony Sprent for their coutesy and encouragement.

I am especially indebted to Jon Osborn who has been the key link to directing me towards the different methodologies that resulted in a viable solution to the mapping problem.

There have been innumerable people who have (metaphorically) lent me their ears. It was following meeting William Douglas from Minnesota in 1996 that I was reinvigorated after a period of slow progress. While discussing my problems one-day with John Parslow from CSIRO Marine Laboratories, he wrote out the mirror transformation equations on a scrap of paper, without error.

My thanks to Richard Coleman for the use of Surfer 3-D graphics software; to Robert Anders for programming the Bursa-Wolf equations; to Andie Smithies at the Clinical Library for assistance through several frustrating literature searches, trying to find the key search words, before the advent of CD or on-line services; to Matthew Kirkcauldie for enhancing the colour photographs in the thesis; to Gordon Sanson at Monash University for his guidance on mapping and measuring small objects and for assistence with the use of the reflex microscope; and to Harvey Mitchell from Newcastle University for the generous use of DS Match proprietary software without which the project could not have proceeded.

My special thanks to my supervisor, Lee Weller, for clear insightful discussions that have spanned almost a decade. I am eternally grateful that I live mostly in the world of private clinical practice. However, I have been struck by the generosity of time and spirit that I have encountered throughout the myriad of Faculties in numerous institutions that I have had contact with during the course of this project.

I am especially indebted to my long-suffering wife Susan for the recruitment of subjects, the taking of impressions and indeterminate patience with my long years of study.

CONTENTS

Chapter 1 – Introduction

1.1 An Observation

Ear canal morphology changes upon smiling, talking and chewing (Morgan 1987). Casual observation suggests that there is wide variation in the types of movement possible between individuals. A standard reference, Cunningham's Textbook of Applied Anatomy 11th ed., when discussing the external ear canal simply states "When the head of the mandible moves forward e.g. on opening the mouth, the cartilaginous part is widened".

Changes in ear canal morphology frequently impact upon the practice of audiology and the fitting of hearing-aids. It was observed that a patient's ear canal occluded upon opening the mouth (speech). This prevented the patient from speaking and hearing at the same time, inhibiting modulation of the voice. A subsequent hearing-aid fitting was inhibited by discomfort in the canal as a result of the canal portion of the hearing aid impinging on the soft tissues when the mouth was opened (Grenness 1990).

Cunningham's description does not seem adequate to explain this observation which provided the impetus to investigate movement in the ear canal related to jaw movements.

1.2 Terminology

The external ear consists of the auricle (pinna), attached to the side of the head, and the external acoustic meatus (ear canal) leading from it to the tympanic membrane and middle ear (Fig.1.1).

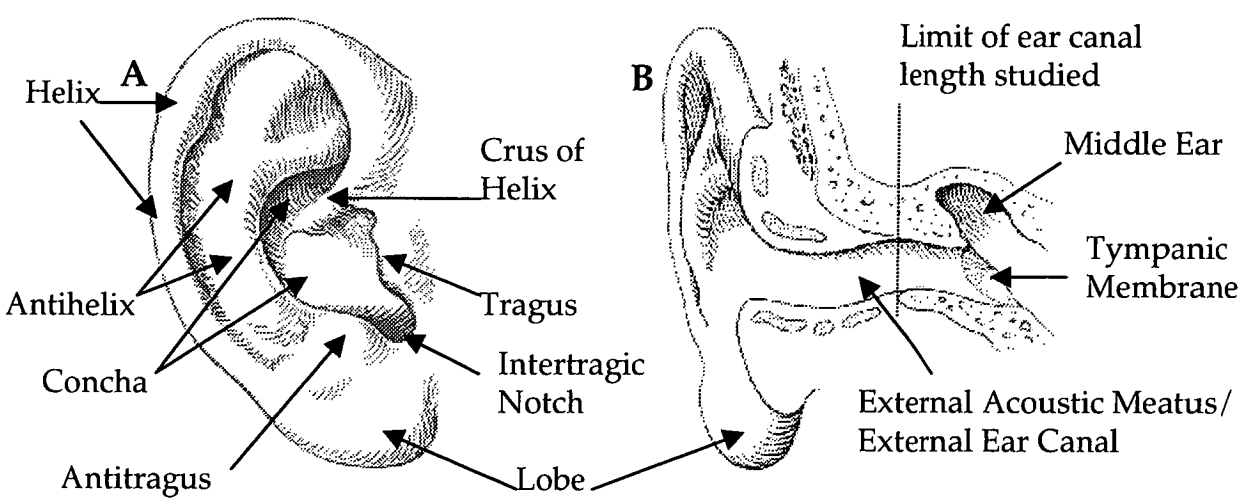

Fig. 1.1 Auricle. **A**: Lateral view, **B**: Frontal section through canal, Source: modified from Feneis (1976).

Hearing-aids are broadly classified according to their size and position in the external ear. These are:

Behind- The –Ear (BTE)
In-The-Ear (ITE)
In-The-Canal (ITC)
Completely-In-the–Ear (CIC)

The use and development of hearing-aids is outlined in section 1.6.

1.3 Previous Investigations

Van Willigan (1976) while investigating craniomandibular disorder reported that ear canal volume increased on mandibular opening. It also appeared that, with a change in mandibular position, not only the ventral wall of the external ear but the entire meatus changed form.

A selection of anecdotal clinical observations illustrates the influence that neighbouring structures can have on ear canal morphology. Hawke et al (1987) reported on a patient who had bilateral spontaneous temporomandibular joint herniation into the external auditory canal. The centre of each herniation was 30 mm medial to the lateral surface of the tragus. Heffez, Anderson and Mafee (1989) reported on two patients who were observed to have a bulge in the anterior wall of the ear canal caused by defect of the tympanic plate and a resultant intrusion of the mandibular condyle displacing retrodiscal tissues into the ear canal. The bulge converted to a depression upon wide mandibular opening.

Oliveira et al (1992) obtained silicon impressions of a subject at varying degrees of jaw opening. Transaxial diameters of the impression canals were measured with a digital caliper. Approximately a 25% change in this subject's ear canal with different jaw positions was observed in the antero-posterior (A-P) plane with essentially no change in the superior-inferior (S-I) plane. This was equivalent to an average increase, in the A-P direction, of about 0.7 mm in a typical adult over the length of the canal. He also reported upon a case with asymmetrical changes in which a 6% change occurred in the right ear, and a 21% change in the left ear.

Pirzanski (1996) reported on qualitative movement in ear canals relative to the concha region and described an "open-jaw" impression technique. He reported that:

1. Mandibular movement affected 20% to 60% of subjects having impressions taken,
2. The cartilage in some subjects stretched up to 2mm,
3. The majority of changes in the ear canal occurred in the anterior direction,
4. Minor changes were observed in the inferior direction, and

5. No changes or minimal changes were found in the posterior and superior part of the canal.

He reported that the areas most susceptible to deformation were:

1. The ear aperture,
2. The middle canal section, and
3. The second turn of the canal.

These changes may occur separately or may all be present in one case.

Oliveira (1997) reported on MRI studies using an MRI enhancer fluid in the ear canal, measuring volumetric changes in the ear canal at varying degrees of mandibular opening and relating these changes to underlying tissues. He concluded that the most significant changes that occurred in ear canal dimension with jaw motion were between the first and second turns of the canal.

This review of the literature has revealed an increasing awareness and reportage of problems associated with ear canal movement and its impact upon hearing-aid fitting and comfort.

This review also indicated that the major deformation of the canal occurred in the anterior wall. Very small changes occur in the S-I plane and in the posterior wall of the canal. There has been no information provided about movement within the concha region, although Pirzanski (1996) used it as his means of aligning pairs of open-jaw and closed-jaw impressions.

The focus of Oliviera (1997) and Pirzanski (1996) most recent papers was the fitting of CIC hearing-aids. These hearing-aids lay entirely within the canal. Changes within the canal impact upon the fit and comfort of these aids irrespective of other changes that may be occurring.

However, ITE are still the most commonly fitted hearing-aids, particularly amongst elderly patients. Their larger size leads to easier handling and manageability. These hearing-aids consist of a larger bowl that fills the concha region of the pinna and a smaller canal section that extends into the ear canal as fair as comfort and access allows. The concha part of the hearing-aid provides the major retentive element of the appliance. Forces applied to the canal section of the hearing-aid by adjacent anatomical structures are resisted by the greater bulk of the concha area. The hearing-aid as a whole must accommodate changes that occur in the canal. If the concha area is unyielding, the accommodation of the movement must occur entirely within the canal.

There is a need to provide quantitative data on movements affecting the entire tissue-fitting surface of earmoulds and hearing-aids. In particular, there is a need to provide quantitative data of morphological changes of the external ear canal relative to the concha region of the pinna associated with facial and mandibular movement.

1.4 Relevance of Ear Canal Movement

Knowledge of the nature and extent of changes in ear canal morphology are relevant to a number of clinical and research situations.

1.4.1 During audiometry

Ventry, Chaiklin and Boyle (1961) reported that pressure produced by audiometer earphones on the pinna might result in the collapse of the external ear canal. He commented that jaw movements tend to pull the cartilaginous external canal forward and downwards, causing an increase in the patency of the canal.

Creston (1965) found that in ten cases of ear canal collapse during audiometry some patients appeared to have some narrowing of the orifice of the canal with a decrease in anterior posterior dimension. In other cases, the orifice of the canal seemed to be placed further anteriorly under the tragus than normal; and in some cases it was noted that slight pressure on the anti helix caused the concha to ride under the tragus, thus compromising the meatus. There was no sex, age or race predeliction for collapse of the canal. The condition was more often unilateral and there was a possible familial tendency.

1.4.2 Affects on the sound attenuation of earplugs

Smith et al (1980) found that a difference of only 0.5 mm between ear canal dimension and earplug size exerted a dramatic effect on the sound pressure level in the ear canal.

Abel et al (1990) found that individuals with straight canals achieved significantly higher attenuation scores than those with twisted canals. The cross-sectional area of the canal at the bone-cartilage junction, gender, type of ear-plug used and the ratio of the concho-meatal and bony-cartilaginous cross-sectional areas all had an effect on the level of sound attenuation achieved.

1.4.3 Development of acoustical model of the ear canal

Zemplenyl, Gilman and Dirks (1985) measured ear canal length in order to correct for errors in sound pressure level (SPL) measurements taken in the ear canal due to the specific location of the microphone probe tip in the ear canal.

Stinson and Lawton (1989) measured entire ear canal geometry in cadavers in order to improve the prediction of sound-pressure level distribution within ear canals.

1.4.4 The fitting and performance of hearing-aids

Morphological changes can give rise to :

1. Impression inaccuracies during impression taking,
2. Acoustic feedback during movement,
3. Occlusion effect during movement, and
4. Discomfort during mandibular function.

Pirzanski (1996) highlighted problems with the manufacture and fitting of CIC hearing-aids as a result of ear canal movements. He noted that this type of hearing-aid was particularly vulnerable to acoustic feedback related to jaw movements, and may slide completely out of the ear while the wearer was eating or speaking.

Skinner (1988) noted that venting an earmould helped to prevent the occlusion effect, that makes the bone-conducted sound of a person's own voice seem loud and hollow. Excessive venting can lead to feedback.

Movement may lead to changes in the amount of the air-gap between a hearing-aid and the adjacent skin surface. Therefore, movement in the ear canal associated with jaw movements can result in an alteration to the amount of acoustic seal or venting by an earmould leading to either in increase or decrease and acoustic feedback or the occlusion effect.

1.5 Anatomy of Ear and Associated Structures

Typically anatomical descriptions of the external ear divide it into the auricle (pinna) and external auditory meatus (ear canal) (Anson and Donaldson, 1967).

Developmentally, it would appear as though the auricle is derived from three tubercles, proliferation of mesoderm, at the dorsal end of the second (hyoid) pharyngeal arch. The tragus derives from three tubercles at the dorsal end of the first (mandibular) pharyngeal arch (Wood-Jones and I-Chuan, 1934).

Functionally it is more sensible to describe the external ear as consisting of all the cartilaginous elements that make up the external ear and the outer portion of the external auditory meatus. The cartilage elements of the auricle and the tragus unite without any trace of their separate origins. Their separate origins could contribute to variable relations.

In the fitting of hearing-aids and the wearing of earplugs it is usual for the earpiece to extend to the limits of the cartilaginous portion of the ear canal. Movement of the cartilaginous meatus relative to the bony meatus during mandibular and facial movements may result in the earpiece causing mechanical irritation to the skin overlying the bone at the bone-cartilage joint. However this is not universally the case and many patients are able to tolerate earpieces that extend beyond this point. For many hearing-aid users this is desirable for reasons related the frequency response of the hearing-aid (Skinner, 1988).

For the purposes of this discussion only the salient anatomical features will be highlighted. It is movement of the antero-inferior aspect of the cartilaginous canal relative to the concha that is of most interest. Elements of the cartilaginous ear and associated structures that are likely to impact upon and lead to movement will be considered.

1.5.1 Pinna

Structure. The pinna is invested on both its medial and lateral aspects by integument that closely follows the irregularities of the underlying cartilage. Thus it is tightly bound to the perichondrium of the lateral surface by subcutaneous areola tissue, but much more loosely attached on the medial surface. In the subcutaneous tissue there is little fat except in the lobule, which is entirely fat and tough fibrous tissue. Hairs are abundant but are for the most part rudimentary. Sebaceous glands are found on both surfaces; sudoriferous glands are few and scattered.

Ligaments. An anterior ligament extends from the spine of the helix and tragus to the zygomatic process, and a posterior ligament from the

eminence on the concha to the mastoid part of the temporal bone. A superior ligament runs from the superior margin of the bony external auditory meatus to the spine of the helix. (Fig. 3 and 4)

Muscles. There are three extrinsic muscles. The anterior auricular muscle arises from the temporal fascia and inserts into the spine of the helix. The superior auricular muscle arises from the galea aponeurotica and the temporal fascia and inserts into the root of the ear; and posterior auricular muscle arises from the mastoid process and inserts into the root of the ear. The extrinsic muscles are not normally used, but can be trained to move the external ear slightly; this power is greater in some people than in others.

Six intrinsic muscles can be distinguished. On the lateral surface there are four muscles: helicis major, helicis minor, tragus and antitragicus (Fig. 1.2). The pyramidal muscle of the auricle, which inserts into the spine of the helix, may be occasionally present.

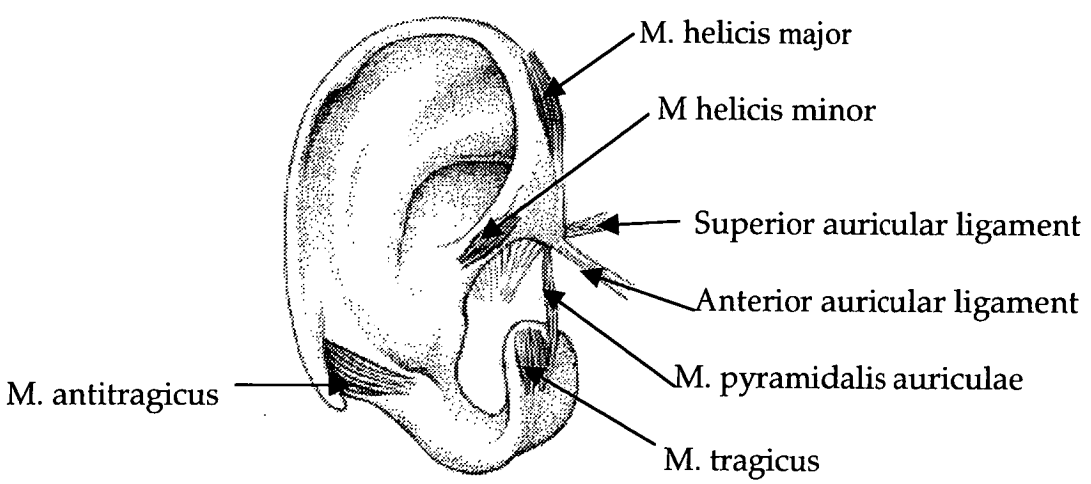

Fig. 1.2 Auricular Cartilage. Lateral view,
Source: modified from Feneis (1976).

Medially there are two muscles: oblique muscle of auricle and the transverse muscle (Fig. 1.3). A muscle of incisure of helix may be occasionally present as caudal continuation of the transverse muscle.

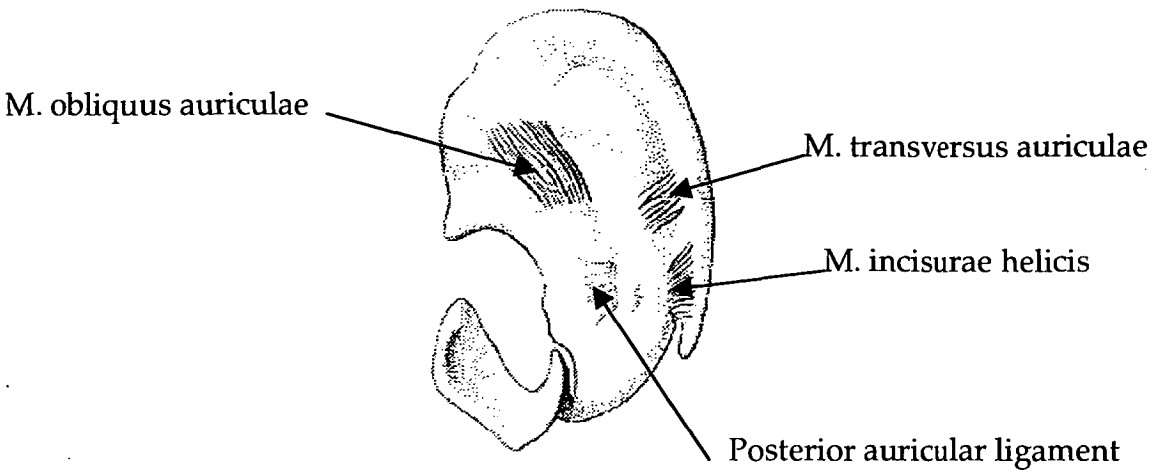

Fig. 1.3 Auricular Cartilage. Medial View,
Source: modified from Feneis (1976).

As with extrinsic muscles, the intrinsic muscles are not normally used, but can be trained to move parts of the external ear slightly; this power is greater in some people than in others.

1.5.2 The external auditory meatus

This passage leads from the lower part of the concha to the tympanic membrane. The cartilage of the meatus is a curved plate, which forms only the anterior and inferior walls, the remainder being fibrous tissue. Medially the cartilage and fibrous tissue are fused to the bony part of the meatus; laterally the cartilage is continuous with the tragus. The cartilage of the anterior wall contains two fissures filled with fibrous tissue, the incisurae cartilaginous meatus acustici (notches in cartilage of acoustic meatus) (Fig. 1.4).

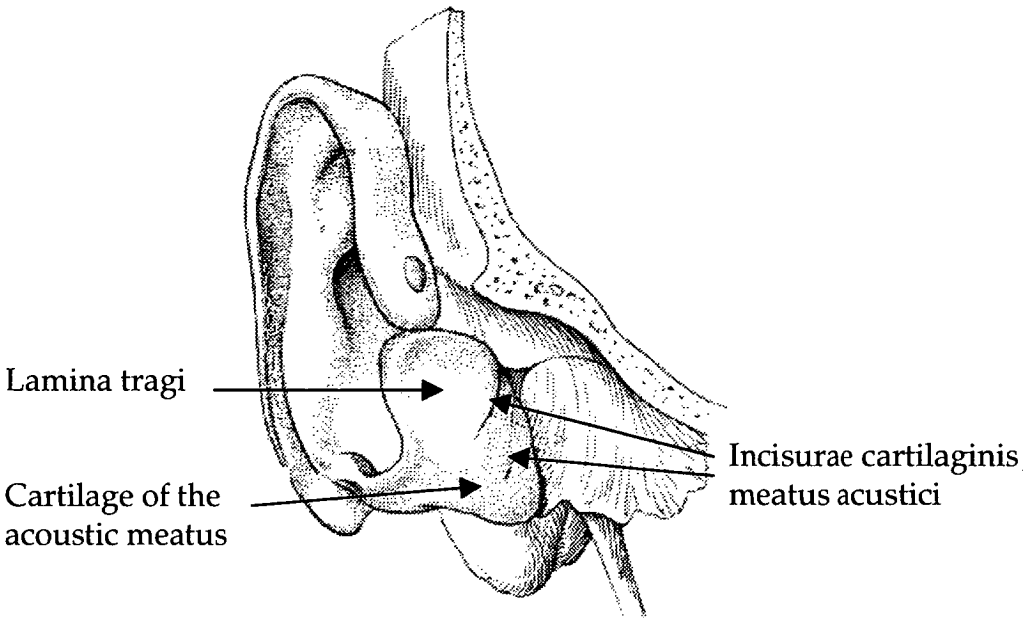

Fig. 1.4 Auricular Cartilage. Anterior view,
Source: modified from Feneis (1976).

The skin of the meatus covers the external surface of the tympanic membrane and is continuous with the skin of the auricle laterally. It is thick in the cartilaginous part where it carries fine hairs and sebaceous glands, the latter continuing along the postero-superior wall of the bony part. Numerous enlarged 'sweat' glands are found in the cartilaginous part. These secrete wax or cerumen and are known as ceruminous glands.

Relations. The anterior wall of the meatus is related to the mandibular fossa medially and the parotid gland laterally. The inferior wall is closely bound to the parotid gland.

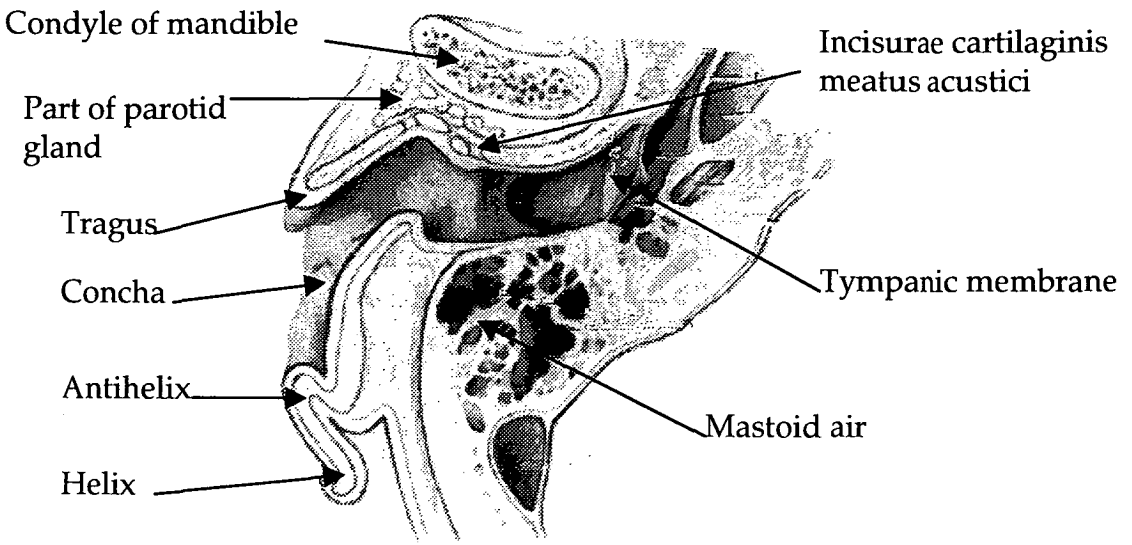

Fig. 1.5 Horizontal section through right ear canal. viewed from below, Source: Cunningham's Textbook of Anatomy (1972).

1.5.3 Movements of the external ear

It is assumed that for practical purposes the concha area does not deform during movements of the entire pinna and canal. This is based on published information reference texts, which show the absence of muscles within the concha area (Figs. 1.2 and 1.3). This assumption was tested during this study.

Reviewing Fig. 1.5 and simple observation suggests that as the condyle of the mandible moves forwards that portion of the tragus adjacent to the condyle may also move forward. At the same time the lateral portion of the tragus may be pulled anteriorly, or medially and possibly posteriorly. Flexion of the cartilage of the anterior wall of the canal would be likely to occur principally at the notches in the cartilage of the ear canal. The bend that occurs in the ear canal at this point is clearly defined in ear impressions as the first bend. When subsequent ear impressions are taken with the mouth closed and open, i.e. the condyle fully seated in the glenoid fossa or positioned anteriorly on the articular eminence, the firs bend in the impression becomes more clearly defined (Grenness 1990).

However, anterior movement of the tragus may not be an automatic consequence of anterior movement of the condyle. Wilkinson and Crowley (1994) conducted a histological study of the TMJ retrodiscal tissues in the open and closed jaw positions. They found that the upper stratum was folded on itself in the closed position and only became stretched near maximal opening. They concluded that the primary role of these components was to provide a volumetric compensatory

mechanism for pressure equilibration. Their study did not support the concept of an elastic upper stratum to the tissues that has a recoil mechanism to control TMJ disc movement.

The study by Wilkinson and Crowley (1994) leads to the conclusion that it cannot be automatically assumed that as the condyle moves forward it must take all that is behind it, with it.

In subjects where the M. pyraidalis auriculae is present, it is possible that the tragus may be pulled superiorly relative to the concha (Fig. 1.2). Movements of the pinna as a whole must also be considered. Should the pinna as a whole be pulled anteriorly at a greater rate than the anterior wall of the canal, the result would be a narrowing of the canal.

Neame (1988) presented a clinical case in which a 12-year-old girl was able to occlude her external auditory meatus voluntarily by 'flipping' her tragus backward, where it stayed until she actively moved it forward.

Van Willigan (1976) showed changes in ear canal shape and position relative to the position of the maxilla. He found that opening jaw movement caused an increase in volume of the ear canal. However an increase in volume does not equate with an increase in size in all dimensions.

Examination of the diagrams in Van Willigan (1976) clearly show that there is an increase in size in the inferior-superior dimension. At best, it is difficult to evaluate whether there is an increase or decrease in the antero-posterior dimension. Many of the diagrams in this paper suggest that there was a decrease in this dimension upon jaw opening.

That a decrease in the A-P dimension is possible could go some way to explaining the case of ear canal occlusion reported in 1.1 above. If the anterior wall of the canal is generally moving forward then a reduction in the A-P dimension can only be reasonably explained by a greater movement forward of the entire pinna, including the posterior wall of the canal. A study of movement of the canal relative to the pinna is therefore warranted.

1.6. Hearing-Aid Use

Hearing-aids consist of electronic circuitry with a microphone, receiver (speaker) and various volume and tone controls. These components may be contained in a housing that sits behind the ear and the sound is delivered to the ear canal via a tube that is held in the ear by an earmould. Alternatively the components may be housed within the earmould in the case of ITE, ITC and CIC hearing-aids.

1.6.1 Aim of hearing-aid fitting

The goals of hearing-aid fitting are to make speech and other important sounds comfortably loud in the frequency regions between 250 and 6000 Hz and to limit the maximum acoustic output so that the sounds are not uncomfortably loud (Skinner 1988).

Five factors that help determine the utility of hearing-aids (in order) are:

1. Improves speech audibility,
2. Cosmetic and psychological acceptance,
3. Comfortable to the ear,
4. Good sound quality, and
5. Maximum speech discrimination.

The importance of the third factor, that a hearing-aid must be comfortable or it won't be worn on a regular basis, almost goes without saying. "Anyone who has tried wearing a hearing aid with an ill-fitting ear-mould, for example, knows from personal experience that it almost can't be done"(Killion 1982).

1.6.2 Development of hearing-aids (Katz 1985)

Prior to 1955, body aids were essentially the only available wearable type of hearing-aid. These are usually worn under clothing on the chest with an earpiece passing to the ear. The distance between the microphone (at the chest) and the receiver output (at the ear) of the body aid reduced the possibility of acoustic feedback at higher output levels. Body aids came with a range of stock earpieces, the one of best fit being chosen. An effective acoustic seal was not required due to the large distance between the microphone and the receiver output.

The invention of the transistor led to the development of smaller BTE hearing-aids. The parallel development of hearing aid components, such as microphones, receivers, capacitors and integrated circuits contributed to today's hearing-aid technology. The BTE aids fit behind the pinna are rugged and easily serviceable. The output of the hearing-aid is delivered to the ear canal via a custom made earmould. Clinical

and laboratory techniques for the fabrication of these earmoulds were derived directly from dentistry.

The availability of very small, efficient electret microphones, correspondingly small receivers and further battery miniaturization has facilitated packaging the entire hearing-aid within the concha and ear canal: In-The-Ear (ITE) hearing-aids. The further development of circuits in which the input is phase-shifted such that the output is out of phase with the input has enabled greater amplification with less feedback. Most ITE aids are of the 'custom' type with the components built into a shell made from an impression of the user's ear. 'Modular' ITE aids are built into a case of fixed shape that fits into a matching depression in the custom ear-mould (Katz 1985).

More recently Completely-In-the-Canal (CIC) hearing aids have been developed to be inserted deeper into the ear canal with a handle to facilitate their removal. This type of hearing aids has proved to be particularly vulnerable to acoustic feedback related to jaw movements. In addition, when the wearer is speaking or eating, the CIC may continuously slide out of the ear (Pirzanski 1996).

Despite improvements in the electronic technology the fit and comfort of hearing-aids is still vital to successful fitting.

1.6.3 Acoustic feedback

Acoustic feedback either positive or negative occurs when amplified sound escapes via the ear-mould or the ear canal and arrives back at the hearing-aid microphone. When the escaping sound, after processing by the hearing-aid produces a level in the ear canal equal to or greater than the level generated by the leaking sound, oscillation can occur if the phase conditions are right. The result may be variously identified as whistling, squealing, buzzing, humming or howling.
There are three major possible effects of acoustic feedback:

1. Oscillation can occur, making the hearing aid useless,
2. The frequency response of the aid can be greatly altered, even if oscillation is not occurring, and
3. Major alterations in response e.g. the creation of sharp peaks as oscillation is approached. These sharp peaks result in poor transient characteristics or "ringing" when sounds are processed by the hearing-aid (Lybarger 1982).

The miniaturization of hearing-aids has also brought the microphone closer to the source of sound leakage. This, together with the advent of higher-powered hearing aids has resulted in acoustic feedback becoming a greater problem. Higher sound pressure levels increase the sound leakage from the receiver back to the external environment to be re-amplified by the hearing-aid circuit. Macrae (1988) reports that 10%

of the clients to whom the National Acoustic Laboratories (Australia) provides aids require high-powered hearing aids (2 cc coupler gains of 65 dB or greater).

Skinner (1988) lists ten means by which feedback can be prevented within certain unspecified limits.

1. Reducing size of or eliminating vents.
2. Damping resonant peaks.
3. Reducing the high frequency response.
4. Notch filters (Macrae 1982).
5. Using thick walled tubing.
6. Using soft instead of hard material for the ear-mould (or using a soft material with a hard body in the ear-mould).
7. Using dental liner material around the ear canal and concha surfaces of a Lucite ear-mould (pp270).
8. Increasing the length of the canal.
9. Improving the fit of the ear-mould, particularly in the region of the tragus.
10. Using the three-stage impression technique developed by Fifield.

Items 6 to 10 relate to different prosthetic aspects of the ear-mould, i.e. mould material, geometry (length and fit) and impression technique.

1.7 Hearing-aid Manufacture

Hearing-aid manufacture starts with the taking of an impression of the external concha region of the pinna and the ear canal as far medially as is required for the design of the aid. The impression is processed into a hollow shell for an ITE or CIC hearing-aid or an earmould of varying design for a BTE hearing-aid.

1.7.1 Impression technique

Typically a foam or cotton block attached to cotton thread is placed just beyond the point in the ear canal to be recorded by the impression. Impression material, either silicone based or ethyl methacrylate is syringed into the ear being careful to avoid voids in the material, not to distort the ear and to record the detail of the tissue surface (Juneau 1983, Morgan 1987).

There is differing opinion on the subject of mandibular position and movement during impression taking.

Boothroyd (1965) noted that the commonest cause of badly fitting earmoulds was imperfect impression technique on the part of the clinician. He reported that greater control of the extent of the

impression is obtained if it is built up in stages, using a suitable packing tool. No recommendation regarding mandibular position was made.

Babbington (1975) recommended that when taking ear impressions for hearing-aids, due to shape changes in the meatus during jaw movements, the patient should be placed in a comfortable sitting position and asked to relax. The teeth should not be clenched nor should the mouth be completely slack.

Sullivan (1975) states that "it is proper to make a precise, accurate fit rather than a tight, expanded one.... An impression taken with no consideration of the occlusion (of the ear orifice) and the ability of the ear to stretch can not give you true measurements to be used in the construction of an earmould".

Fifield, Earnshaw and Smither (1980) in describing the multi-stage impression technique made no recommendation concerning jaw movement or position during impression taking. They did recommend jaw movement while testing the effectiveness of the seal under pressure.

Morgan (1987) recommended that jaw movements be encouraged during taking of impressions. He stated that when impressions were made with natural movements occurring, the impression noted these changes. He provided no evidence for this statement. It would appear that the final shape of the impression would be achieved when the impression material had set to a sufficient extent to render further movement uncomfortable. Pirzanski (1996) commented that this view was still widely recommended in impression-taking manuals. Anecdotal evidence also suggests that this is a very commonly held clinical opinion.

Macrae (1989) reported that the chance of sealing the ear with ear-moulds made with the multistage impression technique was 88%. Ear-moulds that were lubricated and ear impressions that were 'patted down' produced hearing-aids with more feedback (more transmission loss).

Pirzanski (1996) stated that patients should be advised to open their mouth at least 2/3 of the way. Stabilizing the jaw with a mouth prop prevents accidental closure.

1.7.2 Impression materials

Ear impressions may be taken with a variety of impression materials of varying viscosities. Many of these are unsatisfactory for making ear-moulds for high-powered hearing-aids because of inadequate elastic properties and poor dimensional stability.

Lear and Earnshaw (1987) pointed out that most impression materials designed for the hearing-aid industry have a non-reacting oil added to the base paste. This allows the material to be mixed in the hands and provides good separation of the set impression from the relatively dry skin lining the ear canal. This also results in poor accuracy and poor dimensional stability. Lear and Earnshaw recommended dental addition-cured silicone elastomeric impression materials were dimensional stability and accuracy were required. (e.g. Reprosil, Dentsply/Caulk, USA).

Morgan (1987) also advocated the use of silicone impression materials over ethyl methacrylate, both, which seemed to be in wide use.

Despite the apparent importance of the impression material's physical properties Pirzanski (1996) concluded that the technique of impression taking might have a greater impact than the material used for fabricating earmoulds.

1.7.3 Impression modification

It is routine practice to apply a coating of wax or other polymer to the impression prior to processing. The purpose of the spacer is to:

1. Ensure that the finished ear-mould fits snuggly into the ear in order to prevent acoustic feedback,
2. Compensate for polymerization shrinkage of the mould during curing,
3. Eliminate surface defects and irregularities,
4. Provide a smooth tissue-fitting surface for hygiene and aesthetics, and
5. Compensate for surface material loss during polishing.

General wax build-up: A general wax build-up is applied to the entire surface of the impression by dipping the impression into a wax bath. The distribution and thickness of the wax varies depending on the temperature of the molten wax, the thermal capacity of the impression material, the length of time that the impression is left in the wax and the number of times that the impression is dipped (Boothroyd 1965).

Volatile acrylic cements may also been applied by dipping or with a fine brush to impressions to achieve a thinner coating of more uniform thickness (Pither 1988).

Special wax build-up: Wax may also be selectively applied to the impressions with a wax knife in the region of the tragus or the canal segment of the impression dipped. The purpose of this practice is to allow the processed earmould to apply positive pressure to the fitting surface of the ear resulting in a 'snug' fit. The placement of the amount

and location of this special wax build-up can best be defined as an art. There are no formal guidelines as to how this should be applied. Technicians learn the art through experience. The amount of build-up may be varied according to the amplification of the hearing-aid.

Macrae (1989) supported applying special wax build-up to impressions in a review of ear impression and ear-mould technology. He reported that applying special wax build-up eliminated feedback in all but 6% of adults who use high-powered post-auricular hearing aids.

1.7.4 Earmould/Shell manufacture

Earmoulds may be made directly in the ear using self-curing acrylics or silicones. They are more commonly made indirectly by making a replica of the ear from an impression. The earmould is then made into the replica.

Many articles have addressed the subject of ear anatomy, ear impression materials and technique and mould manufacture (e.g. Sullivan 1975, Juneau 1983, Fifield, Earnshaw and Smither 1980).

Earmoulds are made from either rigid or flexible materials. Impressions are invested with a variety of materials e.g. dental duplicating media (agar agar) or gypsum products. When the impression is removed from the investment a negative mould space is left into which is packed the ear-mould material, which is then cured or processed. The cured mould is removed from the investment and finished with the placement of a tubing hole, ventilation hole if required, shaping of the mould as is required by the case and the finishing and polishing of the tissue fitting surface. Hearing-aids have electronic components inserted after the shell has been fabricated. Highly polishing the tissue fitting surface results in some loss of material and alteration in the fit of the earmould.

1.8 A Clinical Problem

Macrae (1989) recommended further study into the distribution of the build-up that occurs to multi-stage impressions to give guidelines for the application of special wax build-ups. Taking a further step back, there appears to be limited information available on the morphological changes that can occur in human ear canals or the potential for displacement of tissue.

Furthermore this practice appears to be successful in reducing feedback, however it is fraught with danger as is illustrated by the following case (Grenness 1990):

A long-term hearing-aid user attended an Audiologist complaining of feedback. It was confirmed that the feedback was caused by sound leakage past an ill-fitting earmould. An impression was taken and a new mould ordered from the manufacturer. Upon fitting, the hearing-aid still feedback excessively. A further impression was taken. The laboratory took additional care in applying a special wax build-up to the tragus region of the ear impression, and processed the mould. This was successful in alleviating the feedback problem. The patient returned twelve months later again complaining of feedback. A new mould was ordered and the problem eliminated. A further six months later the patient returned with feedback and a new mould was made. The cycle was then repeated three months later, then every four to five weeks. Finally an earmould could not be made that did not feedback. In addition the patient was now experiencing temporo-mandibular joint pain dysfunction syndrome. It was not determined how long this occurred for and a thorough examination was not undertaken to reveal the extent of the problem. However it was a significant problem to the patient.

The practice of applying positive pressure to the tissue bearing areas of an ear canal is not without consequence. It has been shown that the ear canals of hearing-aid users are of a larger cross-sectional area than non-users (Kokot-Schimdt 1979). This is readily evident to any practicing clinician. It could be expected that displacement of tissue for long periods will induce permanent changes, either atrophy or hypertrophy. In the case of ear canals, atrophy of dermal, subcutaneous, cartilage and/or bone tissue elements results in an enlargement of the ear canal.

The use of general wax build-up dates back to at least the early '70's. The use of special wax build-up dates back about 16 years. As the years pass and more and more patients are aggressively treated using these techniques there may be a large pool of patients who are entering a stage where their ear canals cannot be expanded further to achieve the desired aim of feedback reduction.

Current methodologies may not be adequate in all cases. This case was ultimately resolved (at least to date) by taking a medium-viscosity silicone impression of the ear canal with the patient's mouth open (open-jaw impression). No wax build-up either general or special was applied to the impression prior to processing. Why this should be the case is not immediately obvious. Other similar cases have been assisted with patients adopting a variety of postures, e.g. with head between the knees.

1.9 Aim

The purpose of this investigation was to study:

1. Movement of the tragus/canal region of the ear canal relative to the concha area in order to demonstrate the range and direction of movement and determine whether the narrowing of the canal does occur.
2. Movement within the concha region of the ear in order to demonstrate whether this region undergoes deformation.
3. Movement within the tragus/canal region of the ear in order to demonstrate the range of deformation.
4. Precision/Accuracy of the measuring system

Chapter 2 – Method

2.1 Overview

Pairs of open-jaw and closed-jaw ear impressions were taken of patients. Subject selection was not intended to be representative of any group or the population as a whole. Practical issues relating to collecting data and developing a successful method of analysis limited the sample size. The sample size was intended to be large enough to draw conclusions about the range and extent of movement. It was not expected that conclusions could be drawn about specific groups of subjects.

The concha and the anterior surface of the tragus/canal regions of the impressions were mapped separately using a Reflex microscope.

The resultant 3D coordinate data was manipulated:

1. Transposition of coordinates plotted via a mirror using Cartesian Geometry (Parslow, 1994) so that concha and tragus/canal fields were in their correct spatial relationship and in the same coordinate system.
2. Alignment of the concha region of impression pairs using proprietary area-matching software, DS Match, utilizing a least-squares solution (H. Mitchell, version 23, 1995).
3. Application of transformation parameters from area-matching using seven parameter similarity transformation equations (Harvey 1995) to tragus/canal regions

This resulted in the tragus/canal fields from impression pairs being in the same coordinate system with their respective concha fields coincident.

The manipulated data was analyzed:

1. The area-matching software applied to the paired concha fields was used to evaluate distortion within the concha region that may have occurred as a result of opening the mouth.
2. The area-matching software was applied to the paired tragus/canal fields to evaluate distortion within the tragus region that may have occurred as a result of opening the mouth.
3. Analysis and Visualisation software, Surfer (Golden Software, version 6.04, 1997) was applied to the paired tragus/canal fields to evaluate movement in the tragus/canal region relative to the concha as a result of opening the mouth.

Statistical analysis was performed on data collected to determine the accuracy and precision of the recording system and error in the manipulated data.

Flow Chart:

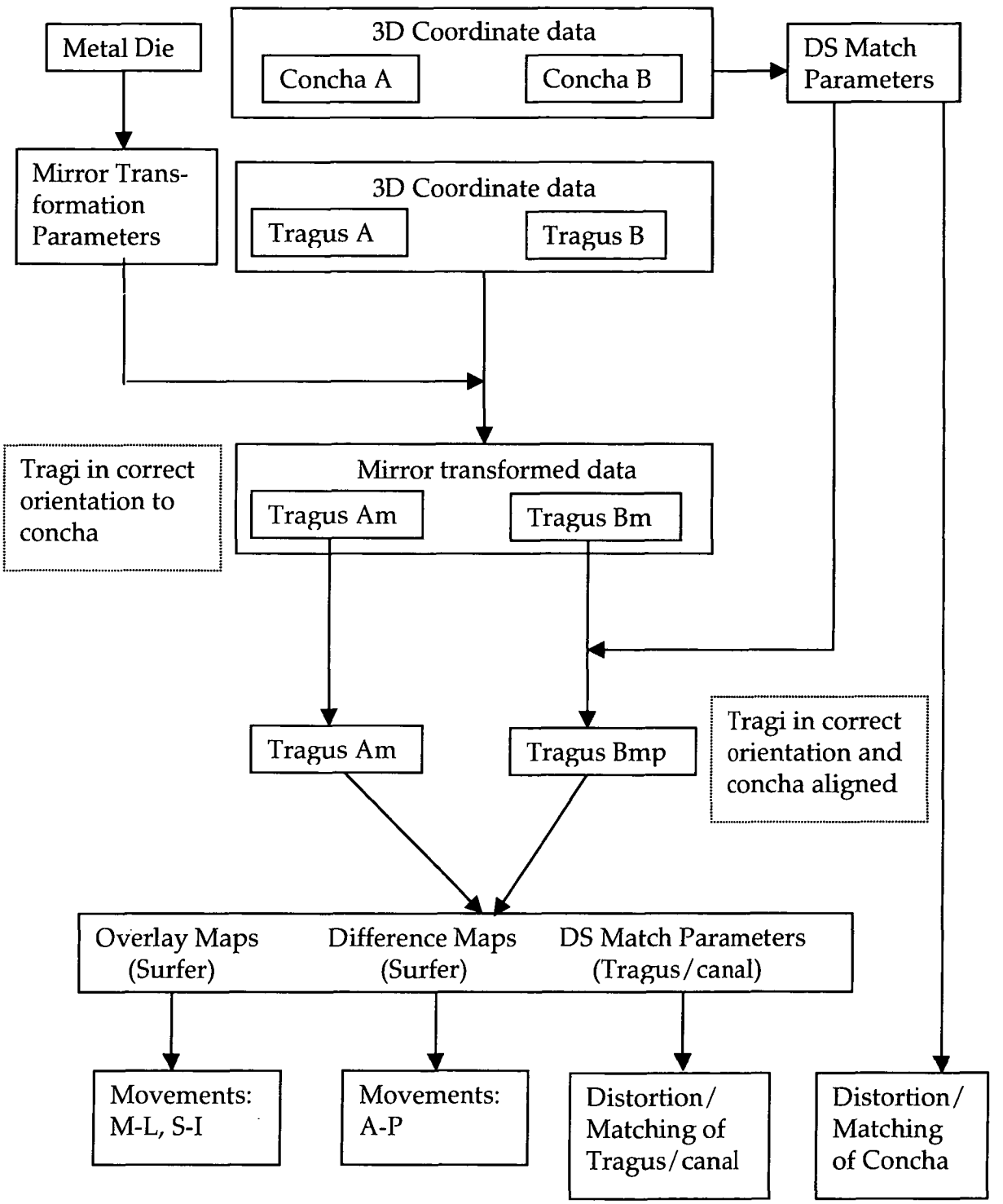
Metal Die
3D Coordinate data
Concha A
Concha B
DS Match Parameters
Mirror Trans-formation Parameters
3D Coordinate data
Tragus A
Tragus B
Tragi in correct orientation to concha
Mirror transformed data
Tragus Am
Tragus Bm
Tragus Am
Tragus Bmp
Tragi in correct orientation and concha aligned
Overlay Maps (Surfer)
Difference Maps (Surfer)
DS Match Parameters (Tragus/canal)
Movements: M-L, S-I
Movements: A-P
Distortion/ Matching of Tragus/canal
Distortion/ Matching of Concha

2.2 Previous Investigations

Ear canal geometry has been measured using a variety of means.

Boothroyd (1965) measured moulds at two convenient places with a micrometer screw gauge and the results compared with the corresponding dimensions of the ear. Sufficient data was not published to determine the accuracy of the method.

Van Willigan (1976) compared sections of ear impressions that were sectioned at depth of 6, 8, 10, and 12 mm from the ear opening. Sections were compared with each other by photographing them and projecting the negatives on top of each other. No measurements were taken but the changes in morphology were represented visually.

Smith et al (1980) used ear canal calibrators in 8 different sizes ranging from 5 through to 12 mm in diameter to measure the major and minor axes on the canal. Each of the calibrators was measured with precision calipers prior to the investigation and found to be accurate in size.

McHugh and Purnish (1984) used a caliper to measure the diameter of cylinders of set impression material to the nearest 0.1 mm.

Zemplenyl, Gilman and Dirks (1985) used an operating microscope (Zeiss OPMI, with 250 mm focal length objective lens whose depth of focus was less than 1 mm) to focus on the umbo of the eardrum. The microscope was then refocused on a point at the end of an earpiece in the ear canal. The difference between the two points was determined by measuring the distance that the microscope head traveled along its track. This distance was measured with calipers. In no individual did the repeated ear canal measurement differ by more than +/- 1mm.

Kamel, Kunov and Abel (1986) reproduced standard ear impressions in polymethyl-methacrylate. The reproduced mould was encased in a mixture of polyester resin, hardener and talcum powder; the encasement included notches to act as fiducials and to facilitate the alignment of the sections later during digitization. The mould was sectioned, destroying 1mm thickness of the mould with each slice. The sections were photographed and a computer system was used to digitize the serial sections.

Lear and Earnshaw (1987) tested various impression materials according to International Standard ISO 4832 (1984). Elastic recovery after compression was measured using a dial gauge comparator to an accuracy of 0.01 mm. Dimensional accuracy and dimensional stability of impressions of a steel block bearing engraved markings were measured using a travelling microscope (toolmakers microscope) with an accuracy of +/- 1 mm.

Macrae (1988) measured impressions and earmoulds using a Sylvac digital caliper with reported resolution of 0.01 mm, accuracy was 0.03 mm and repeatability of measurements of 0.01 mm. All measurements were carried out under binocular x2 magnification. Each measurement was repeated three times and the mean of the three values was taken as the estimate of the true value. Five dimensions of each object were measured:

Major axis (long axis) at the meatal entrance,
Minor axis (Short axis) at the meatal entrance,
Meatal length,
Major axis at the meatal tip, and
Minor axis at the meatal tip.

In order to assess the repeatability of measurements carried out with the digital caliper each of the five dimensions of a single impression was measured 100 times. The average standard deviation from the mean values was 0.1032 mm.

Stinson and Lawton (1989) obtained rubber moulds with a setting time of 20 minutes from human cadavers. Each earmould was orientated with the canal pointing vertically on a turntable. A probe was mounted horizontally on a three-axis movement micrometer. X, y and z data from the probe was combined with angle data from the turntable to produce x, y, z, coordinate data. Approx. 100 points were collected over the surface along the canal. Accuracy was reported at about 0.03 mm. This study was conducted for the purpose of measuring ear canal volume.

Abel et al (1990) measured impressions using calipers to measure the maximum and minimum diameters at the concho-meatal angle and the cartilaginous-bony angle. "Because there were no fiducial points on the canals from which measurements could be taken, there was no guarantee that the measurements of these diameters could be faithfully reproduced". Accuracy on repeated measurement was 1 mm.

Oliveira et al (1992) used silicone ear impressions and a digital caliper on one subject to measure the effect of jaw position and magnetic resonance imaging to define the three-dimensional structure of the canal and visualize key underlying tissues.

Egolf at al (1993) used a computer assisted tomographic (CT) scanner in two steps to make radiographic images of parasagittal cross sections at uniform levels along the length of the canal. Accuracy was evaluated by comparing areas of cross sections appearing in radiographic images of a cadaver ear canal to cross sectional areas of the corresponding microtome slices of an injection mould of the same canal. The reported accuracy of 9.65% differences between the radiographic images and the

mould of the same canal. This equates to accuracy in the order of +/- 1 mm.

Pirzanski (1996) demonstrated changes in canal morphology by placing a closed-jaw impression into the bisected open-jaw impression reverse. Hollow spaces were seen between the closed-jaw impression and the bisected investments prepared from the open-jaw impressions. The method demonstrated gross qualitative change. No quantitative measurements were recorded.

Malard et al (1997) found that CT scan measurements in the lateral portion of the external ear canal were not reliable, quantitative usefulness being limited to the bony meatus.

Oliveira (1997) reported on volumetric changes in the ear canal, using MRI upon an ear canal filled with an MRI enhancer fluid to enable imaging of the of the canal space itself.

None of these methods provide reliable quantitative data on ear canal movement relative to the concha region of the pinna.

2.3 Ear Measurement

In order to quantify changes in morphology of the surface in the external (third) ear canal relative to the concha area during functional movements of associated structures it was necessary to map the surface features of the canal and concha region in three dimensions (3D).

2.3.1 Subjects

Ear impressions were taken of patients attending the Tasmanian Centre for Hearing, Hobart, for new or replacement hearing-aids, and staff. Subjects were selected on an ad hoc basis to provide:

1. Male and female subjects,
2. A wide age range,
3. Known hearing-aid fitting difficulty,
4. Existing hearing-aid users, and
5. Non hearing-aid users.

Subject selection was not intended to be representative of any group or the population as a whole.

2.3.2 Sample size

Practical issues relating to collecting data and developing a successful method of analysis limited the sample size. The sample size was intended to be large enough to draw conclusions about the range and extent of movement. It was not expected that conclusion could be drawn about specific groups of subjects.

2.3.3 Ethics approval and consent

Ethics approval was sought and approved by the University Ethics Committee (Human Experimentation), University of Tasmania.

A consent form was drafted outlining the aim of the project, the subject's involvement and material risks, and included a no disadvantage clause.

2.3.4 Confidentiality

Once taken, impressions were numbered. A secure register was maintained to record relevant patient details and impression identifying numbers. Impressions were stored in hard plastic containers with only their identifying number in the lid. The identifying number was used as the reference for all subsequent analysis stages.

2.3.5 Ear impression

The starting point for 3D reconstruction of the canal was an impression of the ear canal and concha in an elastomeric (dental) impression material. This relates to the clinical situation where earmoulds/shells for hearing aids are fabricated starting with an impression of the ear (concha and external third of canal down to the bone-cartilage joint). The material used for this investigation was a medium viscosity condensation silicone dental impression material (Xantopren H (green), Heraeus/Kulzer, Germany). This material has been in use at the Tasmanian Centre for Hearing for many years. It gives good surface detail without being so fine that it is likely to cause significant trauma to the lining epidermis upon removal. The manufacturer reports recovery from deformation equal to or greater than 98.0 % and linear dimensional change of equal to or less than –0.90 %.

Ear impressions were taken with the jaw in either the 'closed' or 'open' position as described by Pirzanski (1996). The subject was seated upright looking forward. A small sponge was inserted in the subject's ear to prevent penetration of the impression material to the eardrum. In the case of 'closed-jaw' impressions the patient was asked to sit still but not given any specific instruction regarding jaw position. In the case of 'open-jaw' impressions, the patient was asked to open their mouth and a bite block, 30mm thick, was inserted between the upper and lower incisor teeth. The impression material was syringed into the canal and concha areas of the pinna. The impression was allowed to set for 8 minutes and then removed carefully from the ear (Fig. 2.1). The impression was then examined for surface flaws and defects (bubbles, stretch marks, and tears) and repeated if necessary. The impression was labeled, wrapped in cotton wool and placed into a specimen jar.

Open and closed-jaw impressions of the same ear were taken immediately after each other. Thus a pair of impressions was obtained from each ear.

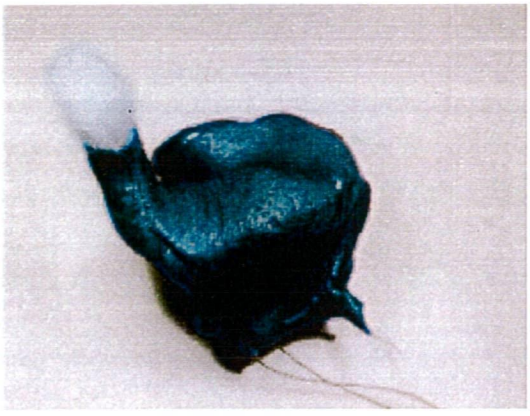

Fig. 2.1 Ear impression, cotton block in place

2.3.6 Measurement systems

The ear canal is relatively inaccessible to measuring instruments. In practice it is not practical to measure an ear canal directly. One must rely on an indirect method. A number of systems reported from past investigations were considered for this task. They can be separated into:

1. Contact,
2. Non-contact

A replica of an ear canal may be more able to tolerate a mechanical contact system, but is also not suitable for measurement due to its inaccessibility. Thus either a direct impression of the ear using an elastomeric material must be used or a replica of that impression fabricated from a more rigid material. A rigid replica was required for mechanical measuring systems to prevent distortion of the direct impression during measurement. However the additional manufacturing stages involved in producing an impression replica result in distortion of the replica when compared to the original impression.

Due to the elasticity of impression materials it was necessary to use a non-contact measuring system. Non contact systems include stereo-photogrammetry, confocal imaging and reflex plotting. More recently laser-plotting systems have become available. In this study a reflex microscope was used to map the impressions.

2.3.7 Three-dimensional measuring instrument – Reflex microscope

The Standard Reflex microscope is a non-contacting instrument enabling direct measurement in 3D of small objects (up to 110 mm) which can lead to 3D computer representations. The observer views the object through an ordinary stereoscopic microscope. A small light spot appears in the field of view, and it can be guided to coincide with desired points on the surface. The x, y and z coordinates are monitored by Moiré fringe encoders, and the counting interface passes the position on request to a computer through an RS232 link.

The object is carried on a conventional two-dimensional (x, y-axis) slide. The slide was first translated to give the observer a view of the point to be measured. This is done either by a track ball or computer program. The microscope, mirror and measuring spot are carried on a vertical (z-axis) slide, and the observer translates the microscope using stereoscopic vision to judge the height coincidence of the light spot with the object point. The vertical slide was moved via a finger slide. Multiple views of an object can be recorded and combined where there are common points to each view.

The microscope magnification is selectable as x 5, x 10, and x 20. Accuracy and precision of measurements is dependent upon the visual acuity of the operator. The measuring mark may have a diameter of 20 μm, 10 μm, and 5 μm. A full description and explanation of the reflex principle, the Reflex microscope, and examples of its application may be found in a paper by Scott (1981).

The Reflex microscope has also been used to: measure the dimensions of the glenoid fossa (Owen, Wilding and Adams 1992), measure areas of dental caries in teeth (Neilson and Pitt, 1993), measure the cement thickness of porcelain crowns (Shearer, Gough and Setchell 1996), measured tooth morphology and wear in two small animals (Bezels and Sanson, 1997), measure tooth movement on sequential casts during orthodontic treatment (Battle and Ryan, 1998), and measure palatal clefts defects (Owman-Moll, Katsaros and Friede 1998).

2.3.8 Accuracy and precision of the Reflex microscope

Accuracy and precision is limited by the design of the instrument, but is also dependent on the operator.

Accuracy is a measure of the closeness of an observation to its true value. If the observational errors are normally distributed and free from systematic error then the mean of a set of observations can be used as the best estimate of the true value. When a true value is not known then it is necessary to use measures of precision, and demonstrate that the

observations are free of systematic errors (or that any systematic errors will not influence the results or conclusions).

Speculand, Butcher and Stephens (1988) reported on the accuracy and precision of the reflex microscope. They found a mean under-measurement of 0.28%, i.e. 0.14 mm per 50 mm. They found no systematic error between the three microscope lenses. They also found that increased magnification does not necessarily confer greater accuracy. The explanation for this was concerned with point identification being a matter of 'decision' and not 'vision'. It is necessary to choose the degree of magnification most appropriate to the size of the object.

The microscope was calibrated according to the manufacturer's instruction. All measurements were taken using x20 magnification and the 20 μm measuring spot.

Analysis of coordinate data (section 2.6) involved the subtraction of paired datasets to produce difference data. Systematic error affecting one dataset would affect its pair in the same way. Thus any small systematic errors are likely to cancel rather than accumulate.

Precision is a measure of the repeatability of the measurements. It is indicated by the standard deviation of the recorded values from their mean value. Evaluation of precision was an important function when performing analysis and drawing conclusions from datasets that which involved several measurements and which had undergone several mathematical manipulations.

All impressions were plotted as ordered-grids (section 2.4.3) and the precision of recordings was determined by the instrument. Precision in the x and y-axes was determined by the precision of the Moiré fringe encoders, reported by the manufacturer as 1μm.

Precision of z-axis values
The precision of the reflex system (including operator error) z-axis values was tested by scanning the same profile (30 points) 14 times on a single ear impression. Points were collected using a ordered-grid routine. The data was placed into a spreadsheet consisting of 14 columns, each column representing a profile. The mean value for each point was calculated. The standard deviation from the mean of the 30 coordinates was then calculated. The mean of the standard deviations was calculated. This was taken as the average precision of the z-axis measurements.

2.4 Ear Impression Plotting

The areas to be plotted, the anterior surface of the tragus/canal and the concha, were at near right angles. They could not be viewed directly from the same direction, as the microscope required. A fixed mirror was required to optically transpose the tragus/canal into the same plane as the concha. Determination of the parameters of that transposition allowed the placement of the tragus/canal into the correct spatial relationship with its corresponding concha.

2.4.1Design of object mount

The object mount consisted of a brass mounting plate 120mm x 120mm with a platform 25 mm x 25 mm raised 10 mm above the base. The platform had two deep grooves and locating holes engraved into its surface. The ear impression was seated on the raised platform with the concha region approximately horizontal and the tragus/canal region pointing vertically. Adjacent to the platform was a 50 mm diameter optical flat mirror, lambda 4, set at approx. 45 degrees to the platform (Fig. 2.2).

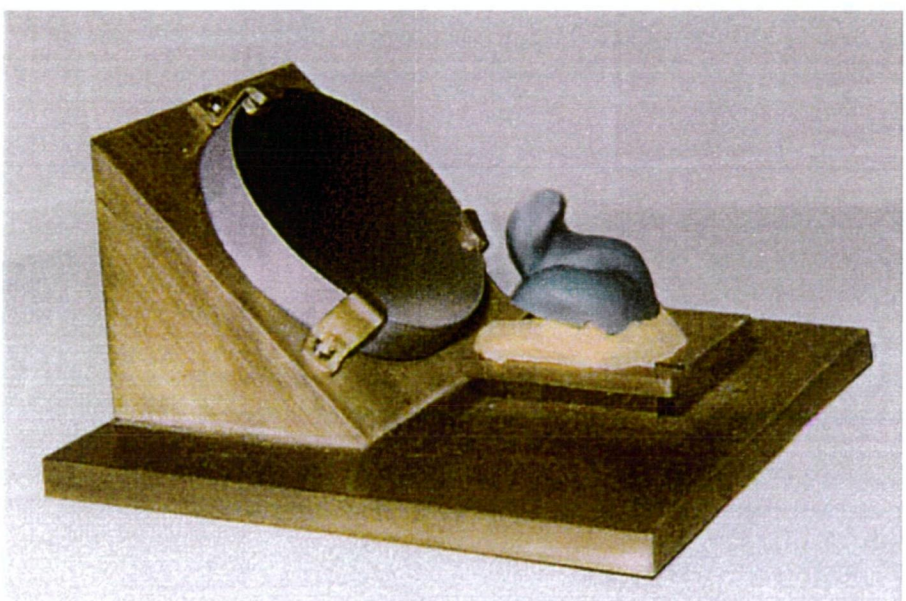

Fig. 2.2 Object mount with impression and mirror in place.

Plotting coordinates via the mirror increased the optical distance from the microscope to the object. The surface plotted through the mirror appeared to be below the base of the microscope stage, beyond the recording range of the instrument. As a result the specimen mount was raised by approximately the distance from the object to the mirror (4 cm). The object mount and 4 cm block were fastened securely to the microscope stage with toolmakers clamps.

When viewed through the microscope, the concha region could be seen directly. The anterior surface of the tragus/canal could be seen through the mirror. The two areas were moved into the viewing range of the microscope by the x, y slide (Fig. 2.3).

2.4.2 Alignment and securing of object

A system of aligning and securing the impressions to the mount was required to allow for the alignment of the concha of both impressions from each impression pair into approximately the same position. Subsequent area-based matching of the concha fields was more reliable when the fields to be matched with already in close alignment.

1. Trimming the impression: The lateral surface of each impression was cut to a plane with a scalpel. Deep locating notches were then cut into this plane.
2. First impression base: The object platform, described above, had a dollop of polyether (Permadyne, Espe, Germany) elastomeric impression material (coloured purple or pink) placed onto it. While the material was still workable, one impression from each pair was seated into the polyether with the canal part of the impression pointing vertically. A minimum thickness of 2mm of polyether was maintained. Thus an impression base consisted of a surface with large ridges to fit into the base of the impression, and a surface with two small ridges and plugs to fit onto the platform.
3. Register: The polyether impression base was trimmed flush with the edges of the brass platform. The platform, polyether and impression were boxed with dental modeling wax. Bite registration material (Automix Bite Registration material, 3M, USA) was injected into the wax box, around the ear impression to create a register. The tragus region of the impression was not covered. The wax box was carefully loosened. The register and impression were removed. The other impression from the impression pair was fitted to the register and together with the wax box re-fitted around the platform.
4. Second impression base: Different coloured polyether (either pink or purple) was injected into the space between the impression and the platform and allowed to set. Each impression pair consisted of two impressions with two differently coloured bases, allowing for remounting of impressions.
6. Identification: Impression pairs were placed into separate boxes with identifying numbers.

The horizontal plane correlated to the mid-sagittal plane of the human body. The x-axis was close to the A-P direction. The y-axis was close to

the S-I direction. The z-axis was close to the medio-lateral (M-P) direction

2.4.3 Collection of 3D coordinate data from impressions

The microscope had a number of recording routines that could be used to aid in the collection and recording of data of which two were used: free-format and ordered-grid.

Free-format. The measuring mark was moved to any desired point using the track ball to move the x, y stage, and the finger wheel to move the measuring mark onto the surface of the object (z coordinate). A foot switch was pressed to record the x, y, z coordinates of the mark, as monitored by the moiré fringe encoders. Accuracy and precision of each x, y, and z value was dependent upon the operator.

Ordered-grid, with parallel profiles in y direction. Parameters were set for x and y-axis intervals. The measuring mark was moved to the southern, left-hand point of the field. Activation of the foot switch moved the mark to the next predetermined x, y location. The finger wheel was used to adjust the z position of the mark. The foot switch was pressed, the coordinates of the mark were recorded and the step motors moved the stage to the next point. Accuracy and precision of the x and y values was determined by the instrument, and the z value was dependent upon the operator.

The ordered-grid routine recorded the first coordinate of each routine as 0,0,0. The x and y-axis values were changed as the x, y slide moved to the next predetermined point. In order to place multiple fields from the same object into the same coordinate system it was necessary to record the x, y, z coordinates of the mark, as displayed on the monitor, which coincided with 0,0,0.

Coordinate data was collected from two fields on each impression:

1. The anterior surface the tragus/canal was plotted via the mirror, and
2. The concha region was plotted directly.

Each field was plotted using a separate free-format routine. Several separate measurement files were used to collect data points on some fields. Coordinate data was recorded as ASCII files of x, y and z columns of numbers. Fields were plotted on a 1000 μm x 1000 μm grid, with points along the edge of the southern border of object recorded every 500 μm (Fig. 2.3).

Concha fields ranged between 9 to 12 mm in the x-axis (Antero - posterior) and 20 to 30 mm in the y-axis (superior – inferior).
Tragus/canal fields ranged between 9 to 20 mm in the x-axis (medial – lateral) and 10 to 19 mm in the y-axis (superior – inferior).

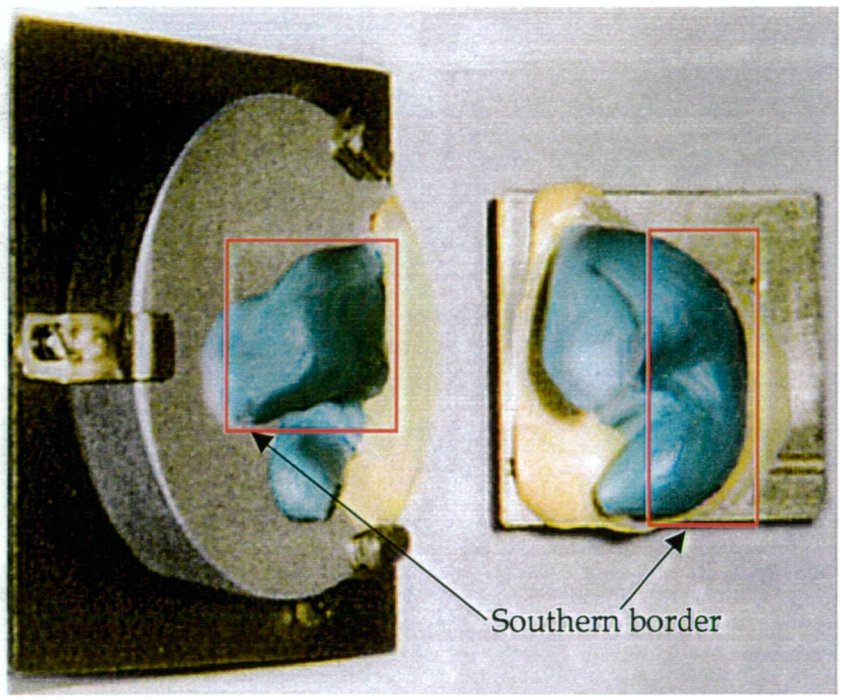

Fig. 2.3 Object mount, viewed from above, showing concha field (right) and tragus/canal field (left).

2.5 Data Manipulation

2.5.1 Determination of mirror transformation

In order to transform coordinate data recorded as a mirror image into a direct image it was necessary to derive transformation parameters from common points that could be viewed directly and through the mirror. No such common points existed on ear impressions due to their morphology.

A brass triangular block was fabricated with a square base and a square plane set at approx. 45° to the horizontal. The sloping surface of the triangle was scored with numbers fine grid lines. The brass block was placed on the mount so that the grid lines could be viewed through the microscope directly and through the mirror. At the beginning of each measurement session, between 18 and 30 common points were plotted using a free-format routine. The coordinates were used as inputs to

equations based on Cartesian geometry to derive unit vectors and a constant (Parslow 1994).

The final equation followed the general form:

$Xr = X - (b)\ (xi)$ where X was the direct coordinate
Xr was the mirror image coordinate
b was a constant derived from the coordinates
xi was the unit vector.

A full explanation and the equations appears in Appendix 1.

The unit vectors and constant were used to calculate coordinates in the direct plane from the tragus/canal coordinates plotted via the mirror. This resulted in the tragus/canal fields being in the correct spatial relationship with their respective conchae.

2.5.2 Alignment of coordinate data from concha fields

To achieve the aim of measuring movement in the ear canal relative to the concha region it was necessary to precisely align the surface plots of the concha fields of each impression pair. Care was taken in the alignment of the impressions during the mounting procedure. However the precision of the alignment can be further enhanced by using computer software to match the coordinate data from the fields to be matched. Two methods were explored:

Feature-based matching: This involves the detection of distinct features in an image, the description of these features in mathematical terms and a decision as to whether two descriptions refer to the same element in the data being matched. In image matching, feature-based methods are usually faster, more reliable (less susceptible to gross error i.e. mismatches), and is likely to find a match with poor a priori orientation values (Fryer, McIntosh and Oh, 1998).

In this case skin pores were readily identifiable on individual impressions. Attempts to identify common pores on impression pairs failed. Attempts to mark suspected common points were unsuccessful.

Area-based matching: This involves finding the orientation of best correlation between corresponding fields in images that are being matched. In image matching, this method is usually more precise than feature-based matching (Fryer, McIntosh. and Oh 1998), but may not be as reliable as feature-based matching because it is more likely to match areas that do not correspond. (This is discussed below).

The concha fields were area-matched using proprietary software: DS Match (version 23, H Mitchell, 1995). This program triangulated the data points to produce common grid-nodes for both datasets. It subtracted the z-axis values of one surface from the other to produce

difference or residual data, and used an iteration process to shift the two surfaces. The parameters resulting from each iteration were used as inputs for the next iteration. The iteration process converged to a solution by minimizing the differences between the two surfaces. Iteration stopped when the differences were less than a specified amount. The version of software used accepted convergence when the most recent corrections to all unknowns, i.e. rotation and translation parameters, were less than +/- 0.00001. When convergence occurred, the mean of the differences (residuals) between the two surfaces was 0.000000. The root mean square (RMS) of the residuals gave a measure of the coincidence of the two surfaces.

Reflex microscope recordings were in microns. Data files were adjusted to millimeters so that convergence was accepted when the last correction to the translation parameters was .01 μm and the last correction to the rotations was 0.00001 decimal degrees.

DS Match required a 'threshold for exclusion of points', in addition to the two input files to be matched. This enabled the exclusion of points where the fields did not overlap and of points that were grossly divergent from the rest of the field, either through error or gross distortion of the surface. The solution was affected by the choice of threshold limit. Threshold limits of 100, 200, 300 and 400 μm were run for both concha field matching and tragus field matching.

DS Match allowed for the number of parameters used in the matching process to be varied from 2 to 6. It allowed the input of starting parameter values. The program ran for 8 iterations before displaying the parameters that resulted from the last iteration, the size of the last correction and the number of equation included in the solution. At this point the solution could be accepted, dropped, or the data reiterated with 3, 4 or 6 parameters. Even if the surfaces had converged (according to the criteria of the program) the iteration process could be restarted using the last set of transformation parameters as the starting values for the next iteration.

The DS Match output file included the standard deviations of the parameters. These statistics could be influenced by close but incorrect fits, and so indicated the closeness of the fit, not the validity of the criteria used, i.e. threshold for the exclusion of points and size of last correction.

The results of area-based matching the concha field were used to re-orientate the data from impression pairs with their concha co-incident.

2.5.3 Application of transformation parameters to tragus/canal field.

The transformation parameters to match the second concha field to the first were applied to the corresponding second tragus/canal field. This was done using Bursa-Wolf seven parameter similarity transformation equations (Harvey 1995).

In this way the surface maps of the two tragus fields from open and closed jaw impressions from the same ear of the same patient were now aligned in the same coordinate system, with their respective concha regions aligned. The spatial relationship of the tragus/canal fields to each other, i.e. the movement that had occurred between the taking of open and closed jaw impressions was now available for comparison.

2.6 Data Analysis

2.6.1 Movement within the concha

Area-matching software was applied to the concha datasets of open and closed-jaw impressions. The resultant transformation parameters (section 2.5.3) were used to align the data sets of each impression pair.

Statistics derived from the matching process were used to evaluate the changes that occurred in the concha upon opening the mouth. The key statistical measure for the alignment or non-alignment of the two surfaces was the RMS residuals.

The residual data was mapped with Surfer 3D analysis and visualisation software and overlaid with a contour map of the concha from the closed-jaw impression. This enabled visualisation of the regions of the impression where matching occurred within the cutoff limits of the program and where data points were excluded, representing those areas where matching was not within the cutoff limits.

2.6.2 Movement within the tragus/canal

Area-matching software was applied to the paired tragus/canal fields to evaluate movement within the tragus region that may have occurred as a result of opening the mouth.

The pairs of tragus/canal datasets, transformed into the same coordinate system with concha fields aligned, were matched using DS Match with threshold cut off limits of 100, 200, 300 and 400 μm.

The origin (0,0,0,) of the transformed fields was distant from the fields themselves. When DS Match was applied to these data files this

resulted in large translation parameters as a consequence of the rotation effect of the solution. In order to minimise to rotation effects the origin of the fields was moved to the centre of the field. Common x, y, and z-axis translations were added to each impression pair. Neither this or previous operations introduced distortion of the fields.

Following application of the mirror transformation parameters, the transformed fields were orientated in a vertical direction. DS Match was found to work only on fields that were essentially orientated in the horizontal plane. The x- and z-axes were swapped to re-orientate the field into horizontal fields. This did not alter the geometry of the fields.

The results of area-based matching of the tragus/canal fields were used to evaluate distortion that had occurred in this region during jaw movement.

The residual data was mapped with Surfer 3D analysis and visualisation software and overlaid with a contour map of the tragus/canal from the closed-jaw impression. This enabled visualisation of the regions of the impression where matching occurred within the cut-off limits of the program and where data points were excluded, representing those areas where matching was not within the cutoff limits.

2.6.3 Movement of tragus/canal relative to the concha

The datasets from the pairs of tragus/canal regions, transformed into the same coordinate system with concha fields aligned, were further analysed and visualised using Surfer software. The x and z-axes were swapped so that the imported files were orientated as horizontal surfaces. The x-axis correlated with the M-L direction, the y-axis correlated with the S-P direction (unchanged) and the z-axis correlated with the A-P direction. (refer to section 2.4.2)

Movement in the Frontal plane (x, y axes)
Data sets were converted to "grid files' by Surfer. Gridding parameters were set at 500 μm for both x and y-axes. Triangulation and interpolation was accepted as the gridding method. Fields were plotted as contour maps with contours at 500 μm intervals. Closed-jaw impression contour maps were coloured black. Open-jaw impression contour maps were coloured magenta.

Open and closed-jaw impressions were overlaid into the same coordinate system in Surfer using the automatic 'overlay maps' command. This provided a visual representation of spatial relationship between the two tragus/canal fields in the frontal plane.

The open-jaw contour map was then clicked and dragged over the closed-jaw map until it achieved an alignment of best fit. Best fit was determined subjectively by balancing considerations of:

The highest contour of the plot (bend in canal),
The ridge extending from the highest point to the inferior aspect of the canal, and
The superior and inferior borders of the canal.

The x and y-axis translations that occurred while manually aligning the two maps were determined using the 'digitize' function of Surfer. This represented movement in the frontal plane.

Movement in the Sagittal Plane (z-axis)
Gridding parameters were set as above. In addition, maximum and minimum grid lines were matched for each pair of data sets. This allowed difference data to be generated by Surfer by subtracting the open-jaw data from the closed-jaw data. Difference contour maps were generated with a contour interval of 500 μm and overlaid with a contour map of the corresponding closed-jaw dataset. The difference data represented movement in the Sagittal (A-P) plane.

Rotational movements
The pairs of tragus/canal datasets, transformed into the same coordinate system with concha fields aligned, were matched using DS Match (section 2.6.2) The rotational parameters were used to evaluate the rotational component of the movement.

Chapter 3 – Results

3.1 Subjects

Fourteen pairs of open and closed-jaw impressions from 10 subjects, 4 males and 6 females were included for analysis (Table 3.1). Their ages ranged from 15 to 58 years. There were 6 left ear impression pairs and 8 right. There were 6 pairs of impressions from males and 8 from females.

No.	Subject	Sex	Age (years)	Ear
1	1	Male	55	Left
2	2	Female	33	Right
3	3	Male	59	Left
4	4	Female	46	Right
5	5	Male	40	Left
6	5	"	"	Right
7	6	Male	45	Left
8	6	"	"	Right
9	7	Female	15	Left
10	7	"	"	Right
11	8	Female	43	Left
12	8	"	"	Right
13	9	Female	58	Right
14	10	Female	44	Right

Table 3.1 Subjects, by sex, age and ear.

3.2 Accuracy and precision of data

Several stages were involved in the manipulation of coordinate data for analysis. Each data point consisted of an x, y, and z value. Each data point could be thought of as having a cloud of uncertainty around it, the dimensions of the cloud varying in each axis.

3.2.1 Plotting of coordinate data from impressions

Precision in the x and y-axes was determined by the precision of the Moiré fringe encoders. This is reported by the manufacturer as 1μm.

Accuracy and precision in the z-axis was limited by the design of the instrument, but was also dependent on the operator. The precision of the z-axis scale is reported as 1 μm, however, the consistency of the operator to place the measuring mark upon the surface of the object in the same manner limited the precision of recordings.

The mean of the standard deviations of the differences (30 points plotted 14 times) on the z-axis was measured on several occasions and is shown in Table 3.2.

Date	St Dev (μm)
27 Jul 1994	44.3
2 Dec 1994	36.0
19 Jul 1996	33.6
8 Nov 1996	19.9
20 Feb 1998	16.3

Table 3.2 Reflex microscope, z-axis precision.

Table 3.2 indicates a progressive improvement in precision with familiarity with the measuring system (as also noted in Speculand, Butcher and Stephens 1988). All ear impression measurements were taken on or after 20 Feb. 1998. The conservative figure of 20 μm was taken as the precision of the z-axis measurements.

In summary, the precision of plotted coordinates was:

x-axis: 1 μm
y-axis: 1 μm
z-axis: 20 μm

3.2.2 Mirror transformation of tragus field into direct coordinate system

Coordinate data of tragus fields was plotted as a mirror image and then transformed into a direct image. Using a metal die and a free-format routine, common points were plotted as direct points and mirror points. These pairs of points were used to calculate transformation parameters, which were applied to tragus fields to transform them from mirror images to direct images.

Only one pair of points was required to produce the vectors and constant for the equations. Measurement error in these two points would be reflected as error in the parameters. Increasing the number of points and averaging the parameters resulted in an increase in the accuracy of the parameters. The errors in the transformed coordinate data are more relevant than the error in the transformation parameters themselves.

The precision of the method was taken as the standard deviation of the mean of the differences between a sample of direct points and the same points plotted through the mirror and transformed into direct points (i.e. calculated direct points) (Table 3.3). The RMS of the standard deviations for the three axes combined was 28.4 μm.

Date	No. of Points	Standard Deviations		
		x-axis (μm)	Y-axis (μm)	z-axis (μm)
8Nov96	30	26.3	9.2	33.4
20Feb98	28	33.9	13.4	33.8
21Feb98	18	23.7	26.9	24.7
19Feb99	18	41.0	17.7	49.6
Mean		30.9	15.5	35.0

Table 3.3 Precision of Mirror transformation, by x, y and z axes.

To determine whether there was any systematic error, the mean of the differences between the direct and calculated points was calculated (Table 3.4). The mean of the differences for the x, y, and z-axes was close to 0 μm. This indicated that the error was random in nature and did not favour any particular axis.

Date	No. of points	Mean of Differences		
		x-axis (μm)	Y-axis (μm)	z-axis (μm)
8Nov96	30	-2.11	0.45	2.49
20Feb98	28	-0.97	-1.25	0.89
21Feb98	18	2.37	-3.87	0.87
19Feb99	18	4.01	1.75	-2.01
Mean Diff.		0.26	-0.63	0.84

Table 3.4 Precision of Mirror transformation, assessment of systematic error.

The mirror transformation parameters that were applied to each individual x, y and z value required inputs from all three axes. (See Appendix 1.) The error values for the three axes are of the same order of magnitude (Table 3.3). Table 3.4 does not give rise to any suspicion that error is greater in any one of the axes.

In summary, the precision of mirror transformation was taken to be +/- 30 μm in each of the x, y and z-axes. This led to an RMS standard deviation of 52 μm for the three axes combined.

3.2.3 Parameters derived from area-matching concha fields

The full area-matching solutions from the concha field data appear in spreadsheet form in Appendix 2 with various summaries on pages 98 and 99.

Error in the parameters derived from area-matching was dependent on the surface shape, the perimeter shape, and the number of equations used to determine the solution and the coincidence of the two surfaces (RMS residuals). This in turn could be affected by the threshold limit set for the exclusion of data.

Area-matching was performed with cut-off threshold limits of 100, 200, 300 and 400 μm. A summary of the percentage of equations included in the solutions, and RMS residuals is provided on page 4 of appendix 2. The mean values for the percentage of equations and RMS values for the 100, 200, 300 and 400 μm cut-off exclusion limits on datasets 2 - 14 are presented in Table 3.5.

Threshold limit (μm)	Mean % of equations	Mean RMS residuals (μm)
100	58	49
200	82	78
300	87	97
400	90	108

Table 3.5 Concha area-matching, varying the threshold limit.

The mean percentage of equations with cut-off limits of 200 to 400 μm was in excess of 80% (Table 3.5). Each profile of the concha fields accounted for between 8 and 10 percent of the points. If a pair of concha fields did not overlap by one profile, then 10 percent of the points would be lost to the solution. If they did not overlap by two profiles then up to 20 percent of the points would be lost to the solution.

Along the inferior, posterior and superior borders of the concha field the surface fell away very steeply. Points recorded in these areas were subject to increased measurement error due to the steep angle at which the surface intersected with the measuring-mark. The error associated with this phenomenon was not tested. However many of these edge points are likely to have been excluded from the solution. The number of points excluded for this reason could approach 10 percent.

It was also accepted that the coordinates of a number of points would be recorded incorrectly because of operator error; principally recording a point with the foot switch before the measuring-mark had been properly positioned upon the surface of the object. No assessment of

the rate of this error was made. The purpose of the cut-off limit was to exclude these points. No attempt was made to assess the percentage of points that fell into this category but an upper limit of 5 percent would seem a conservative estimate, one point in a profile of twenty points.

In summary, loss of equations from the solutions were due to:

Lack of overlap at the first or last profiles	<10%
Steep inclines at southern and northern border	<10%
Recording error	<5%.

An exclusion of around 20% of equations is consistent with a correct match between two closely fitting surfaces.

Thus the figure of 82% for the 200 μm cut-off limit is consistent with the data and measuring system. The figures of 87% for the 300 μm cut-off limit and 90% for the 400 μm cut off limit are consistent with inclusion of a further 5% and 8% of points as more inaccurate points and more edge points are included by the higher threshold limit.

An RMS of 82 μm (200 μm cut-off, Table 3.5) is consistent with the RMS calculated for the metal die (52 μm) given the observation points (x, y grid) do not coincide exactly.

Parameters derived from a cut-off of 200 – 400 μm are generally close together. The parameters derived from a cut-off of 100 μm vary markedly from the parameters derived from the 200 – 400 μm cut-off limits in four cases. In these four cases the % equations falls below 50% (nos. 1, 2, 9 and 10). The range of the transformation parameters derived from a cut-off of 200 - 400 μm is provided on page 4 of the Appendix. The mean values of the range of each parameter are in are presented in Table 3.6.

Parameter	Range
Tx	173 μm
Ty	167 μm
Tz	117 μm
Rz (Kappa)	0.65°
Rx (Omega)	0.28°
Ry (Phi)	0.27°

Table 3.6 Concha area-matching, mean of the range of parameters derived from 200, 300 and 400 μm cut-off limits.

Table 3.6 results indicate that the solutions based on 200, 300 and 400 μm appear relatively stable.

On the basis of the data in Table 3.5, the need to include the highest number of equations was balanced with the need to keep the value of residuals as low as possible and parameters based on a threshold limit of 200 μm were accepted as inputs into further analysis.

The means of the standard deviations for the transformation parameters, based on a cut off of 200 μm, are presented in Table 3.7. These values are indicative of the closeness of the match of the two surfaces using different solutions. The RMS of the x, y and z-axis standard deviations in Tables 3.7 was 73.82 μm.

Parameter	Standard Deviation
Tx	48 μm
Ty	36 μm
Tz	43 μm
Rz (Kappa)	0.12°
Rx (Omega)	0.07°
Ry (Phi)	0.12°

Table 3.7 Concha area-matching, standard deviations of parameters.

In summary, concha fields were area-matched using a cut-off limit of 200 μm. They matched with a RMS of residual values of 78 μm, and a RMS on the standard deviations of the translation parameters of 74 μm.

The same general considerations apply to area-based matching of the tragus/canal fields. These results appear in section 3.4.

3.3 Movement within the Concha

Fourteen impression-pairs were area-matched using DS Match with threshold cut-off limits from 100, 200, 300 and 400 μm. The parameters based on a cut-off limit of 200 μm were accepted as the best estimate of the true solution. The actual parameters are of no importance when considering movement in the concha.

The RMS of the residuals and the percentage of equations involved in the solution give a measure of the coincidence of the two surfaces (3. 8).

Imp. No.	No. of Points	No. of Equations	% Equations	RMS Residuals (μm)
1	442	202	46	102
2	237	177	75	71
3	380	334	88	64
4	283	181	64	91
5	319	252	79	73
6	236	215	91	75
7	301	250	83	87
8	314	256	82	73
9	254	219	86	87
10	234	197	84	77
11	262	211	81	77
12	206	169	82	70
13	270	215	80	90
14	321	286	89	73
Mean			82	78

Table 3.8 Concha area-matching, % equations and RMS residuals.

Note: *Data set 1 was excluded from the calculation of the mean because the area-matching result was unreliable, with a lower number of equations and higher RMS residual value (Table 3.8).*

As discussed in section 3.2.3 the figure of 82% is consistent with the data and measuring system. The figures of 87% for the 300 μm cut-off limit and 90% for the 400 μm cut-off limit are consistent with inclusion of a further 5% and 8% of points as more inaccurate points and more edge points are included by the higher threshold limit.

Table 3.8 shows that the concha region of open-jaw and closed-jaw impression sets 2 – 14 conform, with a mean RMS or residuals of 78 μm derived from coordinate data with a measurement error of 20 μm and plotted on a 1 mm grid.

The residual data was mapped with **Surfer 3D analysis and visualisation software** and overlaid with a contour map of the concha from the closed-jaw data (Appendix 4). The residual data was gridded on a 1 mm interval with triangulation and interpolation, and contoured between –0.2 mm and +0.2 mm with contour intervals of 0.1 mm. The closed-jaw data contour map was gridded on a 0.5 mm grid with triangulation and interpolation. All maps have been displayed such that the inferior border of the concha is at the bottom of the map and the section leading to the external acoustic meatus is to the left. For example, the map of impression no. 10 is displayed below (Fig. 3.1).

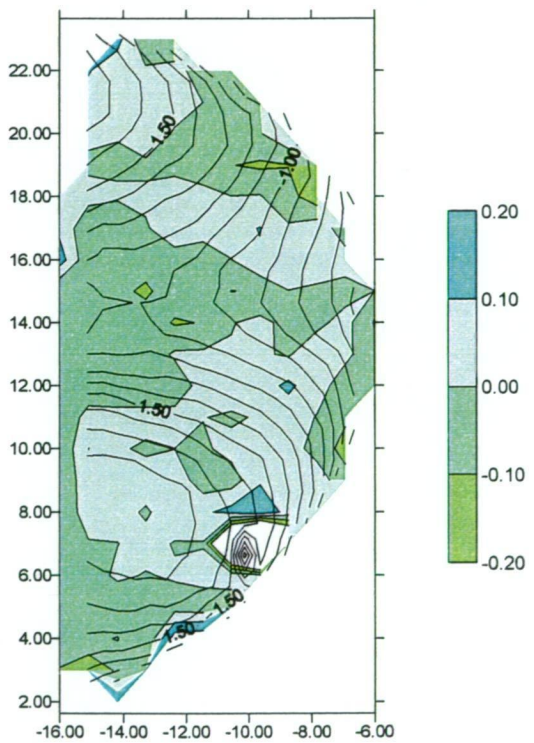

Fig. 3.1 Impression no.10. Concha field, area-matching residual data contour map, overlaid with closed-jaw data. All units in mm's. (from Appendix 4)

Examination of the maps generally reveals:

Broad areas of residual data between +/- 0.1 mm,
Discrete areas of residual data between +/- 0.1 and 0.2 mm,
Blank area at some edges where data points have been excluded.

Two maps, nos. 1 and 3, show larger areas of excluded points. This is in line with their lower % of equations included in the solution (Table 3.8). Map 5 also has a larger area of excluded points but is a much larger ear.

The remaining eleven maps typically show exclusion of points:
Along the left axis corresponding to the first profile, or
Along the border between the concha and the antihelix.

This latter region is associated with an increasing slope and therefore the exclusion of points due to:
Increased measurement error,
Reduction in effective sampling rate,
Movement in the region.

Regions where the residual data is between +/- 0.2 mm are typically:
Along the border with the antitragus,
In the region of the crus of the helix (nos. 11 – 14),
Within the body of the map.
Points in this latter region are likely to be as a result of measurement error. Points in the first two regions above are likely to result from:
Increased measurement error,
Reduction in effective sampling rate,
Movement in the region.

3.4 Movement within the Tragus/Canal

The full area-matching solutions from the tragus/canal field data appear in spreadsheet form in Appendix 3 with various summaries on pages 103 and 104.

Fourteen impression pairs of tragus/canal regions, transformed into the same coordinate system with concha fields aligned, were matched using DS Match with threshold cut-off limits of 100, 200, 300 and 400 μm. Non-convergence indicated movement and distortion beyond the convergence limits set by the program (see section 2.5.2). Data files had common translations added to all points to bring the origin of the coordinate system (0,0,0) into the centre of the field. This minimized the effect of rotations on the translation components upon the matching solutions. Translation parameters from solutions where rotations were significant were not meaningful, because of the translation effect of the rotations.

Applying a cut-off limit of 200 μm produced the following table (Table 3.9) with a mean percentage of equations of 66% and mean RMS residuals of 96 μm:

Imp. No.	No. of Points	No. of Equations	% Equations	RMS Residuals (μm)
10	208	182	88	85
11	210	175	83	80
7	276	220	80	94
5	342	270	79	91
14	208	164	79	82
12	218	169	78	81
1	619	396	64	81
9	145	90	62	101
4	306	184	60	91
6	297	179	60	89
13	267	153	57	89
8	340	183	54	97
2	195	86	44	97
3	247	101	41	106
Mean			66	96

Table 3.9 Tragus area-matching, 200 μm cut-off, % equations and RMS residuals.

Impression numbers: 5, 7, 10, 11, 12 and 14 converged with a high number of equations (>75%)
Impression numbers: 1, 4, 6, 8, 9, and 13 converged with a moderate number of equations (between 50 and 75%)
Impression numbers: 2 and 3 converged with a very low number of equations (<50%).

Loss of equations from the solutions can have been due to the same reasons as for the concha fields:

Lack of overlap at the first or last profiles,	<10%
Steep inclines at southern and northern borders,	<10%
Recording error,	<5%.

A difference in the shape of the canal at the southern and northern borders, as a result of flattening of the canal during jaw-opening, was also expected to result in loss of points. As with the concha fields, a loss of around 20% of equation from the solutions of matching tragus field is consistent with a correct match of two closely fitting surfaces. The RMS of the residuals measures the closeness of the fit.

Applying a cut-off limit of 400 μm produced the following table (Table 3.10) with a mean percentage equations of 85% and a mean RMS residuals of 136 μm:

Imp. No.	No. of Points	No. of Equations	% Equations	RMS Residuals (μm)
2	97	192	98	139
10	85	199	96	116
11	80	193	92	107
5	91	316	92	141
12	81	198	91	120
7	94	251	91	130
14	82	185	89	114
3	106	221	89	153
9	101	119	82	134
4	91	239	78	150
8	97	261	77	168
6	89	215	72	153
13	89	189	71	150
1	81	408	66	123
Mean			85	136

Table 3.10 Tragus area-matching, 400 μm cut-off, % equations and RMS residuals.

Impression numbers: 2 – 5, 7 - 12 and 14 converged with a high number of equations (>75%).
Impression numbers: 1, 6, and 13 converged with a moderate number of equations (between 50 and 75%).

In summary, six of the impression pairs matched with a cut-off limit of 200 μm, a mean 81% of equations and an RMS residuals value of 86 μm. Five impression pairs matched moderately well with a cut-off of 400 μm, a mean 85% of equations and RMS residuals value of 149 μm. Three impression pairs matched with a cut-off of 400 μm, a mean 70% of equations and a mean RMS residuals of 142 μm.

This points to increased distortion of the tragus/canal field when compared to the concha in 8 out of fourteen impressions. Successful matching of fields generally occurred only when the cut-off limit was increased to 400 μm with a mean RMS of 136 μm (compared with a mean RMS of 78 μm for concha matching).

The residual data was mapped with **Surfer 3D analysis and visualisation software** and overlaid with a contour map of the concha from the open and closed-jaw impressions (Appendix 5). The residual data was gridded on 1 mm interval with triangulation and interpolation, and contoured between –0.4 mm and +0.4 mm with contour intervals of 0.1 mm. The overlaid contour maps of the open and closed-jaw tragus/canal region were gridded on a 0.5 mm grid with triangulation and interpolation. All maps have been displayed such that the inferior border of the tragus/canal is at the bottom of the map and the medial section of the canal is to the centre of the page. For example, the map of impression no. 10 is displayed below (Fig. 3.2).

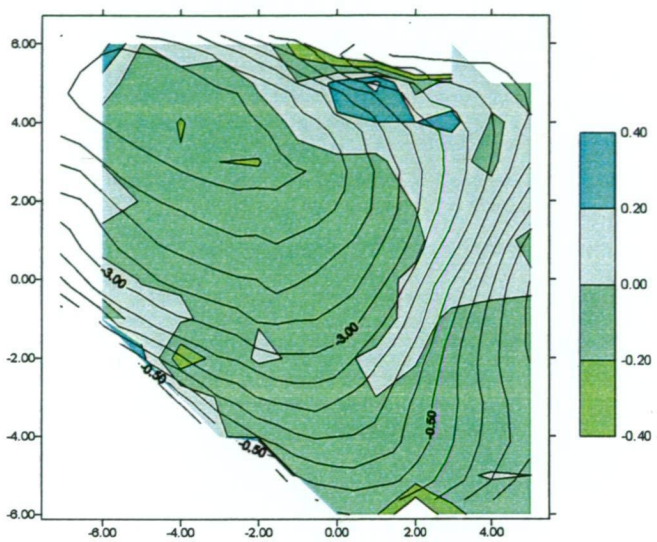

Fig. 3.2 Impression no.10. Tragus/canal field, area-matching residual data contour map, overlaid with closed-jaw data. All units in mm's. (from Appendix 5) *Note: different scale from Fig. 3.1*

Distortion of the tragus could occur in two general areas, within the body of the field and at the edges. The above table and examination of the overlaid contour maps indicates that the influence of loss of data at the edges was significant.

3.5 Movement of the Tragus relative to the Concha

3.5.1. Movement in frontal plane (x, y-axes)

The datasets from fourteen impression pairs of tragus/canal regions, transformed into the same coordinate system with concha fields aligned, were further analysed and visualised using Surfer software. The x and z-axes were swapped so that the imported files were orientated as horizontal surfaces. Gridding parameters were set at 500 μm for both x and y-axes. Triangulation and interpolation was accepted as the gridding method. Fields were plotted as contour maps with contours at 500 μm intervals. Closed-jaw impressions were coloured black. Open-jaw impressions were coloured magenta. Both maps were automatically overlaid by Surfer into the same x, y-axis grid (e.g. Fig. 3.3) and are presented in Appendix 6.

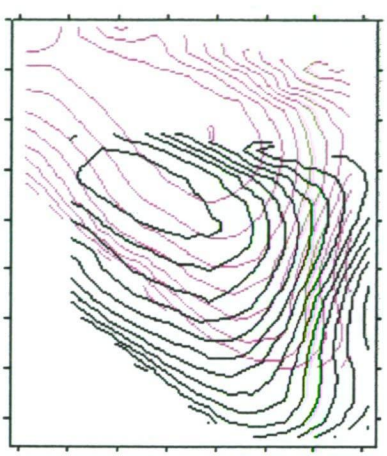

Fig. 3.3 Impression no. 10. Tragus/canal field, Closed-jaw data (black), Open-jaw data (magenta). Maps overlaid into same coordinate system with concha fields co-incident. (from Appendix 6)

The precision of the points on which the contour plots were based upon was calculated from:

Precision of recorded points:	20 μm (section 3.2.1)
Precision of mirror transformed points:	52 μm (section 3.2.2)
Precision of area-based matching:	78 μm (section 3.2.3)

Because the closed-jaw data was recorded, then transformed through the mirror, it had an estimated accumulated error of 56 μm. By comparison the open-jaw data was recorded, transformed through the mirror, and transformed with transformation parameters derived from the concha area-matching, and so had an estimated accumulated error of 97 μm. Contour intervals of 500 μm could be reliably plotted based on this data. Displacements of 500 μm or greater are therefore clearly significant.

All maps were then manually overlaid by clicking and dragging the closed-jaw plot until an alignment of best fit was achieved. Best fit was determined subjectively by balancing considerations of:

The highest contour of the map (bend in canal),
The ridge extending from the highest point to the inferior aspect of the canal, and
The superior and inferior borders of the canal.

The resultant x and y-axis translations were determined using the 'digitize' function of Surfer. The following translations in μm were recorded (Table 3.11). Negative figures represent movement to the inferior (y-axis) or lateral (x-axis).

No.	Subject	X-axis (*um*) Medial-lateral	Y-axis (*um*) Superior-inferior
1	1	0	0
2	2	-3839	-1592
3	3	-364	+823
4	4	-3231	-588
5	5	0	0
6	5	-1248	-1006
7	6	1458	-2716
8	6	2022	-811
9	7	1595	3712
10	7	1489	2372
11	8	-1190	-440
12	8	-2075	0
13	9	-775	-1270
14	10	-647	-1616
Mean (absolute)		1450	1210

Table 3.11 Frontal plane (x, y-axes) movements of tragus relative to the concha.

The mean of the absolute values of the x and y-axis translations were 1450 μm and 1210 μm respectively with a range of 0 – 3839 μm and 0 - 3712 μm.

In general terms, upon opening, the canal moved in the S-I plane (y-axis):

Inferiorly in numbers:	2,4,6,7,8,11,13,14 (8 ears)
Superiorly in numbers:	3, 9, 10, (3 ears)
No S-I movement in numbers:	1,5,12 (3 ears).

In general terms, upon opening, the canal moved in the M-L plane (x-axis):

Laterally in numbers:	2,3,4,6, 11,12,13,14 (9 ears)
Medially in numbers:	7,8,9,10, (4 ears)
No M-L movement in numbers:	1, 5 (2 ears).

3.5.2 Movement in the A-P direction (z-axis)

The datasets from fourteen impression pairs of tragus/canal regions, transformed into the same coordinate system with concha fields aligned, were imported into Surfer as described above. The grid line geometry for each pair of fields was set to the same maximum and minimum limits. Difference data was generated by subtracting the open-jaw data from the closed-jaw data.

Difference contour maps were generated on a 500 μm grid (Appendix 7). Issues of error and significance are the same as in the previous section 3.5.1. Positive values represent movement upon opening in the anterior direction (e.g. Fig. 3.4).

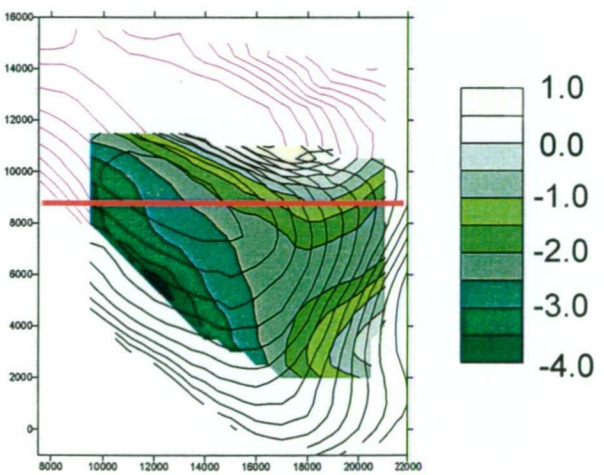

Fig. 3.4 Impression no. 10. Tragus/canal field, Closed-jaw data (black), Open-jaw data (magenta) and closed – open-jaw difference data contour map. Maps overlaid into same coordinate system with concha fields co-incident. Colour scale units in mm.
(from Appendix 7)

The range of values along a horizontal line through the centre of the map was taken as an approximation of the movement in the A- P direction (Table 3.12). The red line in Fig. 3.4 was the region through which difference values were accepted as the A-P movement. This line passes through contour levels of –4.0 mm to –0.5 mm.

Movement ranged from –8.5 mm to +8.0 mm. Movement in 9 of the 14 ears occurred between –3.0 mm and +3.5 mm. The absolute mean of the range was 3.5 mm.

No.	Subject	Z-axis (mm) Antero-posterior	Range (mm)
1	1	4.5 to 5.0	0.5
2	2	-8.5 to –3.0	5.5
3	3	-0.5 to 2.0	2.5
4	4	-2.5 to 3.0	5.5
5	5	0 to 8.0	8.0
6	5	-3.0 to –1.0	2.0
7	6	3.5 to 7.5	4.0
8	6	-2.0 to 3.0	5.0
9	7	1.0 to 3.5	2.5
10	7	-4.0 to –0.5	3.5
11	8	-1.0 to 2.0	3.0
12	8	-1.0 to 2.5	3.5
13	9	1.0 to 3.5	2.5
14	10	1.0 to 2.5	1.5
Mean			3.5

Table 3.12 Sagittal plane (z-axis) movements of tragus relative to the concha.

In general, upon opening, the canal moved in the A-P plane (z-axis):

Anteriorly in nos. 1, 3, 5, 7, 9 and 13 (6 ears)
Posteriorly in nos. 2, 6, 10 (3 ears)
Mixed in nos. 4, 8, 11, 12 and 14(4 ears).

In the mixed group, ears 4, 11and 12 showed anterior movement (widening of the canal) lateral to the first bend and posterior movement (narrowing of the canal) medial to the first bend. Ear 8 showed the reverse.

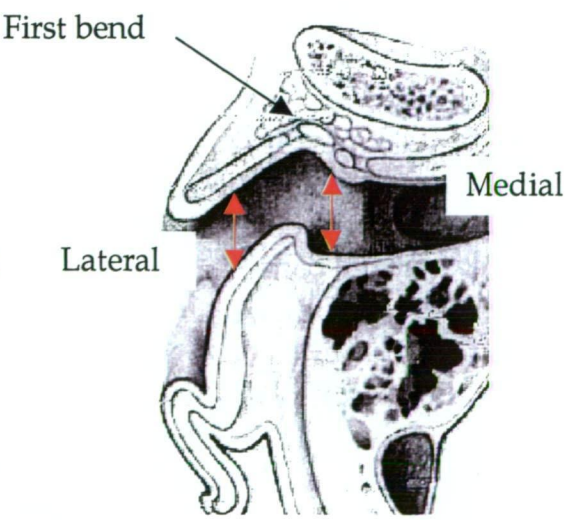

Fig 3.5 Horizontal section through ear canal.
Source: modified from Cunningham's Textbook of Anatomy

3.5.3 Rotational movement of tragus/canal

The datasets from fourteen impression pairs of tragus/canal regions, transformed into the same coordinate system with concha fields aligned, were matched using DS Match with threshold cut-off limits of 100, 200, 300 and 400 μm. (See section 3.4). The translation parameters were not considered for analysis because they were affected by the translation component of the rotation parameters.

The rotational parameters were reviewed to assess the rotational component of the movements. However the rotational parameters could be expected to be affected by distortion of the surfaces without actual rotations occurring. The rotational parameters derived from the 400 μm cut-off limit are displayed in Table 3.13 (from Appendix 3).

Rx related to the M-L axis of rotation or the sagittal plane and could have translation effects predominantly in the A-P direction. **Ry** related to the S-I axis of rotation or the axial plane and also could have translation effects predominantly in the A-P direction. **Rz** relates to an A-P axis of rotation or the frontal plane and could have translation effects predominantly in the S-I direction.

No	Rx	Ry	Rz	% Eq.	RMS
1	1.81	-1.45	-0.77	66	123
2	-1.73	11.28	-4.96	98	139
3	3.88	-1.25	3.09	89	153
4	7.78	-4.29	3.81	78	150
5	-3.71	-2.00	0.65	92	141
6	7.34	5.77	4.50	72	153
7	-13.52	3.93	-2.30	91	130
8	7.36	-6.14	4.56	77	168
9	7.64	-6.64	6.89	82	134
10	-8.72	0.14	-2.38	96	116
11	-1.78	1.92	-4.22	92	107
12	-5.19	-8.19	1.13	91	120
13	5.16	-7.71	-0.77	71	150
14	5.34	0.35	6.72	89	114
Mean (absolute)	6.09	4.54	3.53	85	136

Table 3.13 Rotational movements of tragus relative to concha.

The mean of the absolute values of the x, y and z-axis rotations were 6.09, 4.54 and 3.53 digital degrees respectively. This compares with the mean standard deviation of these parameters of 0.16, 0.18, and 0.13 respectively. (Appendix 3, pp. 104). It is evident that the uncertainty in the transformation parameters is small when compared to the magnitude of the rotations.

The direction of the rotational data displayed in Table 3.13 does not bear a direct relationship to the direction of translations displayed in Tables 3.11 and 3.12. The size of the rotations also does not appear to bear relation to the amount of distortion in the surfaces (Table 3.10).

In general, no statements can be made about rotational movements of the tragus/canal relative to the concha based upon the parameters derived from area-matching.

Chapter 4 – Discussion

4.1 Impressions and Accuracy

Mapping was required to be accurate and precise to a level relevant to clinical practice and the manufacture of hearing-aids.

4.1.1 Subjects

Several impressions thought to be clinically acceptable were rejected for analysis due to flaws and inadequate canal length. In particular, it was more common for males to have increasing amounts of wrinkles and hair growing in the canal with increased age. During manufacture, such flaws are filled with wax and may be adjusted in the clinic. When magnified by the reflex microscope large defects which involved more than one grid point resulted in increased uncertainty as the location of the surface. Where a defect only affected the plotting of one grid point, i.e. in the order of 1 mm or less, the surface of the impression could be extrapolated from the levels and contours of the surrounding surface.

In the early stages of the project it was felt that an increase in skin wrinkles that occurs with age would be advantageous for **feature-based matching**. However this proved unsuccessful and the greater unevenness of the skin surface made evaluation of where the surface actually was less certain. As a result there has been a bias away from older males in the subjects studied.

4.1.2 Practical considerations for accuracy

Clinically, the accuracy of ear impressions can be hampered by the presence of hairs and cerumen. Cerumen can be broadly characterized as being made up of oils, waxy substances and dry flaky skin (Oliviera 1997). These constituents can be present in varying ratios leading to widely varying physical properties. High levels of oil can cause to canal to have easily visible, mobile, soft wax. This can be removed prior to impression taking. Low levels of oil and wax can cause the canal to have predominantly dry skin flakes. Skin flakes and other debri down to around 100 μm can be readily seen without magnification. There are practical limits to the size of particles that can be removed from the ear. It is unrealistic to expect to be able to define and record the 'precise' location of the tissue surfaces in the canal.

As noted in section 1.8, Earmould /HA shell Manufacture, the nature of the materials used and polishing, results in the loss of some material and surface detail. Applying a wax coating can ensure that the finished shell is no smaller in dimension than the original impression, ensuring a 'snug' fit. Heat-cured acrylic resins typically show polymerization shrinkage of 6 to 8 percent (Greener et al 1972). For a mould with a thickness of 2 mm, this could equate with shrinkage of approx. 0.12 -

0.16 mm (in the order of 150 μm). The thickness of wax coatings has not been reported upon and is unknown.

Many hearing-aid moulds are now made from light-polymerized materials. These shrink towards the light source. Manufacturing methods generally involve light application from the outer surface of the mould first, so that the external surface of the mould is cured first. In theory this should minimize shrinkage away from the investment material and optimize the fit of the mould. However light-polymerized materials do not achieve as high a level of polymer cross-linking as heat-cured materials and show reduced hardness. More material is lost from the surface of the mould during polishing. The extent of this problem is unknown. It can be expected to be at least equivalent to shrinkage of heat-cured materials.

As a result of the above considerations, changes in external ear morphology of less than 200 μm are unlikely to have a significant impact upon the dimensions of hearing-aids and earplugs. As noted in section 1.4.2, differences of 0.5 mm exerted a dramatic effect on sound attenuation of earplugs (Smith et al 1980). An error in the order of 100 μm in ear impression maps was accepted as a level of accuracy consistent with the clinical and manufacturing practice.

Mathematical manipulation of the observational data was expected to, and did, introduce error into subsequent results. In order to achieve accuracy in the order of 100 μm in the ear impression maps, it was necessary to achieve accuracy in data collection in the order of 30 μm. This level of error was achieved with the Reflex microscope.

4.1.3 The regions mapped

At the outset, mapping the entire surface of the external ear corresponding to the tissue-fitting surface of ITE hearing-aids was desired. Although it was recognized that the most significant movement occurred in the anterior wall of the tragus/canal.

The geometry of the external ear made the task of mapping the entire surface of impression more complex than initially envisaged. The extensive use of mirrors placed at 45 degrees could not guarantee the visualisation of all surfaces by the reflex microscope. In this study the concha field was orientated horizontally so that the maximum surface area of the concha was visible through the microscope, and therefore available for area-based matching (Fig. 2.3). A mirror was placed to enable visualisation of the anterior surface of the tragus/canal. A mirror at 45 degrees could not be placed to view the entire posterior surface of the canal. The convex shape of the concha obscured the area where the canal joined the concha. If there were morphologic changes in this area it would be worthwhile quantifying.

The angulation of mounting used by Stinson and Lawton (1989) achieved the maximum availability of the full circumference of the canal for mapping by a mechanical probe approaching from the horizontal (Fig 4.1). However the concha area when viewed from above was partially obscured by the canal.

Fig. 4.1 Ear impression no. 4 mounted with canal positioned to allow maximum access of the canal region from the horizontal as per Stinson and Lawton (1989). Note that part of the concha region is obscured from visualisation from above.

The only report to date which has mapped the entire concha and canal regions was that by Kamel, Kunov and Abel (1986). Ear impressions were reproduced in a harder material, then sliced and photographed at 1.0 mm sections. The photographs were aligned and the outline of the ear mould traced with about 20 points per slice (Fig. 4.2).

The method described by Kamel, Kunov and Abel corresponds to an interval of approx. 1mm between points along each section/contour. However this does not mean that the entire ear impression was plotted on a 1 mm grid. The canal part of the impression, which was orientated vertically and sectioned at right angles to its long axis, was indeed plotted on a 1 mm grid. If the concha region was viewed along the plane of the sectioning this would also be the case. However if the concha region was viewed at right angles to the plane of sectioning, the grid size would appear to be very much greater and irregular. Increasing the sampling rate per contour would not provide sufficient data because the contour lines would still be too widely spread.

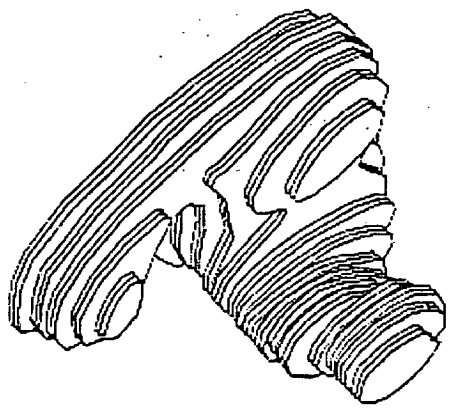

Fig. 4.2 Slicing and reconstruction at right angles to canal.
Source: Kamel, Kunov and Abel (1986).

A typical concha region plotted in this study consisted of 252 points (Table 3.8, Impression no. 5) This was plotted on a 1 mm grid with the southern border plotted at 500 μm intervals. A contour map was plotted using Surfer with 1mm contour intervals. By estimating the length of the contour lines, the number of points that would have resulted from collecting data points at 1 mm intervals along the contour lines was determined as 114 points. This low number is a consequence of the plane of sectioning being parallel to the 'plane' of the concha. While the concha is 'bowl-shaped' it is nonetheless relatively featureless.

Experience from this study shows that the number of points from the concha that result from a slicing method, where the slices are in the sagittal plane, would not be adequate to provide reliable are-based matching.

If slices were taken in the frontal plane or the horizontal plane an adequate 1 mm grid would be achieved. This, of course, is what was achieved with the Reflex microscope: profiles (i.e. slices) in the frontal plane, at fixed 1mm intervals in the horizontal plane. Slices taken in the frontal plane of the canal would only result in a 1 mm grid on the superior and inferior surfaces of the canal (Fig. 4.3). As the circumference of the canal moved to the anterior and posterior, the surface grid lines would become further apart.

Fig. 4.3 Frontal plane slices (red) through the ear canal (black).

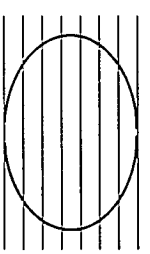

Thus no single orientation of slicing will provide adequate surface data to allow reliable alignment of the concha regions and analysis of the canal region. Either the object requires physical or optical transposition, or the recording system requires physical or optical transposition.

4.2 Area-based matching

4.2.1 The concha field

During the initial matching of concha fields of impressions it was apparent that area-based matching could be unreliable. The circular nature of the first surface maps of concha fields allowed several different 'good matches' with widely varying parameters to be derived from the same pair of impressions. This phenomenon could be described as 'barreling'. Two identical cylinders can be matched in an infinite number of ways when their long axes coincide.

This problem was overcome by enlarging the area of the concha being plotted, and including elements that were less subject to 'barreling'. The most important elements were the edge of the impression, and the hollow of the crus of the helix. Impression numbers 2 to 14 converged (200 μm cut-off limit) with an average number of 11 iterations (range 7 to 18). Impression no. 1 converged after 24 iterations. Further iteration of impression no. 1 could not produce convergence with a higher number of equations.

It can be concluded that the area mapped as outlined in Fig. 4.4, has generally provided a sufficient area for reliable area-matching.

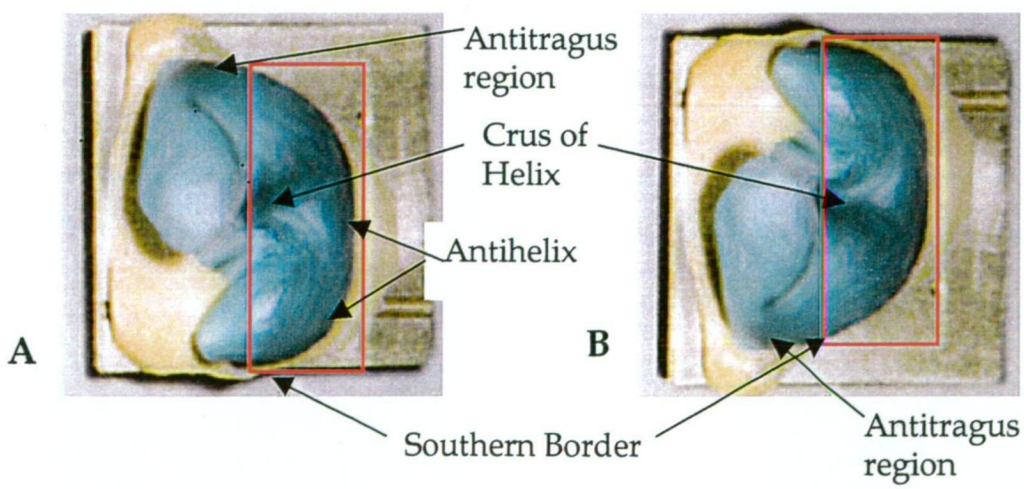

Figure 4.4. Concha regions mapped. **A**, left ear, and **B**, right ear. (Cropped from Fig. 2.3)

4.2.2 Impression alignment

Area matching was more successful when the surfaces to be matched were already closely aligned. During early trials, impressions mounted in the same orientation without the aid of a register (section 2.4.2) did not produce reliable solutions. This was in part due to the lack of edge data as noted above. However, due to a lack of routine in the method of alignment, no assessment could be made as to which solution was correct or whether the solution was reasonable. As a result a method of impression registration was developed to assist in aligning the impressions.

A comparison of the transformation parameters for matching the concha fields (Appendix 2, pp. 99) gives an indication of the effectiveness of the use of a register in aligning each pair of impressions. The abolute mean of the translations on the x, y, and z-axes was in the order of 1000 μm, and the rotations were in the order of 2 degrees. These values were larger than expected and may have been the result an inherent problem with the method or in its application.

The method used was not dissimilar to that used by Pirzanski (1996) in a qualitative study of ear canal movement. A review of the photographs presented in Pirzanski's article reveals apparent buckling of the closed-jaw impression negative or register into which the open-jaw impression was placed.

The region of the impression most likely contributing to this problem was the tragus. In the current study, the anterior surface of the tragus region was excluded from the register because it was known to move relative to the concha. Despite this, the inaccuracy of the impression alignment using the register was greater than expected. This could have been due to flexion at the intertragic notch (incisura intertragica) and movement of the antitragus.

The lateral-inferior aspects of the tragus/canal contour plots (Appendix 6) do represent the anterior wall of the tragus. Examination of these maps reveals large movements along the inferior border of the tragus in this region in the majority of maps. Interestingly, maps that show the least movement along the inferior border in the S-I and M-L planes (Nos. 3, 5, 6, and 11) also show smaller translations and rotations for all six area-matching parameters.

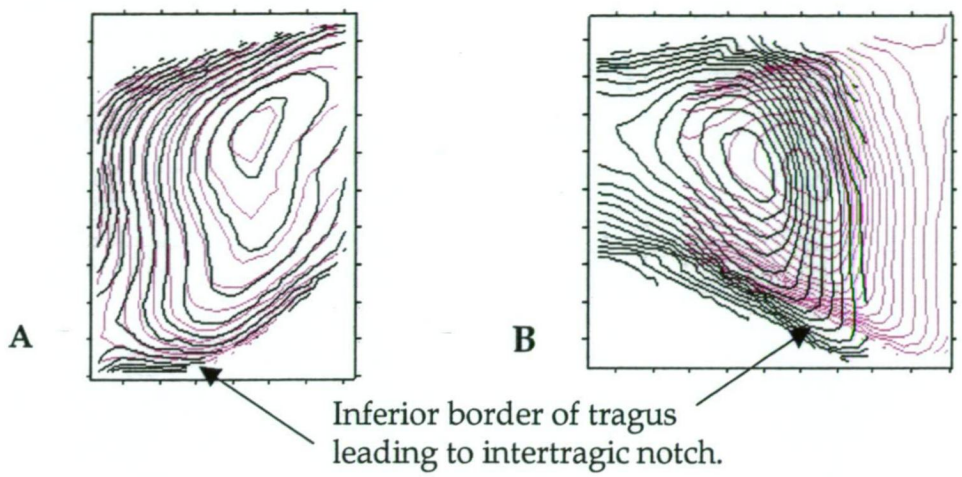

Fig. 4.5 Inferior Border of Tragus. Overlaid contour maps. **A**. Impression no. 5, no S-I, M-L movement along inferior border of tragus. **B**. Impression no. 4, significant M-L movement along inferior border of tragus. (from Appendix 6)

It can be concluded that where there was not significant movement in the intertragic notch region in the S-I and M-L planes, there was less error in the manual of alignment of the impressions with a register.

These movements do not appear to have resulted in distortion of the area of the concha that was plotted, as shown by high number of equations included in all the matching solutions.

Examination of the concha residual data contour plots e.g. Fig. 4.6 (from Appendix 4) shows a small loss of difference data along the inferior border of the map in the region of the antitragus in around half of the datasets. This loss of data, commented upon in the results section 3.3, was due to the increased slope in the region leading to increased measurement error and reduction in effective sampling rate, and possibly distortion in the region.

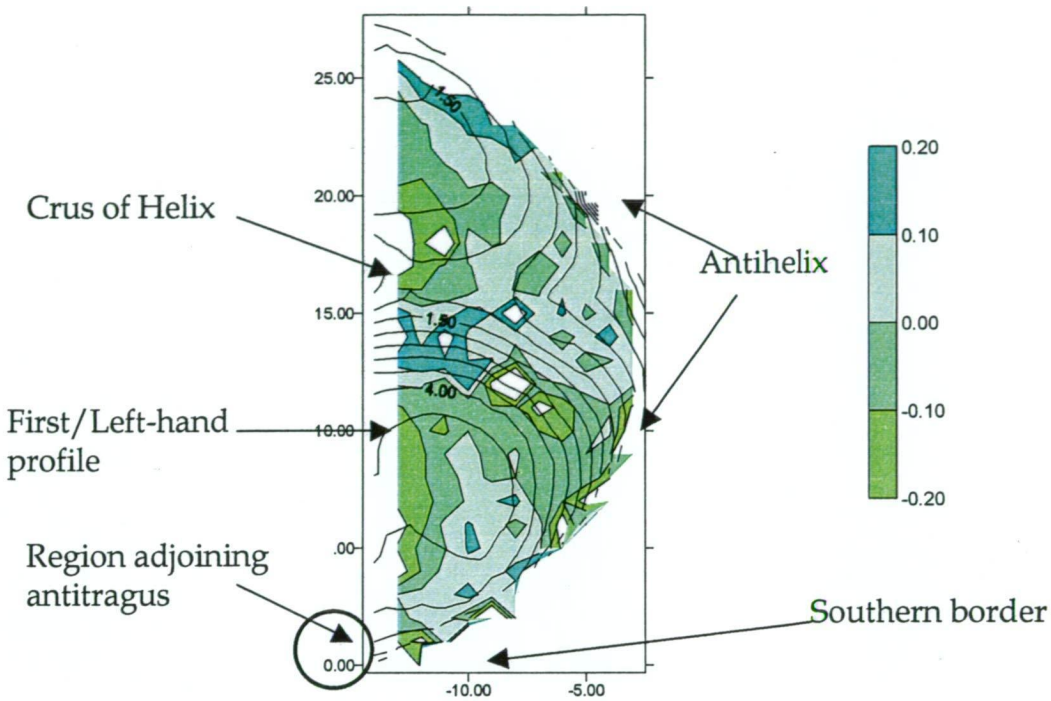

Fig. 4.6 Concha area-matching, loss of data.
Concha field of Impression no. 13: DS Match difference data contoured and overlaid with closed-jaw data contour map (black). (from Appendix 4)

However, the posterior wall of the intertragic notch, i.e. the antitragus region, was included in the register to provide sufficient contact with the impression to aid in the alignment of the impressions. There was a suspicion of movement in this region. Casual inspection of ear impressions frequently shows changes in this area. However the extent and significance of these changes has not been reported or commented on previously and did not form a part of this study. The plane of the antitragus part of the ear impressions was typically at close to right angles to the plane of the concha, and was therefore not mapped. (Fig. 4.7).

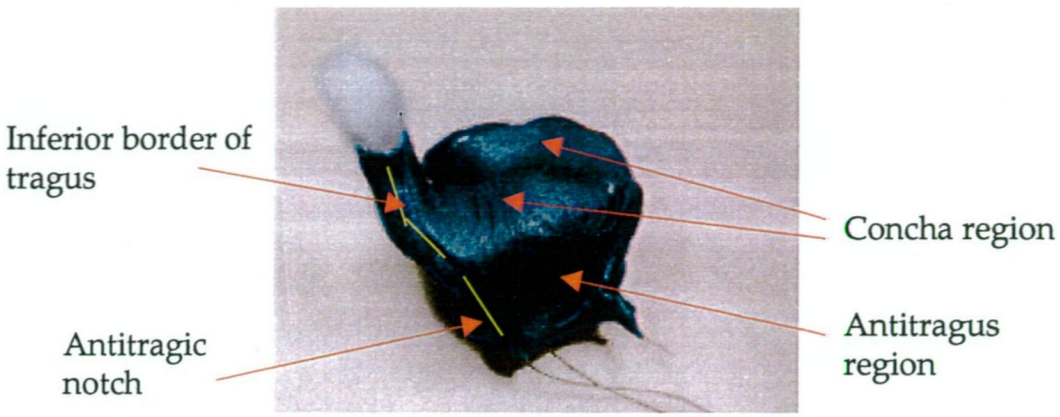

Fig. 4.7 Ear Impression with cotton block in place.

This study has found area-based matching to be a reliable method of enhancing the alignment of coordinate data, within the accuracy and precision requirements.

4.2.3 Multiple best-fit solutions of tragus/canal field

Area-based matching of the tragus/canal region had a propensity to produce multiple solutions. In order to determine the solution of best fit the data was repeatedly iterated with different combinations of 3, 4 and 6 parameters until the highest number of equations included in the solution was determined.

For example, Fig. 4.8**A** shows the residual data of area-matching the tragus/canal of impression no. 5, mapped as a contour map, overlaid with a contour map of the closed-jaw data. A cut-off limit off 400 μm was used, and convergence achieved with 62% of equations and an RMS residuals of 134 μm. Clearly the residual data contour map and the overlaid closed-jaw map do not coincide.

Further iteration of the closed and open-jaw data produced convergence with 92% of equations and an RMS residuals of 141 μm. The resultant map in Fig. 4.8**B** shows good alignment of the residual data contour map and the corresponding closed-jaw impression. Clearly this second solution provides a better match than the first.

Whether this result is the correct match, is a matter of clinical judgement and whether the result provides meaningful information about the relationship between the two surfaces. This issue is discuused further in section 4.4 below.

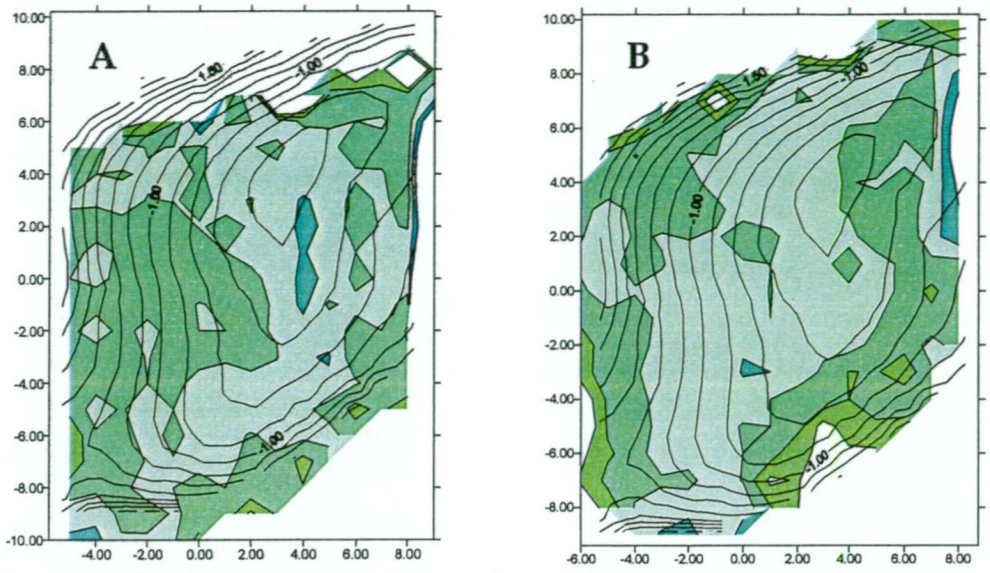

Fig. 4.8 Multiple solutions of tragus/canal fields, Impression no. 5, 400 μm cutoff limit. **A**. Solution contains 62% of equations, **B**. Solution contains 92% of equations.

4.3 Movement within the concha

The results showed that the concha region of open and closed-jaw impression sets 2 – 14 conformed, with a mean RMS of residuals of 78 μm (Table 3.8), derived from coordinate data with a measurement error of 20 μm and plotted on a 1 mm grid.

However, the grid points of the measured coordinates did not coincide. DS Match triangulated the data, interpolated new common grid points and calculated the sum of the squares of the differences. The fields were rotated and translated by an iteration process until the least squares solution was found. It is likely that the triangulation process has introduced some error into the interpolated points, which resulted in a higher RMS residuals value than would have occurred if the interpolated points were equal to the recorded points.

Examination of contour maps of the difference data (Appendix 4 and Fig. 4.8 above) gives visual support to the contents of Table 3.8. The maps demonstrate areas where data points have been excluded. These areas are:

Along the first, left hand profile (No 13 provides a good example of loss difference data along an entire left-hand profile),
Along the border of the antihelix (Nos. 5, 6 show loss in the middle region, nos. 7, 8 and 9 show loss in the superior region),

Along the border of the antihelix (Nos. 5, 6 show loss in the middle region, nos. 7, 8 and 9 show loss in the superior region), The inferior border of the concha, in the region of the antitragus has shown very little loss of points.

Therefore it is possible to conclude that a mean result of 80 um is consistent with the hypothesis that there is no movement in the concha region at all. A more conservative conclusion is that movement in the concha is not significant in clinical or manufacturing terms (refer 4.1).

4.4 Movement within the tragus/canal

4.4.1 Summary

Six of the impression pairs matched very well with a cut-off limit of 200 μm, a mean 81% of equations and an RMS residuals value of 86 μm.

Five impression pairs matched moderately well with a cut-off of 400 μm, a mean 85% of equations and RMS residuals value of 149 μm.

Three impression pairs matched with a cut-off of 400 μm, a mean 70% of equations and a mean RMS residuals of 142 μm.

This points to:

Movement in the anterior surface of the tragus/canal that is not clinically significant in 6 of the 14 ears (Nos. 5, 7, 10, 11, 12 and 14),
Increased distortion of the tragus/canal field when compared to the concha in a further 5 ears (Nos. 2, 3, 4, 8 and 9),
Increased distortion of the tragus/canal field in 3 ears. (Nos. 6 and 13).

The low % equations in impression no. 1 can be explained by a lack of overlap between the two fields.

4.4.2 Increased flexion at first bend

Distortion of the tragus/canal could occur in two general areas; within the body of the field and at the edges.

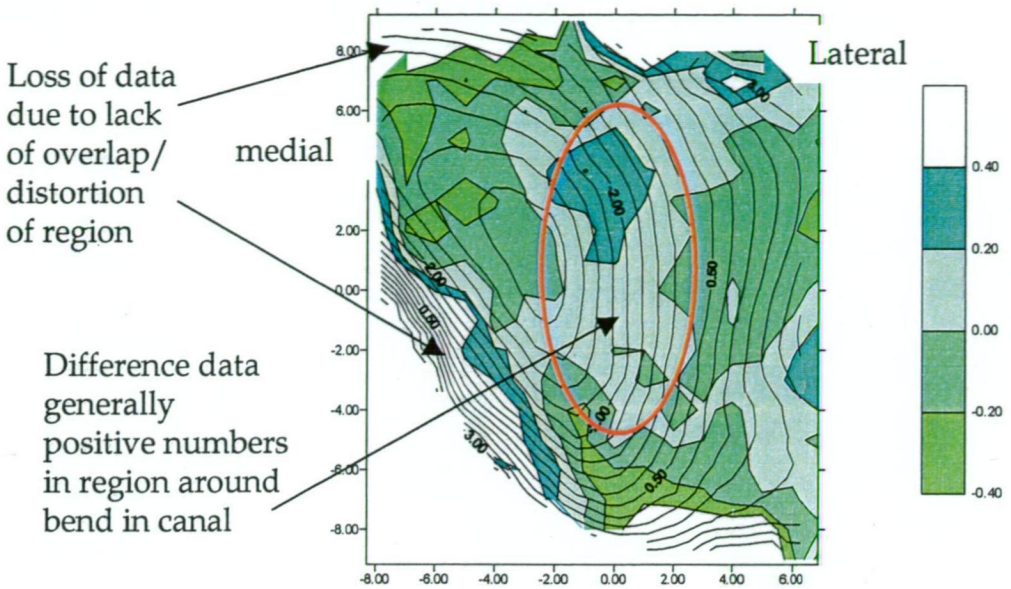

Fig. 4.9 Distortion of Tragus/canal, Loss of data. Impression no.8, DS Match difference data (400 μm cut-off limit) contour map overlaid with closed-jaw data contour map.

Fig. 4.9 shows loss of data due to distortion at the superior and inferior border of the tragus/canal. It also shows a central region near or around the bend in the canal were the difference data is positive, where the rest of the data is negative. This second feature is typical of the majority of tragus/canal difference-data contour maps (Appendix 5). The residual data in Fig 4.9 is based on a cut-off limit of 400 μm, however the same feature is seen in figure 4.8 above which is based on difference data with a cut-off limit of 200 μm.

Fig. 4.10 represents interpretation of the general form of Fig. 4.9. Where the form of the open-jaw impression data (red) passes above the closed-jaw impression data (black), the residual data is positive. Where the open-jaw data passes below the closed-jaw data, the residual data is negative.

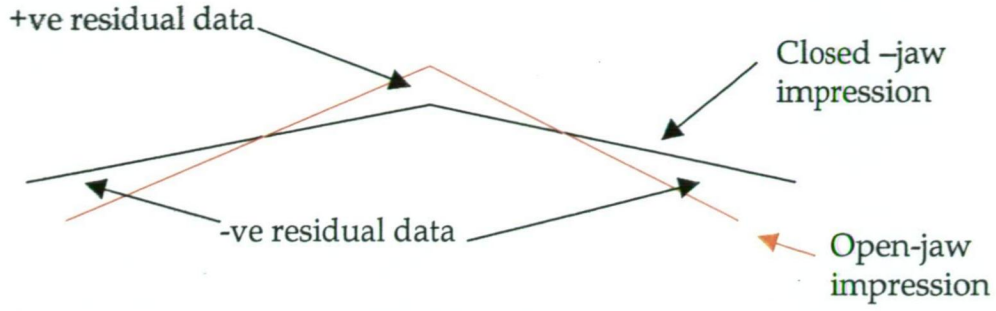

Fig. 4.10 Line drawing representing axial slice through anterior surface of tragus/canal. Increased flexion of canal leads to change in sign of difference data.

Increased flexion of the canal as described above can be seen in 9 of the 14 impressions (2 – 8, 11 and 14). Impression 9 and 10 do not show this feature clearly and are of the same subject.

This finding does seem to support the observation (Grenness 1990) that open-jaw and closed-jaw impressions can be readily identified due to an increased definition of the first bend in the canal.

However, Fig. 4.10 does not represent the movement that has occurred. Area matching has matched the surfaces over their entire surface. The medial aspect of the canal, on the other hand, is fixed as it merges into the bony part of the canal. When Fig. 4.10 is re-drawn such that the medial part of the canals coincide, two general possibilities arise (Fig. 4.11).

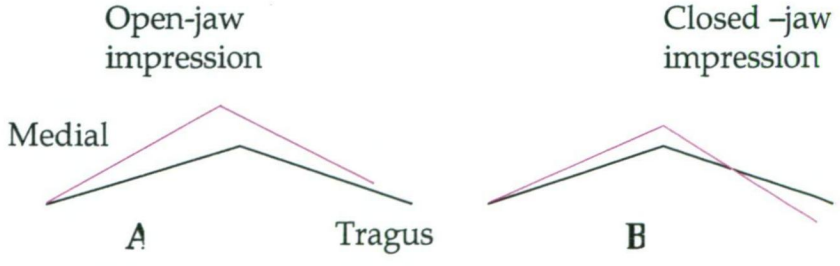

Fig. 4.11 Line drawing representing axial slice through anterior surface of tragus/canal. Left ends (medial) coincide.
A. Larger anterior movement at bend, small anterior movement in tragus. **B.** Smaller anterior movement at bend, posterior movement of tragus

Flexion at the bend in the canal may occur in conjunction with a larger anterior movement at the bend and a smaller anterior movement of the

tragus, or a smaller anterior movement at the bend and a posterior movement of the tragus.

If the difference-data map in Fig. 4.9 had a common factor of 400 μm added across the entire field, this would have the approximate effect of aligning the medial part of the canal into the same frontal plane. The region at the bend in the canal would now show differences up to +800 μm.

This is consistent with Oliveira (1997) who found that the average increase in A-P direction in adults was 0.7 mm.

4.4.3 Future direction

It would be worthwhile area-matching the medial part of the field in order to differentiate between these two general possibilities. However because of the essentially cylindrical nature of the canal in this region area-matching is likely to result in significant 'barrelling' and widely variant multiple solutions and was therefore not trialled. The most likely means of matching this portion of the canal would involve including data from surrounding anatomical structures nor directly a part of the external ear.

4.5 Movement of Tragus/canal relative to Concha

4.5.1 Summary

As noted in the results, mean absolute movement in the **S-I** direction was 1210 μm with a range of 0 to 3712 μm. If impressions where no demonstrable movement occurred in the S – I direction, i.e. Nos. 1, 5 and 12 are excluded from this analysis, the mean absolute value where demonstrable movement occurs was 1540 μm. 8 canals moved inferiorly, 3 ears move superiorly and 3 canals did not move in the S – I direction.

Mean absolute movement in the **M–L** direction was 1450 μm, with a range of 0 to 3839 μm. 9 canals moved laterally, 4 canals moved medially and 2 ears did not move in the M – L direction.

Movement in the **A-P** direction ranged from approx. –8.5 mm to +8.0 mm. Movement in 9 of the 14 ears occurred between approx. –3.0 mm and +3.5 mm.

Rotational parameters derived from DS Match did not correspond with the quantum or direction with the translations derived from manual

overlaying of contour maps. No conclusion was drawn from the rotation parameters.

Greater differences in the A-P direction were associated with the edges of the impression where the contour fell away steeply. Difference in the A-P direction does not necessarily represent the closest distance between the two surfaces. In the central region of the canal, i.e. in the centre of the plots, the A-P difference were taken as an approximation of the closest difference between the surfaces. At the edges of the canals, where the contour lines are closer together, as the slope of the surface becomes steeper, the closest difference between the two surfaces is more likely to be perpendicular to the surface. That is, as the contour lines come closer together, the direction of the closest difference between the surface will deviate from the z-axis (A-P) by increasing amounts.

Thus what appears to be movement in the A-P direction of 8 mm at the inferior border of an impression may a combination of approx. 3 mm A-P movement and 1.5 mm S-I movement and a mean absolute M-L movement of 1450 μm.

4.5.2 Direction of movements

As reported in the results, in general, upon opening, the canal moved in the A-P plane (z-axis):

Anteriorly in numbers:	1, 3, 5, 7, 9 and 13 (6 ears)
Posteriorly in numbers:	2, 6, 10 (3 ears)
Mixed in numbers:	4, 8, 11, 12 and 14(5 ears).

In the mixed group, ears 4, 11and 12 showed anterior movement lateral to the first bend and posterior movement medial to the first bend. Ear 8 showed the reverse.

A summary of the combinations of movements appears in table 4.1.

Move-ment	Inferior			Superior		No S - I
A-P	Ant	Mixed	Post	Ant.	Post	Ant
Lateral	13	4,11,14	2,6	3		
Medial	7	8		9	10	
No M - L		12				1,5

Table 4.1 Distribution of movements.

Movement of the tragus/canal inferiorly, laterally and in a mixed anterior/posterior is the most popular movement of the ears studied.

The sample size was not large enough to draw conclusions in this regard. However the distribution of movements of the ears studies does hint at trends.

Comparing the distribution of movement in Table 4.1 with the tragus/canal area-matching results in Tables 3.9. and 3.10 does not lead to the suspicion that there is a trend between those ears with an increased amount of distortion and direction of movement. In particular, there is no obvious trend between increased distortion and mixed A-P movement.

Each of the movements was recorded as movement of the tragus/canal relative to the concha. It is expected that a substantial component of the movement was a result of the concha moving relative to the tragus/canal. For example, it is not conceived that the tragus/canal region moves significantly in the S-I plane. It is more likely that it is the pinna as a whole that moves in the S-I -plane in these cases.

In the A-P direction, the absolute mean of the range of movement was 3.5 mm (Table 3.12). This figure combines both anterior, posterior and mixed movements, however gives a measure of the quantum of movement. As noted above in section 4.4.2, flexion in the tragus/canal may account for 0.7 mm average movement across the entire field. If movements are considered relative to the skull, up to 80% of the movement may be provided by the pinna and 20% or greater by the tragus/canal.

Posterior movement of the tragus relative to the concha will result in force being applied to the surface of an ITE hearing-aid if present. These findings do not show that the canal itself has narrowed in the A-P direction. However, while a CIC hearing-aid may not extend into the bowl of the concha, the cartilage that forms the concha also provides a portion of the posterior wall of the canal. Thus it is highly likely that anterior movement of the concha (and a portion of the posterior wall of the canal e.g. Fig. 4.12) is responsible for some CIC's continuously sliding out of the ear as described by Pirzanski, 1996.

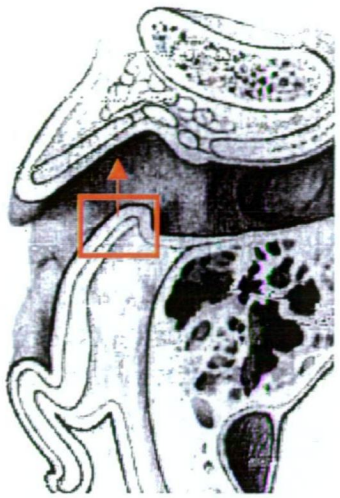

Fig. 4.12 Horizontal section through right ear. Anterior movement of part of concha that forms the posterior wall of the canal.
Source: Cropped from Cunningham's Textbook of Anatomy (1972).

Movements have also been shown in the S-I and M-L directions. These were of a smaller magnitude, approx. 1.5 mm , but are still of clinical significance. M-L movements may provide an additional mechanism for the dislodgment of hearing-aids.

This narrowing of the canal may only occur at its opening into the concha, however the canal continues to narrow the further one travels down the canal. As a consequence, CIC hearing-aids are, in effect, wedge shaped and pressure applied anywhere along its length will result in movement of the hearing-aid out of the canal unless there is a force or barrier counteracting it. The inclusion of the concha part to a hearing aid, i.e. ITE hearing-aid, can provide the necessary barrier to the ejection of CIC hearing-aids from the ear.

4.5.3 Quantum of movements

The quantum of movements are clearly significant when considering the fit and comfort of hearing-aids and easily explain associated problems of impression inaccuracies, acoustic feedback, the occlusion effect and discomfort during mandibular movement (section 1.4.4). They could be expected to affect the attenuation of sound by earplugs in excessive noise environments (section 1.4.2) which result from differences of 0.5 mm between the dimension of the ear canal and ear plugs.

Examination of the difference maps in Appendix 7 also gives insights into the likely effectiveness or ineffectiveness of applying a special wax build-up to the tragus region of impressions prior to the processing of earmoulds. Where the tragus has moved in a posterior direction relative to the concha upon jaw opening (nos, 2, 6, 8 and 10), it would be clearly counterproductive to add additional material to the surface of an earmould. Where the tragus region has moved in an anterior direction

upon jaw opening (numbers: 4, 5, 7, 9, 11 – 14), the addition of material to the mould in this region may be beneficial. These maps show that the distribution of material is likely to vary in both general thickness and distribution in both M-L and S-I directions.

Pereira et al (1996) studied age-related changes of the retro-discal tissues in the TMJ and found a reduced number of fibroblasts, lower distribution of vascular tissue and a higher presence of dense connective tissue. One might have concluded that greater movement with age was likely. However, while the sample size was not large enough to draw conclusions on this issue, the data gives no support to this hypothesis.

4.5.4 Symmetry

A review of the overlaid contour plots (Appendix 6) of left and right ears, subjects 5 to 8, demonstrates a degree of symmetry in both the direction and quantum of movement. The difference in movement between right and left ears in the same subject was approx. 100 to 1200 μm in the x-axis (S-I) and 440 to 1300 μm in the y-axis (M-L). In no case, was there movement in opposite directions between ears, although their was no movement in some cases.

None of the subjects studied had a history of TMJ dysfunction. No subject had a jaw deviation from the centre line upon opening, an indication of restricted joint mobility on the side to which the jaw deviates. If the sample size was increased or subjects selected who had a known history of TMJ dysfunction with a deviation it could be expected that greater asymmetry between the right and left ears might be found.

4.6 Two moments in time

The impressions only capture two moments in time. These two moments do not necessarily represent the two extremes of movement within the external ear. Movement may not have a linear form, but may consist of a circular or elliptical path, returning to a resting position. Even a resting position may change over the course of a day or longer as a subject's general state changes with the passage of time.

The taking of an impression, by way of filling and occluding the ear canal may result in changes in patient behaviour/resting state that may effect the dimensions of the ear canal. It would be advantageous to be able to capture the geometry of the canal at numerous intervals during mandibular and facial movements

The notion that condylar movement is the sole element responsible for movement of the canal is unlikely to be correct. All head and neck muscles, i.e. masticatory, facial, cervical, suprahyoid, infrahyoid, prevertibral, postvertibral will have some role to play. Most of these muscle groups have functions related to jaw motion, but most also have unrelated functions. Simple observation, as well as published reports (section 1.5.3) supports the idea that movement in the external ear can occur completely independently of jaw motion. Jaw motion and position has been extensively studied over very many years and because of its connection to dental hard tissues (teeth) is relatively easy to record. It is for this reason that it has been used to reference the two positions investigated in this and other studies.

4.7 Recent Developments

Recently, papers have been published describing the use CT and MR imaging as the primary data sources for the generation of surface maps and distance measurements.

4.7.1 CT Scanning

Viceconti et al (1999) trialled two algorithms to reconstruct the geometry of a human femur from CT data. They reported an average error comparable to a pixel (0.3 mm), with a peak error lower than 0.9 mm for the Standard Marching Cube algorithm. The other method tested, the Discretized Marching Cube, produced 70% less triangles and a peak error of 1.6 mm.

However, as noted in section 2.2, Malard et al (1997) found that CT scan measurements in the lateral portion of the external ear canal were not reliable, quantitative usefulness being limited to the bony meatus.

4.7.2 MR Imaging

McFall et al (1996) reported on MRI of human lung spaces in association with the inhalation of hyperpolarized nobles gas (He-3) at 20 mm and 6 mm sections. This study has some parallel with that of Oliviera (1992) who used an MRI enhancer fluid in the ear canal so that the canal space itself could be imaged.

Johnson GA et al (1996) reported on MR microscopy (MRM) that permitted in vivo studies down to 50 μm, and in vitro studies where there was an absence of motion, down to 10 μm. Smith BR et al (1998) used MRM to produce isotropic data sets of live, developing rat embryos in utero. Lester et al (1999) reported that high-resolution (<50 μm) MRM had been used to identify brain regions and localisation of lesions in fixed rat brains.

Kim et al (1999) reported on improved sensitivity and specificity of the functional MRI signal from a mapping-each-slice–to-volume method in comparison with a stacked-slice correction method, to overcome inter-slice head motion.

Chen and Ugurbil (1999) reported that the majority of recent studies achieved relatively low spatial resolution (typically with a voxel size of 3.1 x 3.1 x 5.0 mm3), which were incapable of mapping on the millimeter and sub-millimeter spatial scale. They found that high-resolution functional MRI (fMRI) at very-high-magnetic fields (3.0 and 4.0 Telsa) was promising for functional mapping of brain organisation.

In order for MRI to be used successfully to provide a surface map of the entire external ear, it will be necessary to combine series of slices taken in the:

Frontal plane:	concha region of pinna
Sagittal plane:	entire tragus/canal

The horizontal (axial) plane would give insufficient data from the concha for area-matching. In the regions of the concha which slope towards the horizontal, i.e the inferior border leading to the antitragus, the crus of the helix and the superior border leading to the antihelix, a 1 mm rate of (coordinate) sampling would be insufficient for these slopes.

The horizontal plane would also give insufficient data from the superior and inferior regions of the ear canal for the same reasons. While previous studies have not shown significant change in this area, this study has shown significant changes in the order of 1.5 mm between open and closed-jaw positions relative to the concha.

The acquisition of frontal and sagittal scout images and slices is likely to require alterations to the position/inclination of both imaging

equipment and patient. Use of methods such as that descibed by Kim et al (1999) above will be required to overcome interslice movements.

4.7.3 Laser scanning

Wilson et al (1997) described a laser scanning technique to accurately measure changes in facial volume

Coward et al (1997) tested the ability of two assessors to identify landmarks of the ears and face on laser scanned images on two separate occasions. The mean difference between the two sittings of 21 landmarks ranged between 0 and 0.85 mm in the x, y and z axes. The three dimensional mean differences between the two sittings of each landmark ranged between 1 and 2.5 mm.

Marjanovic et al (1998) developed an instrument that scanned a laser displacement sensor over a leg ulcer. Volume was calculated by subtracting the measured topograghy from one calculated using an algorithm to reconstruct a healthy leg surface.

4.7.4 Area matching and alignment

Dastane et al (1996) developed and evaluated a 3-D digitization and computer graphic system to study anatomic tissue and restoration surfaces. They used a profiler assembly for digitization (mechanical plotter), Surfer 3-D graphics package and a public domain data-fitting alignment software. Surfaces were digitized before and after rotation by angular displacement, the digital data were interpolated by Surfer to provide a data grid and the surfaces were computer graphically reconstructed: Misaligned surfaces were aligned by the data-fitting alignment software

Mehl et al (1997) reported on the use of a 3-D optical scanner that utilized the principles of triangulation and a reference-free automated 3-D superimposition software. Gypsum replica tooth surfaces were scanned with a resolution of 250,000 points within a measuring time of 20 to 30 seconds. The results showed that that the precision and accuracy of 3-D data acquisition was dependent upon the surface inclination. Up to 60 degrees, the precision was better than 3 μm, and the accuracy was better than 6 μm. In reference-free measuements the 3-D data acquisition in combination with the automatic matching program can detect tooth wear with an accuracy of 10 μm. If exact repositioning of the object is possible, differences on the surface can be determined with a precision of 2.2 μm.

4.8 Future Directions

Mapping of the entire tissue surface of ear impressions or the actual external ear, together with cranial reference areas remains a valuable project for study.

Two methods present themselves, subject to meeting accuracy requirements:

1. Direct imaging with MRI.

- Imaging the entire external ear (pinna and canal).
- Including an adjacent structure suitable for area-matching.
- Frontal and Sagittal slices.

2. Indirect surface mapping of ear impression.

- Ear impression beyond the second bend.
- Impression referenced to cranium (maxilla).
- Laser scanning of several connected views.

The quantum, direction and combination of movements demonstrated in this study point to the need for a protocol and method of clinical evaluation and/or technique that aids clinicians and hearing-aid users.

Further study is required to determine whether correlations exist between specific patterns of movement and specific clinical problems.

Chapter 5 – Conclusion

The movement of the external ear canal, associated with jaw motion, relative to the concha region of the pinna has been studied. This issue is most relevant to the fitting and function of In-The-Ear hearing aids and the sound attenuation of earplugs. It may also be relevant to ear canal collapse during audiometry and acoustic models of the ear.

5.1 Method

Pairs of open-jaw and closed-jaw silicone impressions were taken of 14 ears from 10 subjects. 3D coordinate data was obtained from the concha region and the anterior surface of the tragus/canal using a Reflex microscope. The canal fields were plotted via an optical flat mirror. Mathematical manipulation of the observational data was expected to, and did, introduce error into subsequent results. In order to achieve accuracy in the order of 100 μm in the ear impression maps, it was necessary to achieve accuracy in data collection in the order of 30 μm. This level of error was achieved with the Reflex microscope.

Proprietary area-based matching software was used to verify the stability of the concha region and evaluate distortion of the tragus/canal region during jaw motion.

The canal data from each pair was placed into the same coordinate system with their respective concha regions aligned using parameters deirved from the area-matching software. Contour and difference maps of the canal data were used to demonstrate the amount of anterior-posterior (A-P), superior-inferior (S-I), and medial-lateral (M-L) movement that occurred between the open and closed-jaw impressions. Rotations were also evaluated.

5.1.1 Data collection

No single orientation of slicing will provide adequate surface data to allow reliable alignment of the concha regions and analysis of the canal region. Either the object requires physical or optical transposition, or the recording system requires physical or optical transposition.

Recording systems ulitizing MRI or laser scanning have been considered and warrant further investigation.

5.1.2 Alignment of impressions

There was less error in the manual of alignment of the impressions with a register where there was not significant movement in the intertragic notch region in the S-I and M-L planes.

Area-based matching has been found to be a reliable method of enhancing the alignment of coordinate data, within the accuracy and precision requirements.

5.2 Movement and distortion

5.2.1 Quantum significance

Biological, clinical, manufacturing and material science issues affecting the quantum of movement and distorton were considered. It was concluded that changes of the order of 200 μm or less were of no clincical significance.

5.2.2 Changes within the concha

The concha regions of 13 out of 14 open and closed-jaw impression datasets conformed, with a mean RMS of residuals of 78 μm. This confirmed that the mapped concha regions did not undergo clinically significant deformation during jaw movement.

5.2.3 Changes within the tragus/canal

The canal regions underwent varying amounts of internal deformation with the majority of canals conforming within an RMS of 149 μm across the entire surface.

The tragus/canal region generally underwent greater deformation than the concha regions. However, the level of deformation was in itself not clinically significant.

Movement of the tragus/canal relative to the bony meatus could not be evaluated. The most likely means of matching this portion of the canal would involve including data from surrounding bony anatomical structures not directly a part of the external ear. However, the above finding is consistent with Oliveira (1997) who found that the average increase in A-P direction in adults was 0.7 mm.

5.2.4 Movement of tragus/canal relative to concha

The majority of canals underwent significant morphologic change relative to the concha.

- Movement of the canal in the M-L plane ranged from 0 to 3.8 mm with a mean of 1.4 mm; 8 canals moved laterally, 5 canals moved medially and 2 ears did not move in the M-L plane.
- Movement in the S-I plane ranged from 0 to 3.7 mm with a mean of 1.3 mm; 9 canals moved inferiorly, 2 canals moved superiorly and 3 canals did not moved in the S-I plane.

- Movement in the A-P plane ranged between +3 mm and –3.5 mm, with 5 canals moving anteriorly, 3 ears moved posteriorly, and 4 ears moving in a mixed fashion.

This study has demonstrated a range of movement combinations in the 3 dimensions. Most significantly, the tragus/canal has moved:

Anteriorly in 5 cases,
Posteriorly in 3 cases, and
A combination of anterior and posterior in 4 cases.

Thus, narrowing or partial narrowing of the ear canal has occurred during jaw opening in 9 out of 14 ears studied. This study does not support previous reports that suggest that the ear canal only widens with jaw opening.

5.3 Clinical implications

5.3.1 Hearing-aid fitting

The movements are clearly clinically significant and help explain the problems of fit, comfort, acoustic feedback, occlusion effect and dislodgment of hearing-aids.

The narrowing of the canal may only occur at its opening into the concha, however the canal continues to narrow the further one travels medially. As a consequence, CIC hearing-aids are, in effect, wedge shaped and pressure applied anywhere along their length will result in movement of the hearing aid out of the canal unless there is a force or barrier counteracting it. The inclusion of the concha part to a hearing aid, i.e. ITE hearing-aid, can provide the necessary barrier to the ejection of CIC hearing-aids from the ear.

Smaller movements have also been shown in the S-I and M-L directions. These were of a smaller magnitude, approx. 1.5mm , but are still of clinical significance. M-L movements may provide an additional mechanism for the dislodgment of hearing-aids.

This study gives insights into the variability in the movements of the ear canal relative to the concha region of the pinna and will be of interest to clinicians involved in the fitting of hearing-aids.

5.3.2 Hearing-aid manufacture

The distribution of movement that has occurred gives insights into the more effective application of special wax build-ups prior to hearing-aid shell manufacture. It is concluded that the application of special wax build-ups to the anterior wall of the tragus/canal are likely to be random in their effect.

Ultimately, decisions about special wax build-ups can only be clinically based. Manufacturers can take no responsibility for the fit and comfort of hearing-aids, other than ensuring that the hearing-aid conforms to the impression supplied by the clinician within the specified standard, e.g. 150 μm.

There is the potential for more successful retention of CIC hearing-aids by changing their essentially wedge shape, particularly at the opening of the ear canal where the cartilaginous posterior wall may impinge upon the CIC during jaw opening. Because of limited space availability within these hearing-aids an alteration of shape in this region may not be easily achieved. Some work in this area may provide more satisfactory outcomes for hearing-aid users.

5.4 Future Directions

5.4.1 Mapping morphologic change in the external ear

Mapping of the entire tissue surface of ear impressions or the actual external ear, together with cranial reference areas remains a valuable project for study.

Two methods present themselves, subject to meeting accuracy requirements:

1. Direct imaging with MRI.
- Imaging the entire external ear (pinna and canal)
- Including an adjacent structure suitable for area-matching
- Frontal and Sagittal slices

2. Indirect surface mapping of ear impression
- Ear impression beyond the second bend
- Impression referenced to cranium (maxilla)
- Laser scanning of several connected views

5.4.2 Clinical evaluation of movement

The quantum, direction and combination of movements demonstrated in this study point to the need for a protocol and method of clinical evaluation and/or technique that aids clinicians and hearing-aid users.

Further study is required to determine whether correlations exist between specific patterns of movement and specific clinical problems.

5.5 Finale

Further detailed study of morphologic change in the external ear, especially the posterior wall, related to jaw and facial movements should yield further insights into the problems associated with the wearing of hearing-aids.

References

Abel, S.M., Rockley, T., Goldfarb, D. and Hawke, M. (1990) Outer ear canal shape and its relation to the effectiveness of sound attenuating earplugs. J. Otolarngol. 19(2): 92-95.

Anson, B.J. and Donaldson, J.A.(Ed) (1967) The surgical anatomy of the temporal bone and ear. W.B. Saunders, Philadelphia. pp 16-48.

Babbington, A.G. (1975) Some observations on some types of materials and unusual earmould designs. In: Scand. Audiol. Suppl.5: 255-259.

Battagel, J.M. and Ryan, A. (1998) Spontaneous lower arch changes with and without second molar extractions. Am. J. Orthod. Dentofacial Orthop. 113(2): 133-143.

Bezzobs, T. and Sanson, G. (1997) The effects of plant and tooth structure on intake and digestibility in two small animals. Physiol. Zool. 70(3): 338-351.

Boothroyd, A. (1965) The provision of better earmoulds for deaf children. J. Larngol. Otol. 79: 320-335.

Chen, W. and Ugurbil, K. (1999) High spatial resolution functional magnetic resonance imaging at very-high-magnetic field. Top. Magn. Reson. Imaging 19(1): 63-78.

Creston, J.E. (1965) Collapse of the ear canal during routine audiometry. J. Otolarngol. Otol. 79:893-901.

Coward, T.J., Watson, R.M. and Scott, B.J.J. (1997) Laser scanning for the identification of repeatable landmarks of the ears and face. B. J. Plast. Surg. 50: 308-314.

Cunningham's Textbook of Anatomy, 11th Edition, Edited by G.J.Romanes, Oxford University Press, London (1972)

Dastane, A., Vaidyanathan, T.K., Vaidyanathan, J., Mehra, R. and Hesby, R. (1996) Development and evaluation of a new 3-D digitization and computer graphic system to study the anatomic tissue and restoration surfaces. J. Oral Rehabil. 23(1): 25-34.

Egolf, D.P., Nelson, D.K., Howell, H.C. and Larson, V.D. (1993) Quantitative ear-canal geometry with multiple computer-assisted tomographic scans. J. Acoust. Soc. Am. 93(5): 2809-2819.

Feneis, H. (1976) Pocket Atlas of Human Anatomy, Georg Thieme Publishers, Germany

Fifield, D.B., Earnshaw, R. and Smither , M. (1980) A new impression technique to prevent acoustic feedback with high powered hearing aids. In: Volta review, 82(1): 33-39.

Fryer, J.G., McIntosh, K.L. and Oh, W.-J. (1998) A resolution enhancement algorithm for digital photogrammetry: Precision and accuracy. The Australian Surveyor. 43(1): 47-52.

Grenness, S.K. (1990) Personal communication. Tasmanian Centre for Hearing. Hobart.

Greener. E.H., Harcourt, J.K. and Lautenschlager, E.P. (Ed.) (1972) Materials science in dentistry. Williams and Watkins. Baltimore.

Hawke, M., Kwok P., Mehta, M. and Wang R-G. (1987) Bilateral spontaneous temporomandibular joint herniation into the external auditory canal. J. Otolaryngol. 16(6): 387-389.

Harvey, B.R. (1995) Practical least squares. The School of Geometric Engineering, University of NSW, Sydney.

Heffez, L., Anderson, D. and Mafee, M. (1989) Developmental defects of the tympanic plate: Case reports and review of the literature. J. Oral Maxillofac. Surg. 47: 1336-1340.

Johnson, G.A., Benveniste, H., Black, R.D., Hedlund, L.W., Maronpot, L.W. and Smith, B.R. (1993) Histology by magnetic resonance microscopy. Magn. Reson. 9(1): 1-30.

Juneau, R.P. (1983) NAEL: Fitting Facts, Part 1: The ear impression. Hearing Instruments, 34(3): 6-7,49.

Kamel, H.A., Kunov, H. and Abel, S.M. (1986) Morphology of the ear canal. (unpublished) Int. Soc. of Photogrammetry and Remote Sensing. Commission 5 Congress, Toronto.

Katz, J. (Ed.) Handbook of Clinical Audiology, 3rd edition, Williams and Watkins, Baltimore (1985)

Killion M.C. (1982) Transducers, earmolds and sound quality considerations. In: The Vanderbilt hearing Aid report. Edited by Sutebaker G.A. and Bess F.H., Pennsylvannia.: Monographs in contemporary audiology.

Kim, B., Boes, J.L., Bland, B.H., Chenevert, T.L. and Meyer, C.R. (1999) Motion correction in fMRI via registration of individual slices into an anatomic volume. Magn. Reson. Med. 41(5): 964-972.

Kokot-Schmidt, M. (1979) Comparative morphometric analysis of the external auditory canal – a study of men with normal hearing and men equipped with hearing aids, Doctoral dissertation, Jahannes Gutenberg University, Mainz.

Lear, A. and Earnshaw, R. (1987) Dimensional accuracy of ear impression materials. Austral. J. Audiol. 9: 55-65.

Lybarger, S.F. (1982) Acoustic feedback control. In: The Vanderbilt hearing-aid report. Edited by Studebaker, G.A. and Bess. F.H., Pennsylvannia.: Monographs in contemporary audiology, 87-90.

Malard, O., Bourdure, P., Gayyet-Delacroix, M., Robert, R. and Legant, F. (1997) Radio-anatomical study of the external auditory canal. Comparison between anatomical pieces and x-ray computed tomography. Ann Otolarngol Chir Cervicofac. 114(3): 59-64.

Marjanovic, D. Dugdale, R.E., Vowden, P. and Vowden, U.K. (1998) Measurement of the volume of a leg ulcer using a laser scanner. Physiol. Meas. 19(4): 535-543.

McHugh, M.A. and Purnish, M.A. (1984) Evaluating the accuracy of earmold impression materials. Hearing instruments. 35(12): 12, 15, 60.

Macrae, J. (1989) Ear Impression and ear mould technology. NAL Audiology Circular, 1989/5. National Acoustic Laboratories, Sydney.

Macrae, J (1988) The acoustic seal of earmoulds. Doctoral dissertation. Macquarie University, Sydney.

MacFall, J.R., Charles, H.C., Black, R.D., Middleton, H., Swartz, J.C., Saam, B., Driehuys, B., Erickson, C., Happer, W., Cates, G.D., Johnson, G.A. and Ravin, C.E. (1996) Human lung air spaces: potential for MR imaging with hyperpolarized He-3. Radiology 200(2): 553-558.

Mehl, A., Gloger, W., Kunzelmann, K.-M. and Hickel, R. (1997) A new optical 3-D device for detection of wear. J. Dent. Res. 76(11): 1799-1807.

Morgan, R. (1987) The Foundation- a good impression. Hearing Instruments 38(4): 20-57.

Neame, J.H. (1988) Mobility of the Tragus. J. Laryngol. Otol. 102: 252-253.

Neilson, A. and Pitt, N.B. (1993) Development and application of a quantitative method of monitoring macroscopic cavitation in smooth surface carious lesions in vivo. Caries Res. 27(2): 140-146.

Oliviera, R.J., Hammer, B., Stillman, A., Holm, J., Jons, C. and Margolis, R.H. (1992) A look at ear canal changes with jaw motion. Ear and Hearing 13(6): 464-466.

Oliviera, R. (1997) The active earcanal. J. Am. Acad. Audiol. 8: 401-410.

Owman-Moll, P. Katsaros, C. and Friede, H. (1998) Development of the residual cleft in the hard palate after velar repair in a 2-stage palatal repair regimen. J. Orofac. Orthop. 59(5): 286-300.

Owen, C.P., Wilding, R.J. and Adams, L.P. (1992) Dimensions of the temporal glenoid fossa and tooth wear in prehistoric human skeletons. Arch. Oral. Biol. 37(1): 63-67.

Parslow, J (1994) Personal communication. CSIRO. Hobart

Pirzanski, C.Z. (1996) An alternative impression-taking technique: The open-jaw impression. The Hearing Journal 49(11): 30-33.

Pither, D. (1988) Personal communication. Audiogene P/L. Melbourne

Scott, P.J. (1981) The reflex plotters: measurement without photographs. Photogrammetric Record. 10(58): 435-446.

Shearer, B., Gough, M.B. and Setchell, D.J. (1996) Influence of marginal configuration and porcelain addition on the fit of In-Ceram crowns. Biomaterials 17(19): 1891-1895.

Skinner, M.W. (1988) Hearing Aid Evaluation. Prentice Hall, New Jersey.

Smith, C.R., Borton, T.E., Patterson, L.B., Mozo, B.T. and Camp, R.T.Jnr. (1980) Insert hearing protector effects. Ear and Hearing 1(1): 263-2.

Speculand, B., Butcher, G.W. and Stephens, C.D. (1988) Three-dimensional measurement: The accuracy and precision of the reflex microscope. B. J. Oral Maxillofac. Surg. 26:276-283.

Stinson, M.R. and Lawton, B.W. (1989) Specification of the geometry of the human ear canal for the prediction of sound-pressure level distribution. J. Acoust. Soc. Am. 85(6): 2492-2503.

Sullivan, E.J. (1975) Anatomy of the ear. Hearing Aid Journal, Feb: 10-32.

Van Willigan, J. (1976) Some morphological aspects of the meatus acusticus externus in connection with mandibular movements. J. Oral Rehab. 3: 299-304.

Ventry, I., Chaiklin, J. and Boyle, W. (1961) Collapse of the ear canal during audiometry. Arch Otolarngol 73: 727-731.

Viceconti, M., Zannoni, C. Tsti, D. and Cappello, A. (1999) CT data sets surface extraction for biomechanical modeling of long bones. Comput Methods Programs Biomed. 59(3): 159-166.

Wilkinson, T.M. and Crowley, C.M. (1994) A histologic study of retrodiscal tissues of the temporomandibular joint in the open and closed position. J. Orofac. Pain 8(1): 7-17.

Wilson, I., Snape, L., Fright, R. and Nixon, M. (1997) An investigation of laser scanning techniques for quantifying changes in facial soft-tissue volume. NZDJ. 93:110-113.

Wood-Jones, F. and I-Chuan, W. (1934) The development of the external ear. J. Anat. (Lond) 68: 525-533.

Zemplenyl, J., Gilman, S. and Dirks, D. (1985) Optical method for measurment of ear canal length. J. Acoust. Soc. Am. 78(4): 2146-2148.

Appendices

Appendix 1 - Mirror Transformation Equations (Parslow, 1994)

For any point there is a reflected point. The line connecting these two points passes normal to the surface of the mirror, the plane of reflection or origin. The distance of each reflected point form the origin is the same as the (direct) point. Thus x,y,z, unit vectors are used to describe the direction each point must travel to produce its reflection and a constant (a) is derived to determine the distance of the point from the origin. The unit vectors are constant so long as the mirror is not moved. The constant (a) varies for every point.

If for an object there is a point: (X, Y, Z),
Then, there is a reflection: (Xr, Yr, Zr),
Difference vectors may be calculated: (X-Xr, Y-Yr, Z-Zr),
The length of the vector is:
l = sqrt((X-Xr)** + (Y-Yr)** + (Z-Zr)**),
Unit Vectors are calculated:
(xi, yi, zi) = ((X-Xr)/l, (Y-Yr)/l, (Z-Zr)/l)
The plane of reflection equals:
=((X+Xr)/2, (Y+Yr)/2, (Z+Zr)/2)
The distance of origin from mirror (a):
a = (X+Xr) * xi /2 + (Y+Yr) * yi /2 + (Z+Zr) * yi /2
Then for any point on the object: (X1, Y1, Z1),
Then the reflected point: (Xr1, Yr1, Zr1),
Is given by: Xr1 = X1 – b * xi
Yr1 = Y1 – b * yi
Zr1 = Z1 – b * zi
Where b = ((X1*xi + Y1*yi + Z1* zi) – a) *2

Only one pair of points is required to derive x,y,z unit vectors. Use of several points should increase the accuracy of the method. The sum of the squares of the vectors or any one point equal approximately 1. However the sum of the squares of average vectors averaged over a number of coordinate pairs may not. In order to correct for this error new unit vectors were calculated:

x_I = average x_I / average l
y_i = average y_i / average l
z_I = average z_I / average l
where l = sqrt (average x_I^2 + average y_i^2 + average $z_i^{2)}$
In this case l = 0.99999998

These equations were programmed into an Excel spreadsheet and applied to the data files from the brass block to determine the mirror transformation. The parameters derived were used to transform data recorded via the mirror into the 'direct' coordinate system.

Appendix 2
Concha Fields
DS Match Solutions: Parameters

Input files: mm unit
Output files: μm units

No.	Cut Off	Tx	Ty	Tz	Kappa	Omega	Phi	Resid	SD x	SD y	SD z	SD Kap	SD Om	SD Phi	Pts	Eqs	%
1	100	-586	4576	-765	0.031	2.420	-1.542	52	181	138	73	0.210	0.076	0.151	442	56	13
	200	-1777	2586	1146	0.570	1.507	2.040	102	142	65	79	0.101	0.078	0.183	442	202	46
	300	-1318	2374	1044	0.594	1.216	1.501	148	183	87	96	0.137	0.104	0.229	442	268	61
	400	-1766	3077	860	1.978	2.801	2.810	195	219	104	124	0.162	0.131	0.276	442	292	66
	500	-1696	3682	973	-0.800	1.462	2.073	195	210	89	113	0.141	0.112	0.244	442	390	88
2	100	2175	-678	-2497	-0.091	-2.513	-4.623	44	45	40	58	0.118	0.095	0.097	237	137	58
	200	2368	-383	-2770	-0.898	-2.602	-5.035	71	59	50	74	0.126	0.093	0.124	237	177	75
	300	2540	-64	-3036	-1.694	-1.817	-5.359	99	70	60	84	0.146	0.111	0.145	237	206	87
	400	2514	-65	-3002	-0.948	-1.694	-5.304	105	75	68	91	0.167	0.120	0.156	237	207	87
3	100	-477	365	-94	0.076	-1.024	0.627	51	12	21	11	0.072	0.029	0.062	380	287	76
	200	-272	87	-189	-0.869	-1.284	0.758	64	9	17	15	0.058	0.033	0.073	380	334	88
	300	-265	36	-176	-1.096	-1.296	0.721	82	10	18	17	0.062	0.036	0.083	380	353	93
	400	-277	59	-172	-1.015	-1.275	0.725	89	11	19	19	0.065	0.039	0.089	380	356	94
4	100	683	2713	-2127	-3.788	-0.053	-1.244	52	52	97	67	0.129	0.098	0.108	283	122	43
	200	539	3060	-1907	-4.470	0.068	-0.879	91	69	124	94	0.282	0.133	0.150	283	181	64
	300	590	3060	-1935	-4.412	0.012	-0.933	127	86	167	117	0.367	0.160	0.189	283	211	75
	400	665	2196	-2059	-2.504	0.112	-1.172	164	103	145	137	0.331	0.163	0.224	283	235	83
5	100	430	188	-349	0.470	-0.203	1.737	48	29	7	22	0.046	0.036	0.074	319	220	69
	200	425	207	-314	0.521	0.136	1.834	73	36	8	30	0.056	0.048	0.099	319	252	79
	300	349	227	-289	0.667	-0.094	1.874	80	41	9	32	0.067	0.052	0.105	319	275	86
	400	339	233	-301	0.689	-0.181	1.829	85	44	10	34	0.071	0.055	0.111	319	277	87

Appendix 2 - continued **Input files: mm units** **Notes: ** denotes**
Concha Fields **Output files: μm units** **non-convergence**
DS Match Solutions: Parameters

No.	Cut Off	Tx	Ty	Tz	Kappa	Omega	Phi	Resid	SD x	SD y	SD z	SD Kap	SD Om	SD Phi	Pts	Eqs	%
6	100	610	71	-739	-1.769	-1.192	-0.756	49	26	16	25	0.064	0.054	0.078	236	170	72
	200	660	48	-780	-1.857	-1.405	-0.985	75	34	20	33	0.081	0.069	0.080	236	215	91
	300	679	23	-820	-1.912	-1.428	-0.797	73	38	22	38	0.092	0.081	0.114	236	222	94
**	400	695	10	-827	-1.962	-1.525	-0.919	88	37	22	37	0.089	0.078	0.090	236	223	94
7	100	1939	905	2096	-0.902	1.761	5.274	50	79	11	37	0.142	0.060	0.085	301	163	54
	200	1213	1021	2226	0.178	2.028	4.662	87	93	14	41	0.156	0.067	0.120	301	250	83
	300	872	958	2341	0.960	2.198	4.837	110	95	15	45	0.161	0.075	0.136	301	277	92
	400	796	940	2334	1.070	2.201	4.692	120	99	16	47	0.169	0.080	0.146	301	283	94
8	100	-3923	-930	-378	5.431	-0.048	-1.848	51	55	13	30	0.097	0.051	0.074	314	216	69
	200	-4133	-963	-282	5.874	0.113	-1.720	73	70	17	39	0.129	0.065	0.097	314	256	82
	300	-4252	-945	-271	6.141	0.151	-1.746	90	75	22	45	0.135	0.075	0.118	314	209	67
	400	-3991	-955	-349	5.571	0.078	-1.948	102	88	20	49	0.158	0.079	0.128	314	274	87
9	100	32	272	-1871	-6.378	0.321	14.164	53	72	82	89	0.300	0.174	0.262	254	46	18
	200	-808	127	1985	-5.582	-5.240	2.240	87	30	33	45	0.141	0.092	0.163	254	219	86
	300	-864	71	1928	-5.997	-5.416	2.090	108	34	36	50	0.149	0.101	0.180	254	239	94
	400	-978	2	2133	-6.227	-5.817	1.558	118	37	37	50	0.153	0.097	0.185	254	248	98
10	100	512	488	492	2.634	1.266	-1.558	48	17	30	24	0.122	0.080	0.093	234	104	44
	200	1028	1121	67	4.812	2.134	-0.450	77	23	35	24	0.129	0.087	0.118	234	197	84
	300	1003	1087	85	4.718	2.084	-0.465	84	24	35	34	0.133	0.094	0.125	234	200	85
	400	1009	1093	96	4.735	2.076	-0.508	87	24	36	36	0.137	0.097	0.130	234	202	86

Appendix 2 - continued **Input files: mm units**
Concha Fields **Output files: μm units**
DS Match Solutions: Parameters

No.	Cut Off	Tx	Ty	Tz	Kappa	Omega	Phi	Resid	SD x	SD y	SD z	SD Kap	SD Om	SD Phi	Pts	Eqs	%
11	100	-340	38	-1096	0.127	2.892	-0.048	47	14	20	25	0.070	0.040	0.090	262	170	65
	200	-341	52	-1054	0.170	2.881	-0.168	77	17	29	24	0.099	0.056	0.098	262	211	81
	300	-397	13	-985	0.040	2.711	-0.299	106	25	36	38	0.122	0.071	0.144	262	230	88
	400	-425	-56	-963	-0.078	2.583	-0.278	116	26	38	40	0.132	0.075	0.159	262	235	90
12	100	992	562	-578	1.793	-0.677	3.186	50	25	23	35	0.088	0.055	0.161	206	136	66
	200	1073	565	-613	1.741	-0.749	3.380	70	31	33	41	0.126	0.071	0.174	206	169	82
	300	1079	478	-647	1.585	-0.710	3.476	96	34	38	48	0.119	0.085	0.209	206	174	84
	400	1172	637	-721	2.250	-0.450	3.553	109	33	38	51	0.150	0.093	0.223	206	187	91
13	100	1008	-1604	-610	-3.336	-0.512	1.798	47	20	22	23	0.084	0.043	0.096	270	141	52
	200	1465	-1437	-853	-1.889	-0.177	2.368	90	33	40	41	0.161	0.068	0.166	270	215	80
	300	1100	-1578	-536	-2.897	-0.485	1.348	116	27	35	45	0.042	0.071	0.180	270	236	87
	400	1446	-1418	-822	-1.775	-0.072	2.139	122	38	47	51	0.188	0.080	0.213	270	242	90
14	100	-166	471	-174	-0.323	-0.640	0.436	47	26	26	16	0.095	0.032	0.069	321	215	67
	200	-333	459	-34	-0.695	-0.851	0.094	73	26	20	24	0.075	0.047	0.086	321	286	89
	300	-260	460	-77	-0.423	-0.683	0.029	96	23	27	31	0.116	0.056	0.132	321	304	95
	400	70	646	-102	0.202	-0.628	-0.020	98	26	28	30	0.097	0.054	0.128	321	307	96

Appendix 2 - continued **Input files: mm units**
Concha Fields **Output files: μm unit**
DS Match Solutions: Statistics

		Impression number													
Cut Off	1	2	3	4	5	6	7	8	9	10	11	12	13	14	Mean (2:14)
		% Equations included in solution													
100	13	58	76	43	69	72	54	69	18	44	65	66	52	67	58
200	46	75	88	64	79	91	83	82	86	84	81	82	80	89	82
300	61	87	93	75	86	94	92	67	94	85	88	84	87	95	87
400	66	87	94	83	87	94	94	87	98	86	90	91	90	96	90
		RMS Residual value													
100	52	44	51	52	48	49	50	51	53	48	47	50	47	47	49
200	102	71	64	91	73	75	87	73	87	77	77	70	90	73	78
300	148	99	82	127	80	73	110	90	108	84	106	96	116	96	97
400	195	105	89	164	85	88	120	102	118	87	116	109	122	98	108
		Spread 200 - 400													
Tx	459	171	12	126	87	35	417	261	169	25	84	99	365	403	173
Ty	703	319	51	865	26	37	81	18	125	34	108	158	160	186	167
Tz	285	266	17	152	25	47	115	78	205	30	92	107	317	68	117
Kappa	1.41	0.80	0.23	1.97	0.17	0.11	0.89	0.57	0.64	0.09	0.25	0.66	1.12	0.90	0.65
Omega	1.59	0.91	0.02	0.10	0.32	0.12	0.17	0.07	0.58	0.06	0.30	0.30	0.41	0.22	0.28
Phi	1.31	0.32	0.04	0.29	0.05	0.19	0.18	0.23	0.68	0.06	0.13	0.17	1.02	0.11	0.27

Appendix 2 - continued **Input files: mm units**
Concha Fields **Output files: μm unit**
DS Match Solutions: Parameters

No.	Cut Off	Tx	Ty	Tz	Kappa	Omega	Phi	Resid	SD x	SD y	SD z	SD Kap	SD Om	SD Phi	Pts	Eqs	%
1	200	-1777	2586	1146	0.570	1.507	2.040	102	142	65	79	0.101	0.078	0.183	442	202	46
2	200	2368	-383	-2770	-0.898	-2.602	-5.035	71	59	50	74	0.126	0.093	0.124	237	177	75
3	200	-272	87	-189	-0.869	-1.284	0.758	64	9	17	15	0.058	0.033	0.073	380	334	88
4	200	539	3060	-1907	-4.470	0.068	-0.879	91	69	124	94	0.282	0.133	0.150	283	181	64
5	200	425	207	-314	0.521	0.136	1.834	73	36	8	30	0.056	0.048	0.099	319	252	79
6	200	660	48	-780	-1.857	-1.405	-0.985	75	34	20	33	0.081	0.069	0.080	236	215	91
7	200	1213	1021	2226	0.178	2.028	4.662	87	93	14	41	0.156	0.067	0.120	301	250	83
8	200	-4133	-963	-282	5.874	0.113	-1.720	73	70	17	39	0.129	0.065	0.097	314	256	82
9	200	-808	127	1985	-5.582	-5.240	2.240	87	30	33	45	0.141	0.092	0.163	254	219	86
10	200	1028	1121	67	4.812	2.134	-0.450	77	23	35	24	0.129	0.087	0.118	234	197	84
11	200	-341	52	-1054	0.170	2.881	-0.168	77	17	29	24	0.099	0.056	0.098	262	211	81
12	200	1073	565	-613	1.741	-0.749	3.380	70	31	33	41	0.126	0.071	0.174	206	169	82
13	200	1465	-1437	-853	-1.889	-0.177	2.368	90	33	40	41	0.161	0.068	0.166	270	215	80
14	200	-333	459	-34	-0.695	-0.851	0.094	73	26	20	24	0.075	0.047	0.086	321	286	89
	Mean	79	468	-241	-0.171	-0.246	0.581	78	48	36	43	0.123	0.072	0.124			82
	Absolute Mean	1174	865	1016	2.152	1.513	1.901										

Appendix 3
Tragus/canal Fields
DS Match Solutions: Parameters

Input files: mm units
Output files :μm units

Imp No.	Cut Off	Tx	Ty	Tz	Kappa	Omega	Phi	Resid	SD x	SD y	SD z	SD Kap	SD Om	SD Phi	Pts	Eqs	%
1	100	273	577	4536	-0.514	1.371	-3.519	47	13	8	4	0.128	0.088	0.083	619	285	46
	200	94	1006	4615	-6.358	2.448	-3.102	81	7	5	5	0.022	0.096	0.095	619	396	64
	300	-67	743	4600	-4.678	1.541	-2.799	104	8	9	7	0.020	0.147	0.125	619	396	64
	400	-255	593	4650	-0.772	1.810	-1.453	123	4	8	7	0.010	0.152	0.065	619	408	66
	500	322	777	4628	-0.759	2.947	-1.865	144	5	7	8	0.010	0.142	0.079	619	453	73
2	100	408	894	-4968	-14.973	-10.476	18.038	47	8	35	22	0.318	0.489	0.267	195	35	18
	200	85	1016	-4687	-9.860	-6.408	22.846	97	71	38	43	0.515	0.337	0.367	195	86	44
	300	2867	1439	-6043	-5.707	-1.145	10.674	141	11	16	14	0.174	0.202	0.176	195	189	97
	400	2730	1437	-5987	-4.959	-1.727	11.282	139	14	18	14	0.189	0.211	0.186	195	192	98
3	100	-600	736	1056	2.687	-4.655	9.911	54	32	30	27	0.300	0.252	0.396	247	35	14
	200	-430	966	851	0.536	-1.378	5.108	106	21	22	18	0.154	0.169	0.260	247	101	41
	300	232	1366	407	3.015	4.028	-3.854	140	17	9	13	0.116	0.135	0.251	247	209	85
	400	-3	1395	584	3.092	3.878	-1.246	153	17	10	16	0.119	0.141	0.243	247	221	89
4	100	4265	1281	-1432	1.494	13.494	-3.524	47	6	16	13	0.052	0.149	0.112	306	47	15
	200	3197	752	-1243	3.160	8.229	-4.201	91	14	16	7	0.078	0.162	0.124	306	184	60
	300	3085	646	-1251	3.857	7.345	-4.539	129	19	21	10	0.101	0.205	0.155	306	226	74
	400	3081	680	-1262	3.809	7.777	-4.294	150	20	21	11	0.115	0.215	0.173	306	239	78
5	100	85	-82	1129	0.693	-2.610	-2.560	50	4	8	4	0.060	0.077	0.058	342	196	57
	200	106	-119	1102	0.845	-3.354	-2.203	91	7	10	6	0.083	0.097	0.085	342	270	79
	300	120	-161	1097	0.850	-3.592	-2.036	113	8	10	7	0.083	0.114	0.101	342	298	87
	400	131	-157	1083	0.654	-3.707	-1.996	141	10	12	9	0.097	0.134	0.122	342	316	92

Appendix 3 - contiued
Tragus/canal Fields
DS Match Solutions: Parameters

Input files: mm units
Output files: mm units

Imp No.	Cut Off	Tx	Ty	Tz	Kappa	Omega	Phi	Resid	SD x	SD y	SD z	SD Kap	SD Om	SD Phi	Pts	Eqs	%
6	100	-135	978	-2534	1.907	5.567	7.549	54	10	15	8	0.103	0.091	0.125	297	69	23
	200	437	1771	-2394	6.845	7.074	4.392	89	13	13	7	0.113	0.085	0.141	297	179	60
	300	829	1823	-2373	5.095	6.908	2.602	124	33	26	10	0.192	0.140	0.219	297	209	70
	400	186	1706	-2408	4.500	7.343	5.772	153	16	12	11	0.078	0.130	0.211	297	215	72
7	100	-1096	-3004	5507	-1.585	-13.279	4.182	49	7	8	5	6.061	0.063	0.056	276	144	52
	200	-1088	-2969	5489	-2.208	-13.330	4.074	94	11	14	8	0.103	0.098	0.086	276	220	80
	300	-1089	-2908	5467	-2.910	13.189	3.899	116	10	2	9	0.054	0.092	0.097	276	238	86
	400	-1054	-2996	5484	-2.304	-13.524	3.927	130	13	13	10	0.105	0.122	0.107	276	251	91
8	100	-2427	766	1057	5.340	5.443	-5.974	52	11	16	9	0.075	0.108	0.116	340	87	26
	200	-2143	1095	946	4.982	7.125	-7.296	97	10	7	9	0.055	0.106	0.115	340	183	54
	300	-1902	1174	743	4.417	6.719	-6.606	124	18	23	12	0.125	0.146	0.137	340	221	65
	400	-1864	1435	684	4.562	7.356	-6.137	168	20	26	13	0.150	0.171	0.163	340	261	77
9	100	-1920	4372	3706	6.586	8.329	-5.264	51	17	2	11	0.127	0.079	0.162	145	77	53
	200	-1933	4405	3712	5.172	6.178	-5.502	101	32	5	22	0.191	0.175	0.330	145	90	62
	300	-1833	4209	3685	7.967	8.433	-6.155	107	30	19	18	0.272	0.219	0.267	145	113	78
	400	-1849	4347	3668	6.891	7.637	-6.638	134	33	6	22	0.191	0.189	0.317	145	119	82
10	100	282	-2748	-914	-2.171	-6.597	0.681	53	15	7	15	0.149	0.143	0.220	208	105	50
	200	140	-3072	-601	-2.246	-8.370	0.758	85	21	12	17	0.135	0.161	0.236	208	182	88
	300	181	-3096	-539	-2.489	-8.752	0.223	103	22	13	17	0.134	0.170	0.246	208	193	93
	400	149	-3109	-531	-2.379	-8.716	0.143	116	24	14	19	0.146	0.190	0.268	208	199	96

Appendix 3 - continued
Tragus/canal Fields
DS Match Solutions: Parameters

Input files: mm units
Output files: μm units

Imp No.	Cut Off	Tx	Ty	Tz	Kappa	Omega	Phi	Resid	SD x	SD y	SD z	SD Kap	SD Om	SD Phi	Pts	Eqs	%
11	100	1500	-953	-146	-4.124	-1.872	1.786	51	11	9	6	0.091	0.107	0.083	210	136	65
	200	1516	-910	-188	-4.217	-1.530	1.643	80	14	11	7	0.122	0.139	0.113	210	175	83
	300	1503	-912	-177	-4.064	-1.743	1.965	102	18	13	9	0.153	0.159	0.134	210	191	91
	400	1502	-916	-179	-4.220	-1.783	1.922	107	18	13	9	0.156	0.164	0.140	210	193	92
12	100	1113	-764	645	0.489	-4.187	-4.824	49	16	8	10	0.114	0.170	0.176	218	64	29
	200	1687	-526	591	1.757	-5.032	-8.259	81	11	8	9	0.093	0.107	0.115	218	169	78
	300	1612	-573	616	1.244	-5.260	-8.082	109	14	10	11	0.095	0.126	0.136	218	191	88
	400	1627	-533	601	1.128	-5.188	-8.187	120	15	10	12	0.104	0.137	0.152	218	198	91
13	100	1013	1727	1929	-3.531	3.276	-8.537	51	13	5	8	0.104	0.092	0.093	267	86	32
	200	1341	1675	1795	-1.194	4.691	-7.875	89	17	10	12	0.138	0.117	0.120	267	153	57
	300	1398	1665	1786	-0.767	5.104	-7.894	119	21	5	14	0.140	0.121	0.150	267	180	67
	400	1347	1683	1812	-0.767	5.164	-7.713	150	24	13	18	0.185	0.170	0.182	267	189	71
14	100	-548	1303	621	6.436	5.273	0.352	53	12	12	9	0.145	0.089	0.119	208	131	63
	200	-619	1300	668	6.270	5.418	0.657	82	15	17	13	0.200	0.122	0.163	208	164	79
	300	616	1277	652	6.734	5.460	0.456	101	17	19	15	0.215	0.143	0.190	208	181	87
	400	-636	1276	654	6.716	5.340	0.347	114	19	20	17	0.238	0.160	0.210	208	185	89

Appendix 3 - continued
Tragus/canal Fields
DS Match Solutions: Statistics

Input files: mm units
Output files: mm unit

	Impression number														
	1	2	3	4	5	6	7	8	9	10	11	12	13	14	
Cut Off		% Equation included in solution													mean (1:14)
100	46	18	14	15	57	23	52	26	53	50	65	29	32	63	39
200	64	44	41	60	79	60	80	54	62	88	83	78	57	79	66
300	64	97	85	74	87	70	86	65	78	93	91	88	67	87	81
400	66	98	89	78	92	72	91	77	82	96	92	91	71	89	85
		RMS Residual value													
100	46.6	47.1	54.3	47.2	50.2	54.4	48.6	51.7	51	52.6	50.9	49.4	51.2	52.8	51
200	81	96.7	106	91.2	90.8	89	93.7	96.8	101	85.4	79.6	81.5	88.9	82.4	90
300	104	141	140	129	113	133	116	124	107	103	102	109	119	101	117
400	123	139	153	150	141	153	130	168	134	116	107	120	150	114	136
		Translations (400um cutoff)						(relative to concha)				(determined by manual translation)			
x-axis	0	-3839	-3231	-1248	-364	0	2022	1458	1595	1489	116	-2075	-775	-647	
y-axis	0	-1592	-588	-1006	-823	0	-811	-2716	3712	2372	-440	0	-1270	-1616	
abs x-axis	0	3839	3231	1248	364	0	2022	1458	1595	1489	116	2075	775	647	1450
abs y-axis	0	1592	588	1006	823	0	811	2716	3712	2372	440	0	1270	1616	1303
		Rotations (400 um cutoff)						(relative to concha)							
Rx	1.81	-1.73	3.88	7.78	-3.71	7.34	-13.5	7.36	7.64	-8.72	-1.78	-5.19	5.16	5.34	0.758
Ry	-1.45	11.3	-1.25	-4.29	-2	5.77	3.93	-6.14	-6.64	0.14	1.92	-8.19	-7.71	0.35	-0.985
Rz	-0.77	-4.96	3.09	3.81	0.65	4.5	-2.3	4.56	6.89	-2.38	-4.22	1.13	-0.77	6.72	1.29
abs Rx	1.81	1.73	3.88	7.78	3.71	7.34	13.5	7.36	7.64	8.72	1.78	5.19	5.16	5.34	6.09
abs Ry	1.45	11.3	1.25	4.29	2	5.77	3.93	6.14	6.64	0.14	1.92	8.19	7.71	0.35	4.58
abs Rz	0.77	4.96	3.09	3.81	0.65	4.5	2.3	4.56	6.89	2.38	4.22	1.13	0.77	6.72	3.54

Appendix 3 - continued
Tragus/canal Fields
DS Match Solutions: Parameters

Input files: mm units
Output files: μm unit

Imp	Cut Off	Tx	Ty	Tz	Kappa	Omega	Phi	Resid	SD x	SD y	SD z	SD Kap	SD Om	SD Phi	Pts	Eqs	%
1	400	-255	593	4650	-0.772	1.810	-1.453	123	4	8	7	0.010	0.152	0.065	619	408	66
2	400	2730	1437	-5987	-4.959	-1.727	11.282	139	14	18	14	0.189	0.211	0.186	195	192	98
3	400	-3	1395	584	3.092	3.878	-1.246	153	17	10	16	0.119	0.141	0.243	247	221	89
4	400	3081	680	-1262	3.809	7.777	-4.294	150	20	21	11	0.115	0.215	0.173	306	239	78
5	400	131	-157	1083	0.654	-3.707	-1.996	141	10	12	9	0.097	0.134	0.122	342	316	92
6	400	186	1706	-2408	4.500	7.343	5.772	153	16	12	11	0.078	0.130	0.211	297	215	72
7	400	-1054	-2996	5484	-2.304	-13.524	3.927	130	13	13	10	0.105	0.122	0.107	276	251	91
8	400	-1864	1435	684	4.562	7.356	-6.137	168	20	26	13	0.150	0.171	0.163	340	261	77
9	400	-1849	4347	3668	6.891	7.637	-6.638	134	33	6	22	0.191	0.189	0.317	145	119	82
10	400	149	-3109	-531	-2.379	-8.716	0.143	116	24	14	19	0.146	0.190	0.268	208	199	96
11	400	1502	-916	-179	-4.220	-1.783	1.922	107	18	13	9	0.156	0.164	0.140	210	193	92
12	400	1627	-533	601	1.128	-5.188	-8.187	120	15	10	12	0.104	0.137	0.152	218	198	91
13	400	1347	1683	1812	-0.767	5.164	-7.713	150	24	13	18	0.185	0.170	0.182	267	189	71
14	400	-636	1276	654	6.716	5.340	0.347	114	19	20	17	0.238	0.160	0.210	208	185	89
	Mean	364	489	632	1.140	0.833	-1.019	136	18	14	13	0.134	0.163	0.181	277	228	85
	St Dev	1528	1953	2898	3.881	6.773	5.544	17.98	6.96	5.6	4.24	0.057	0.030	0.066	114		

Appendix 4

Concha regions: DS Match residual data contour maps overlaid with closed-jaw impression data. Plotted with Surfer software.

Note: All units are millimeters. All maps have the same colour scale except Imp nos 1a and 4a. These have adjacent corresponding colour scales. All maps are orientated with inferior surface to the bottom.

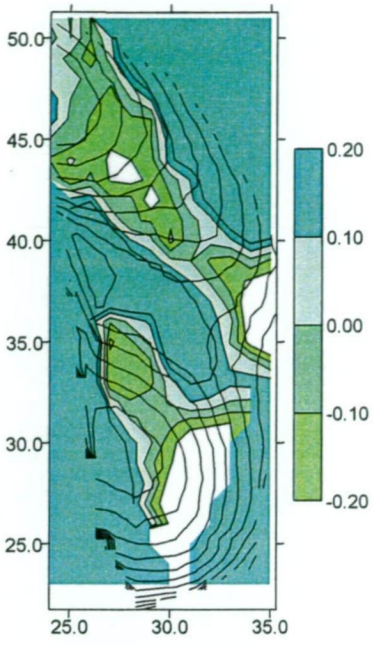

Imp No.1.

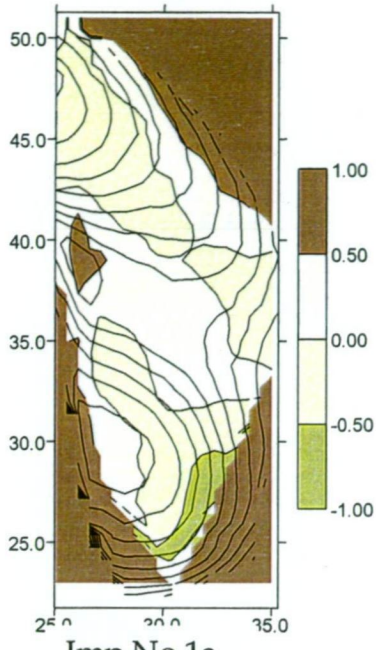

Imp No.1a.

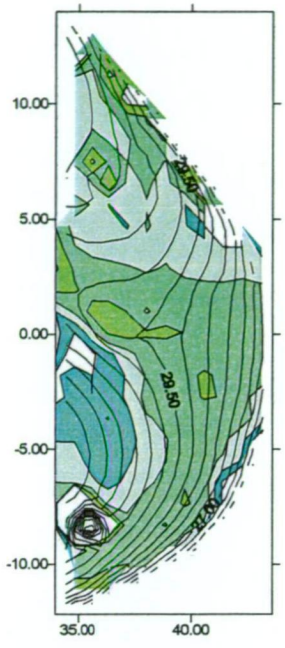

Imp No.2.

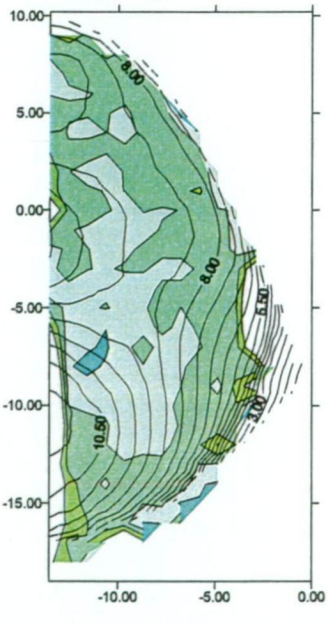

Imp No.3.

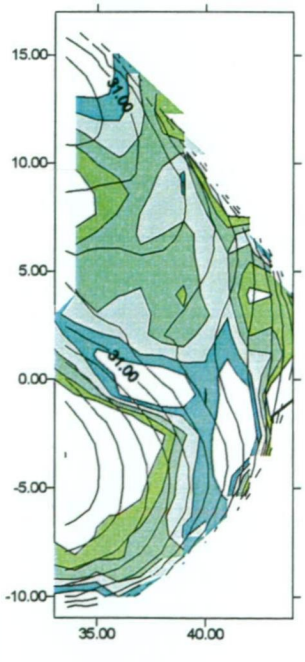

Imp No.4.

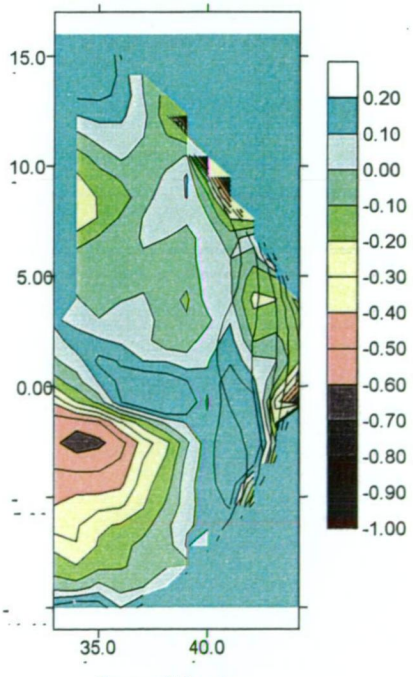

Imp No.4a.

Appendix 4 - continued

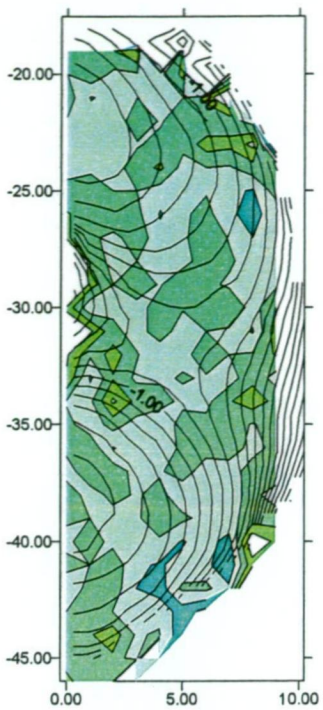

Imp No.5.

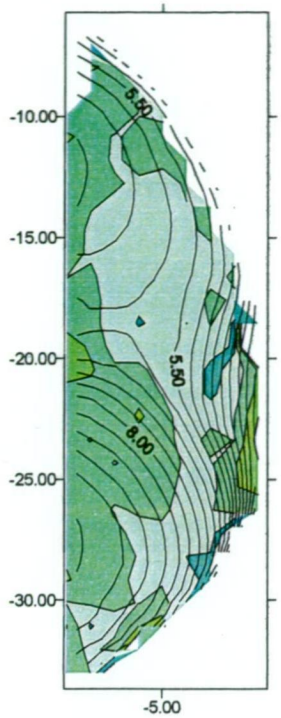

Imp No.6.

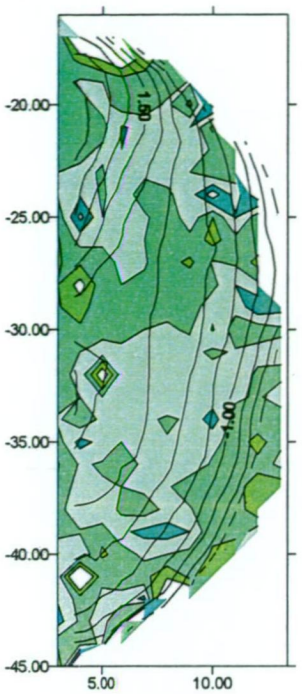

Imp No.7.

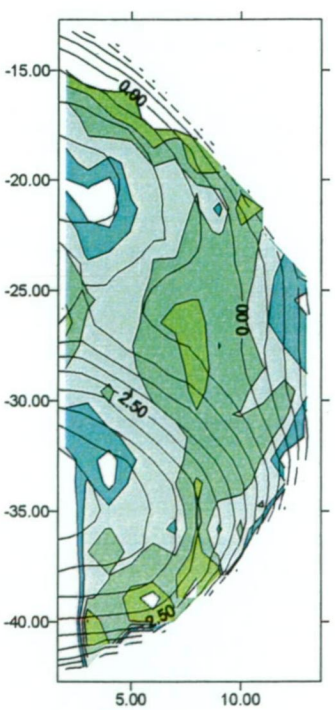

Imp No.8.

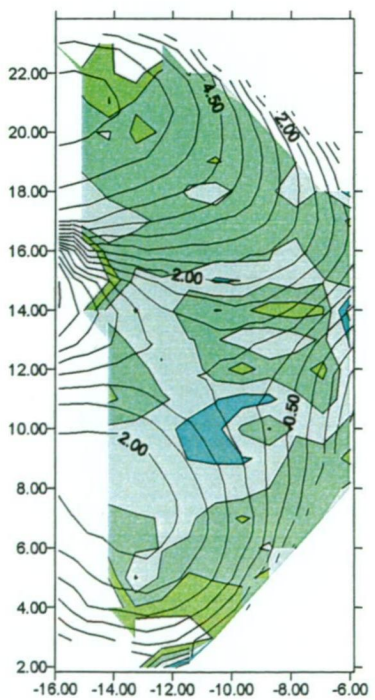

Imp No.9.

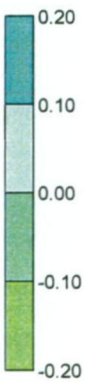

Appendix 4 - continued

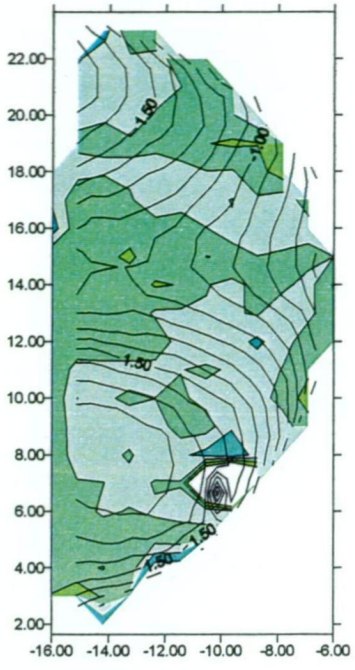

Imp No.10.

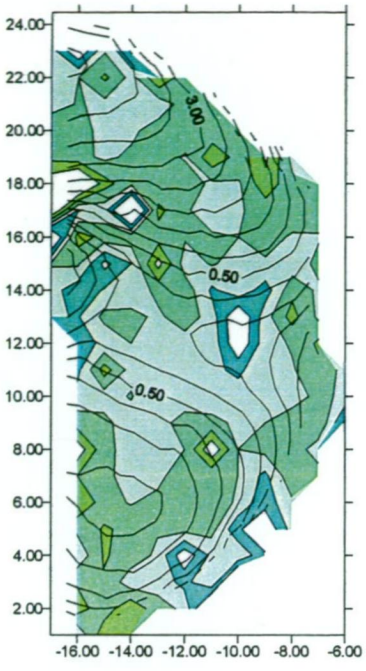

Imp No.11.

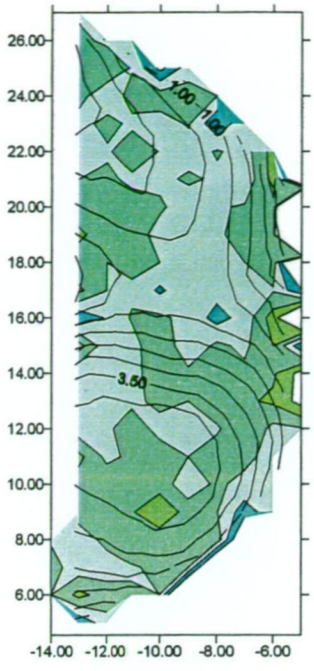

Imp No.12.

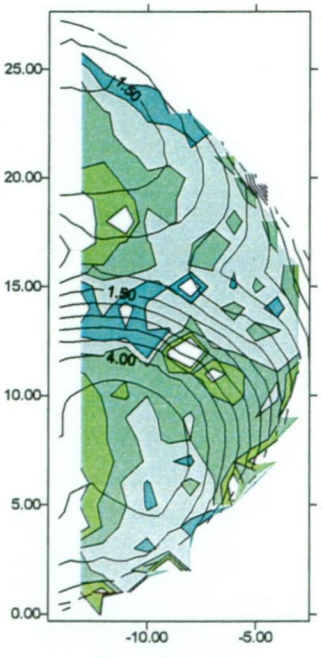

Imp No.13.

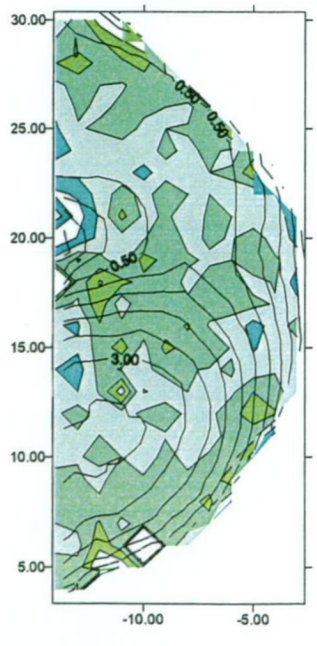

Imp No.14.

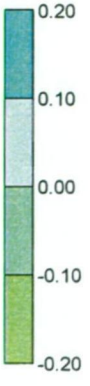

Appendix 5

Tragus/canal regions: DS Match residual data contour maps overlaid with closed-jaw impression data. Plotted with Surfer software.

Note: All units in millimeters. Maps have been orientated so that inferior surface is bottom, medial part of canal is towards centre of page, and lateral part of tragus is towards the outside of page, except map 13, which is a right ear.

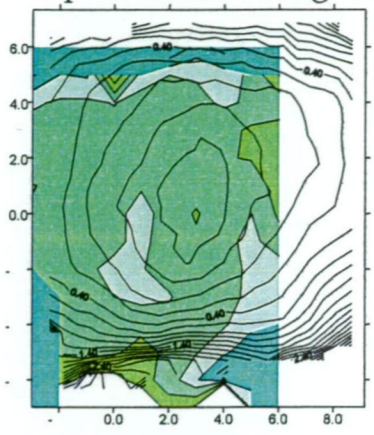

No.1, Subject 1, Left.

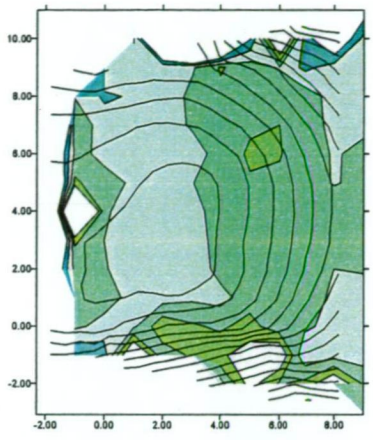

No.2, Subject 2, Right.

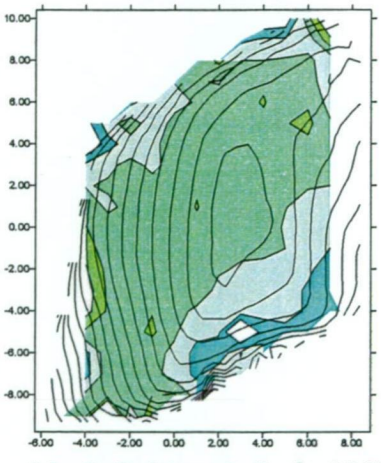

No.3, Subject 3, Left, 89%.

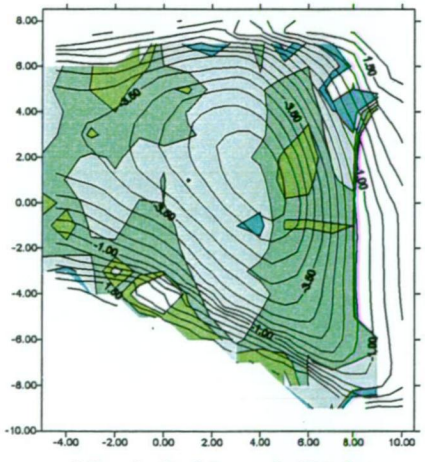

No.4, Subject 4, Right.

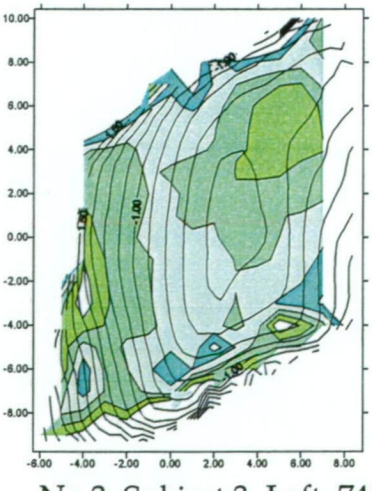

No.3, Subject 3, Left, 74%.

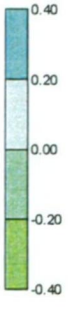

Appendix 5 – continued

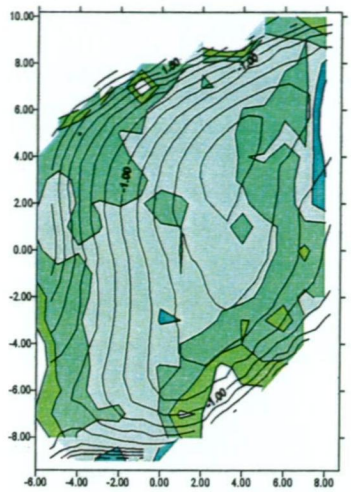

No.5, Subject 5, Left,92% Eq.

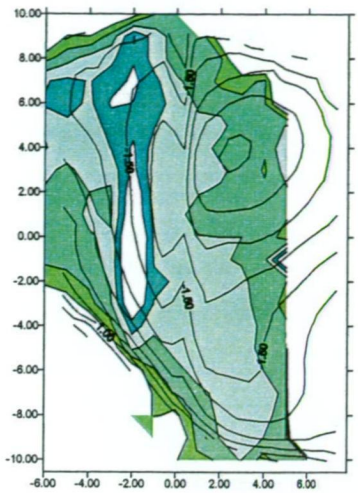

No.6, Subject 5, Right.

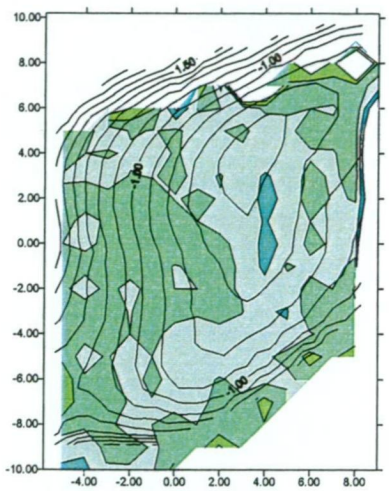

No.5, Subject 5, Left, 62% Eq.

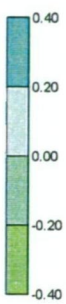

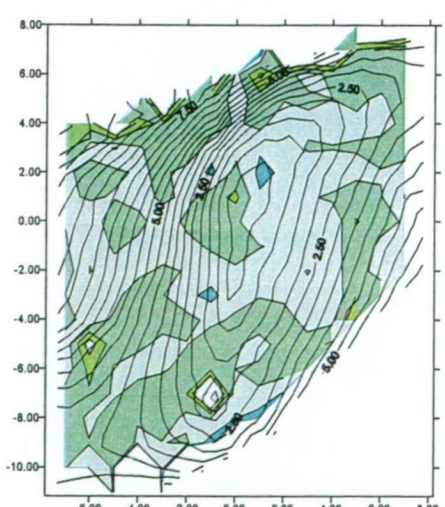

No.7, Subject 6, Left.

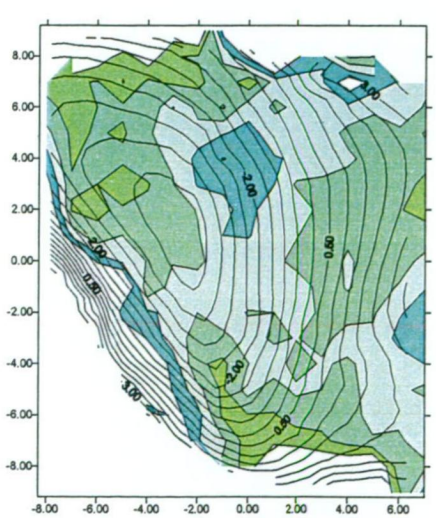

No.8, Subject 6, Right.

Appendix 5 – continued

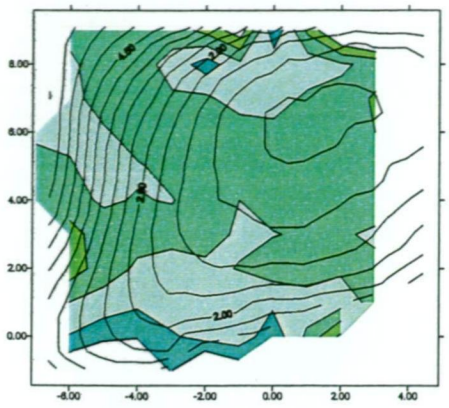

No.9, Subject 7, Left.

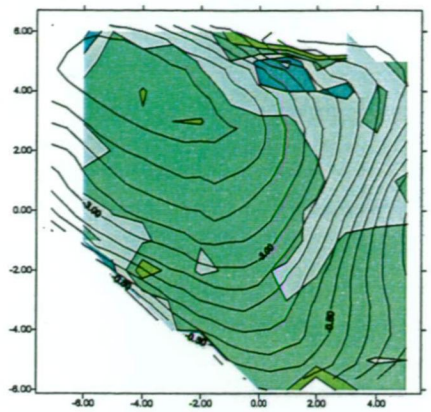

No.10, subject 7, Right.

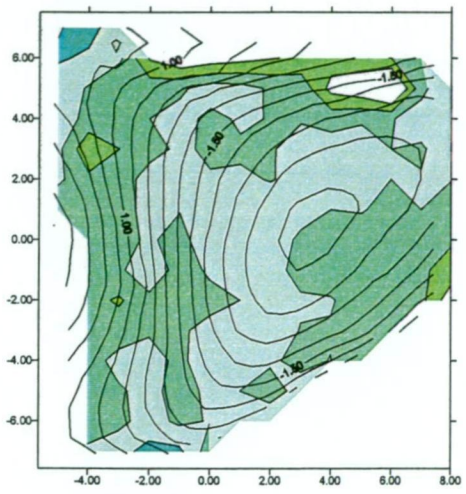

No.11, Subject 8, Left.

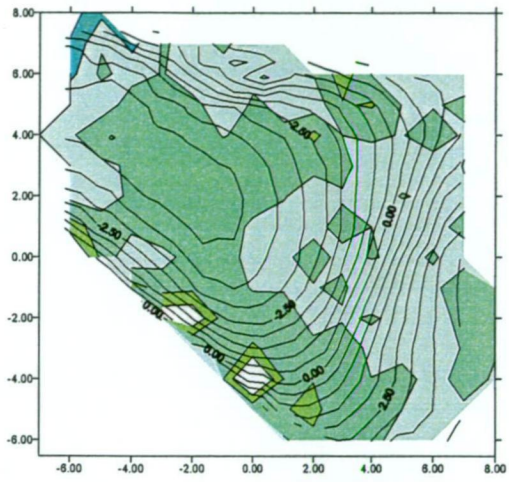

No.12, Subject 8, Right.

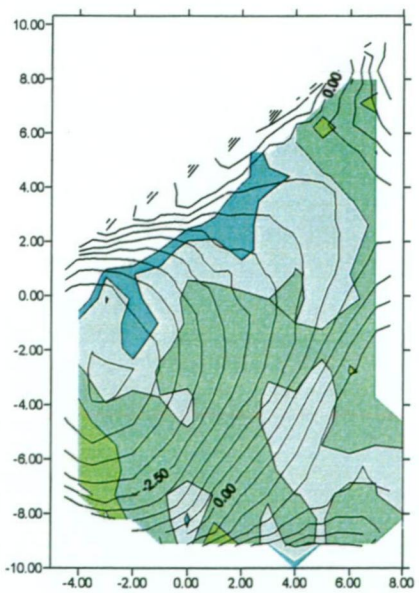

No.13. Subject, 9,Right.

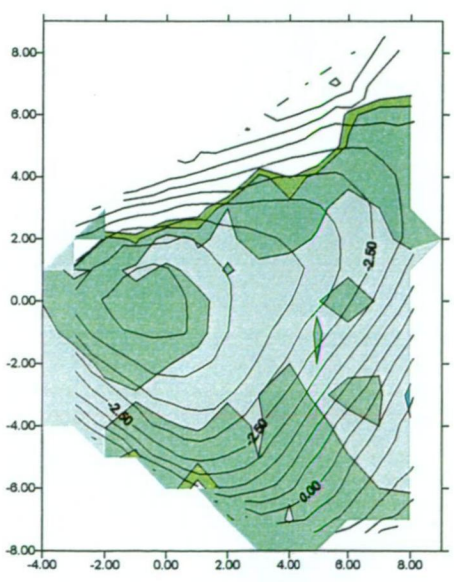

No.14, Subject 10, Right.

Appendix 6

Tragus/canal regions: contour maps overlaid in same coordinate system. Plotted with Surfer software.

Note: All units in microns. Maps have been orientated so that inferior surface of canal is bottom, medial part of canal is towards centre of page, and lateral part of tragus is toward the outside of page, except map 13, which is a right ear.

Closed-jaw Impressions: coloured black
Open-jaw impression: coloured magenta

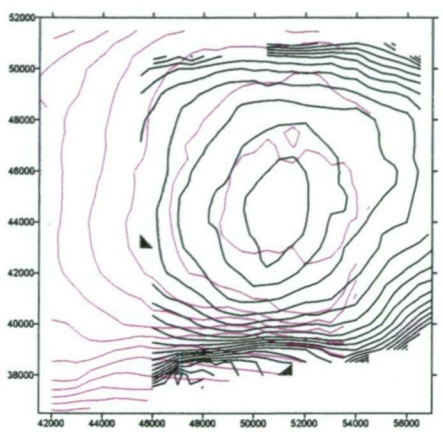

No.1, Subject 1, Left.

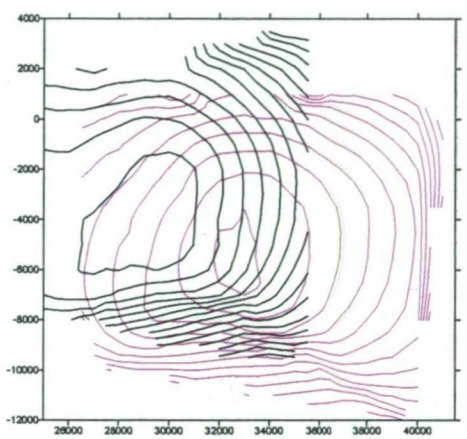

No.2, Subject 2, Right.

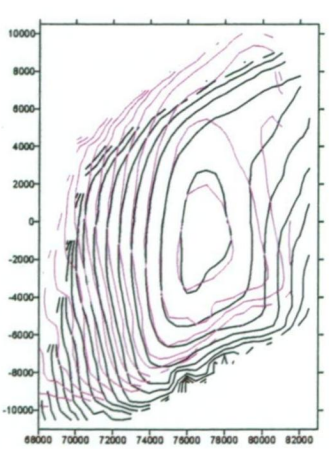

No.3, Subject 3, Left.

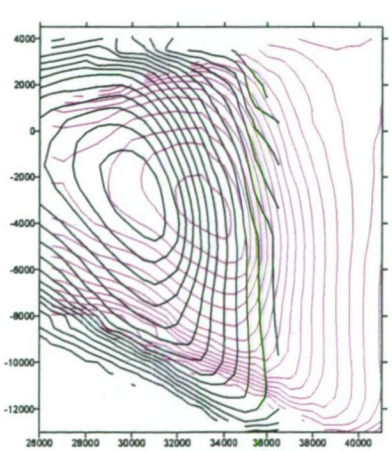

No.4, Subject 4, Right.

Appendix 6 – continued

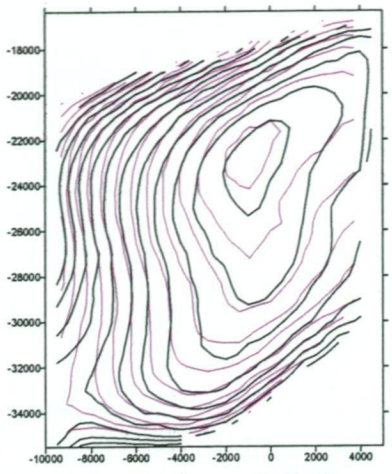

No.5, Subject 5, Left .

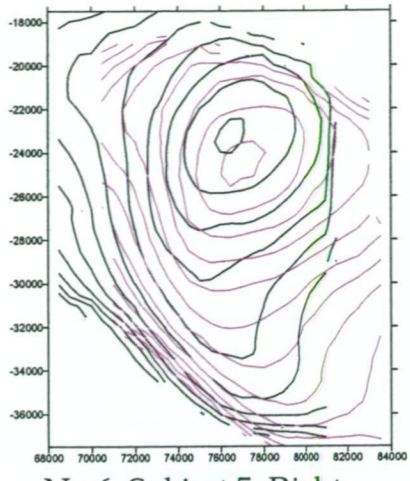

No.6, Subject 5, Right.

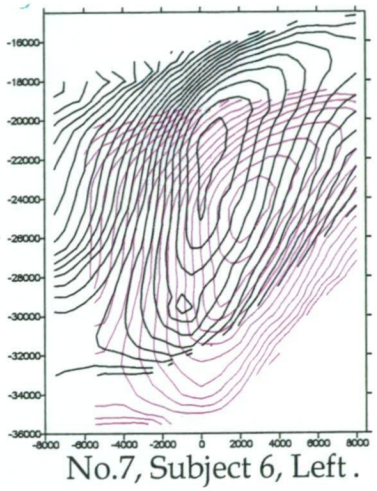

No.7, Subject 6, Left .

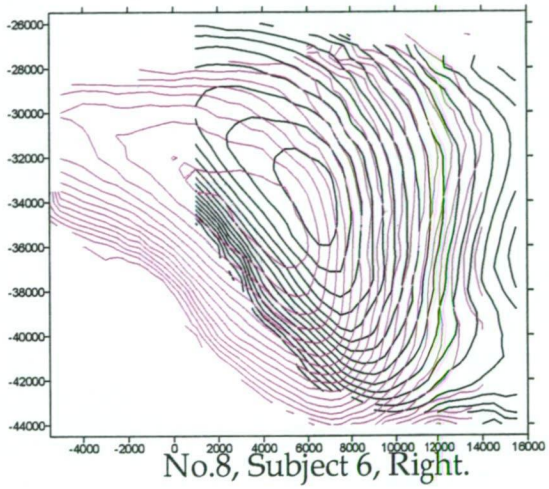

No.8, Subject 6, Right.

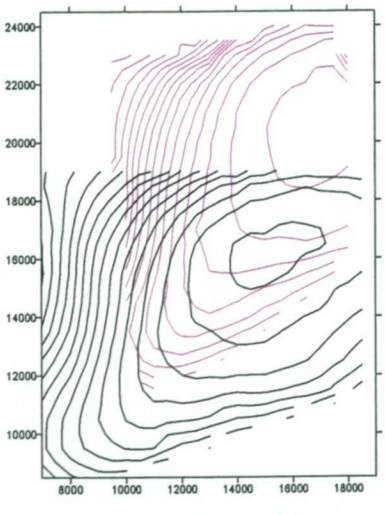

No.9, Subject 7, Left.

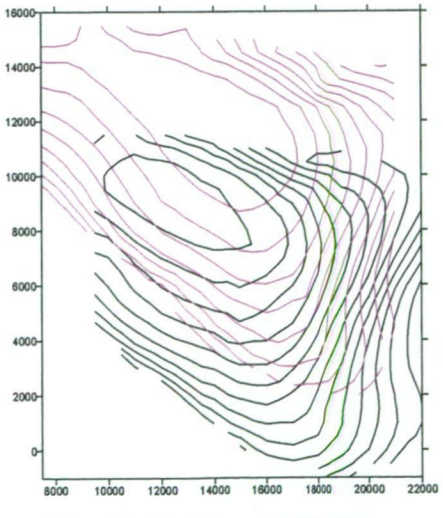

No.10, Subject 7, Right.

Appendix 6 - continued

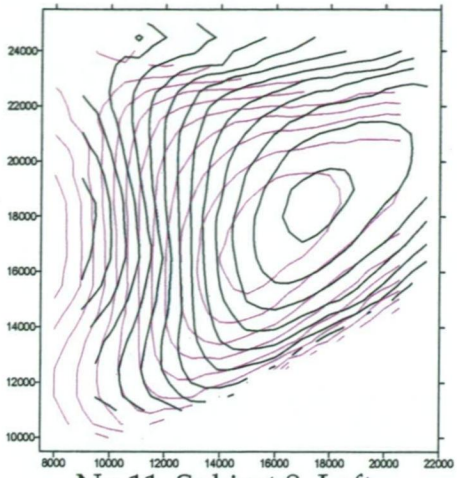

No.11, Subject 8, Left.

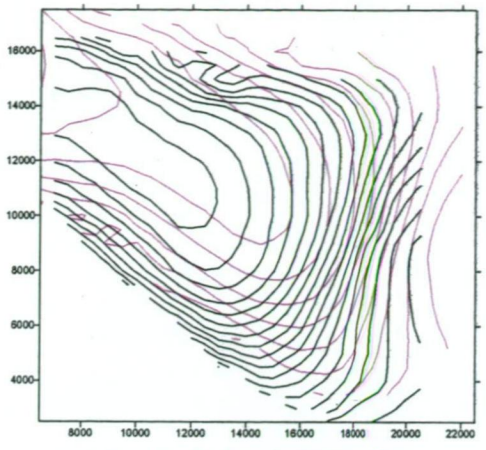

No.12, Subject 8, Right.

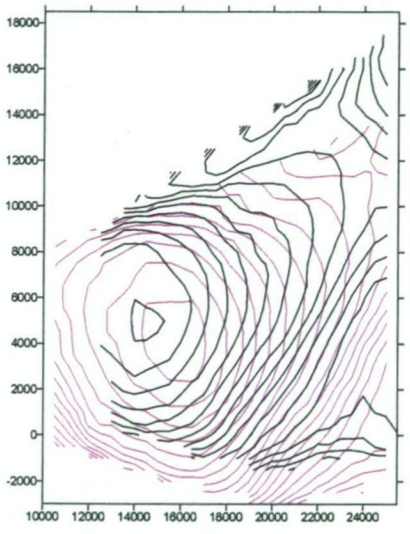

No.13, Subject 9, Right.

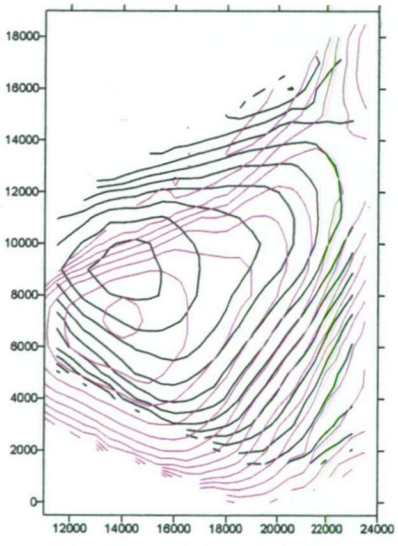

No.14, Subject 10, Right.

Appendix 7

Tragus/canal regions: difference map overlaid with contour maps plotted in same coordinate system with difference. Plotted with Surfer software.

Note: Difference Map = closed-jaw – open-jaw impression
Closed-jaw Impressions: coloured black.
Open-jaw impression: coloured magenta.
All units in microns. Maps have been orientated so that inferior surface on canal is bottom, medial part of canal is towards centre of page, and lateral part of tragus is toward the outside of page, except map 13, which is a right ear.
Positive values (yellow-red) represent anterior movement
Negative values (green-purple) represent posterior movement

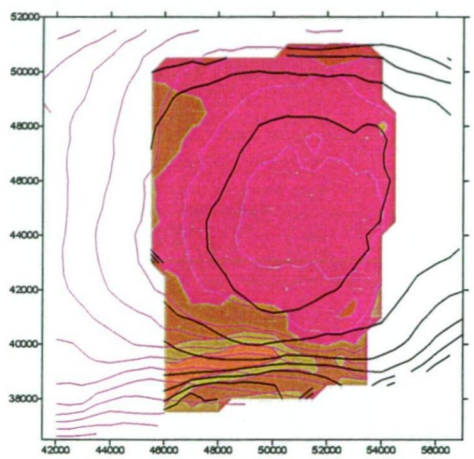

No.1, Subject 1, Left .

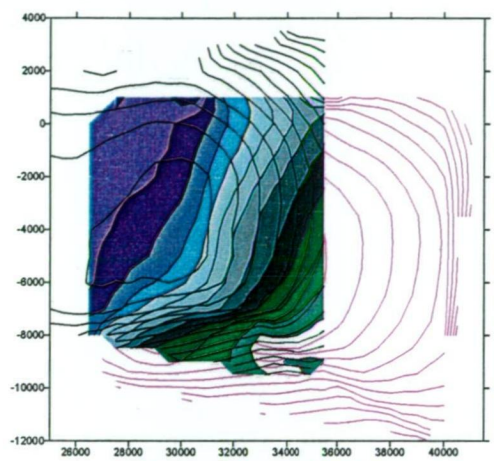

No.2, Subject 2, Right.

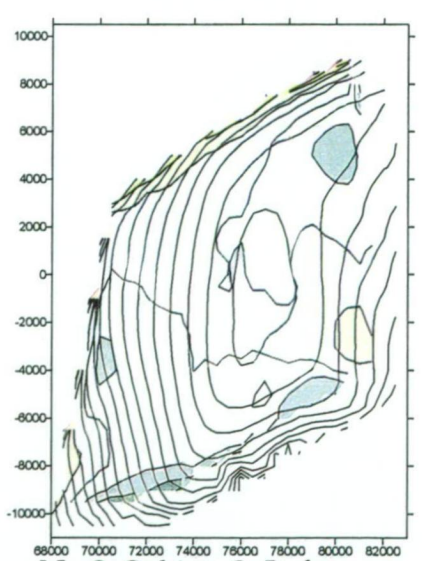

No.3, Subject 3, Left.

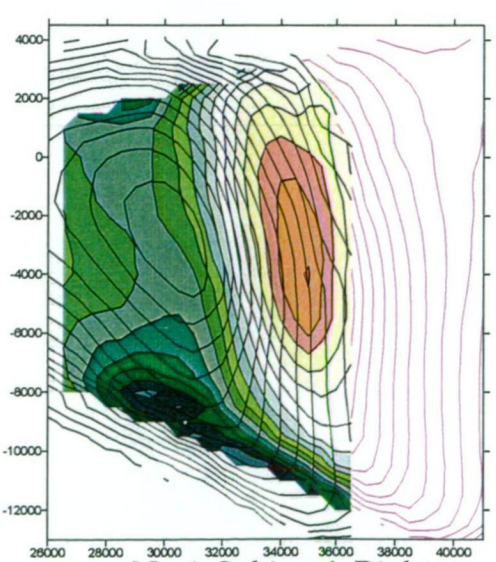

No.4, Subject 4, Right.

Appendix 7 - continued

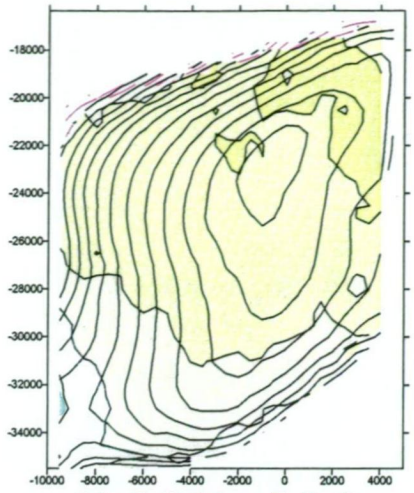

No.5, Subject 5, Left .

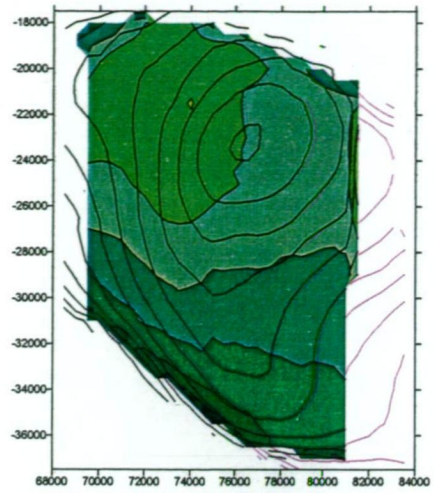

No.6, Subject 5, Right.

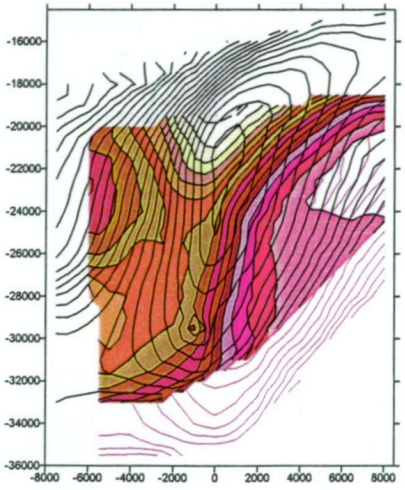

No.7, Subject 6, Left .

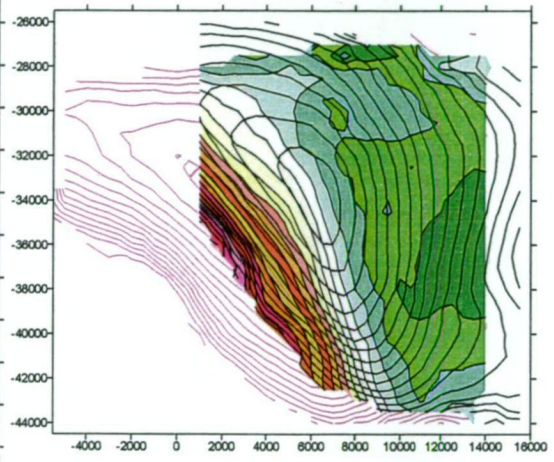

No.8, Subject 6, Right.

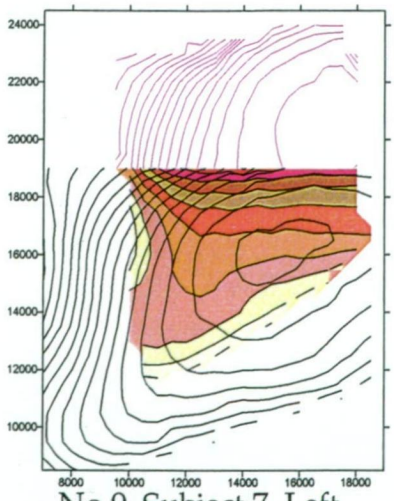

No.9, Subject 7, Left .

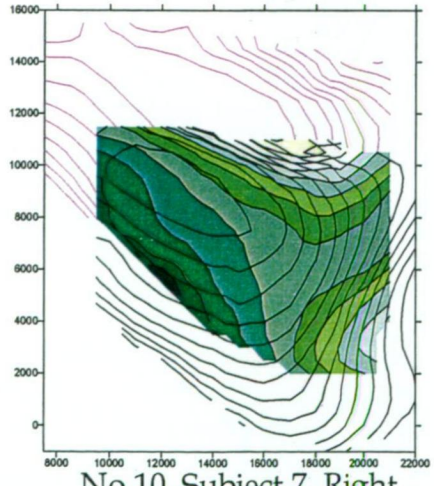

No.10, Subject 7, Right.

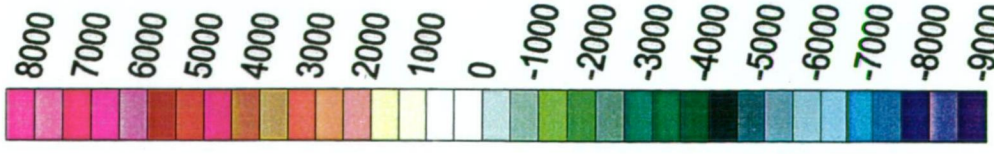

Appendix 7 - continued

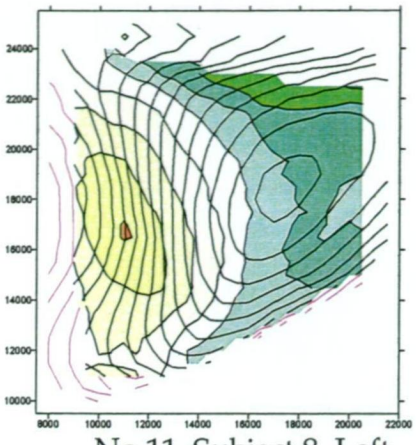

No.11, Subject 8, Left.

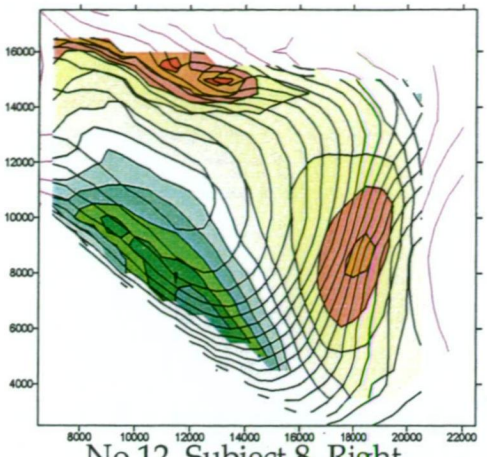

No.12, Subject 8, Right.

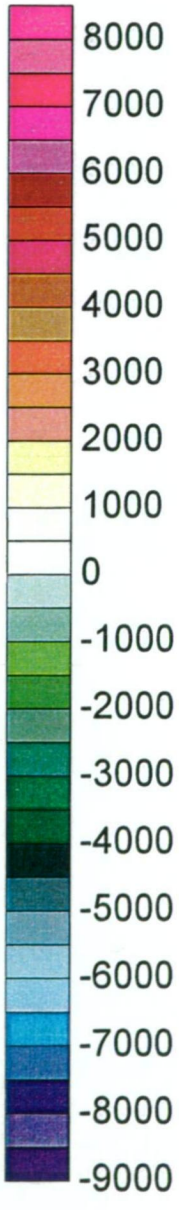

Appendix 7
Colour scale
Units in μm

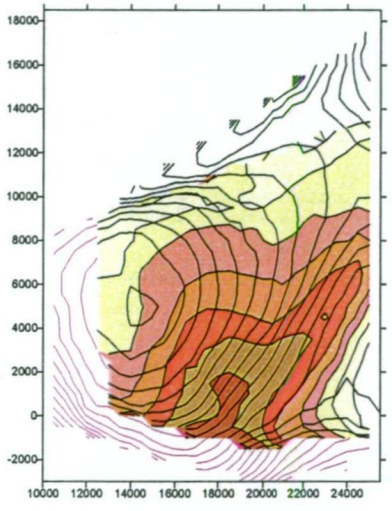

No.13, Subject 9, Right.

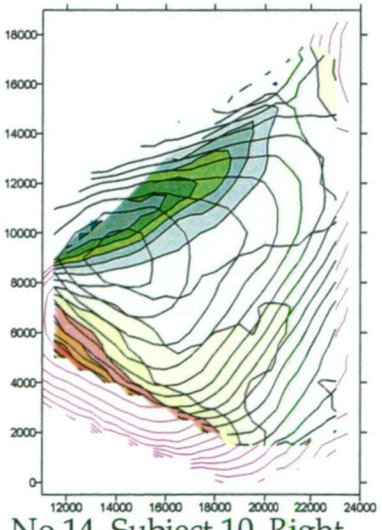

No.14, Subject 10, Right.